CENTER FOR INFRASTRUCTURE ENGINEERING STUDIES

Southview Bridge Rehabilitation in Rolla, Missouri

by

Raffaello Fico

Nestore Galati

Andrea Prota

Antonio Nanni

University Transportation Center Program at

The University of Missouri-Rolla

UTC R103

Disclaimer

The contents of this report reflect the views of the author(s), who are responsible for the facts and the accuracy of information presented herein. This document is disseminated under the sponsorship of the Department of Transportation, University Transportation Centers Program and the Center for Infrastructure Engineering Studies UTC program at the University of Missouri - Rolla, in the interest of information exchange. The U.S. Government and Center for Infrastructure Engineering Studies assumes no liability for the contents or use thereof.

Technical Report Documentation Page

1. Report No.	2. Government Accession No.	3. Recipient's Catalog No.
UTC R103		

4. Title and Subtitle	5. Report Date
Southview Bridge Rehabilitation in Rolla, MO. Volume I: Design and Construction	July 2006
	6. Performing Organization Code

7. Author/s	8. Performing Organization Report No.
R. Fico, N. Galati, A. Prota, and A. Nanni	00001406/0008404

9. Performing Organization Name and Address	10. Work Unit No. (TRAIS)
Center for Infrastructure Engineering Studies/UTC program University of Missouri - Rolla 223 Engineering Research Lab Rolla, MO 65409	11. Contract or Grant No. DTRS98-G-0021

12. Sponsoring Organization Name and Address	13. Type of Report and Period Covered
U.S. Department of Transportation Research and Special Programs Administration 400 7th Street, SW Washington, DC 20590-0001	Final
	14. Sponsoring Agency Code

15. Supplementary Notes

16. Abstract

A research project was undertaken to evaluate the use of post-tensioned FRP for bridge-deck construction. The type of structure selected for this project is a four-span continuous concrete slab having GFRP bars for top and bottom mats and CFRP reinforcement for internal post-tensioning of the bridge deck. This bridge is located in Rolla, Missouri (Southview Drive on Carter Creek). One lane of the bridge was already built using a conventional four-cell steel reinforced concrete box culvert. One lane and sidewalk needed to be added. This additional lane was constructed using FRP bars as internal reinforcement. The combination of prestressed and non-prestressed FRP reinforcement resulted in an economical solution for a deck system with low deflection and high shear strength at a minimum deck thickness. This study includes the design of the FRP portion of the bridge using existing codes when appropriate, the validation of the FRP technology through a pre-construction investigation conducted on two specimens representing a deck strip, construction and field evaluation through load testing of the bridge. The results showed how FRP, in the form of GFRP as passive and CFRP bars as active internal reinforcement, could be a feasible solution replacing the steel reinforcement of concrete slab bridges, and specifically the enhanced shear capacity of the slab due to the CFRP prestressing.

17. Key Words	18. Distribution Statement
Bridge Design, bridge monitoring, concrete deck, GFRP bars, mild reinforcement, CFRP prestresses bars, in-situ load test, structural evaluation, continuous deck, structural health monitoring.	No restrictions. This document is available to the public through the National Technical Information Service, Springfield, Virginia 22161.

19. Security Classification (of this report)	20. Security Classification (of this page)	21. No. Of Pages	22. Price
unclassified	unclassified	190	

Form DOT F 1700.7 (8-72)

The mission of CIES is to provide leadership in research and education for solving society's problems affecting the nation's infrastructure systems. CIES is the primary conduit for communication among those on the UMR campus interested in infrastructure studies and provides coordination for collaborative efforts. CIES activities include interdisciplinary research and development with projects tailored to address needs of federal agencies, state agencies, and private industry as well as technology transfer and continuing/distance education to the engineering community and industry.

Center for Infrastructure Engineering Studies (CIES)
University of Missouri-Rolla
223 Engineering Research Laboratory
1870 Miner Circle
Rolla, MO 65409-0710
Tel: (573) 341-4497; fax -6215
E-mail: cies@umr.edu
http://www.cies.umr.edu/

RESEARCH INVESTIGATION

SOUTHVIEW BRIDGE REHABILITATION IN ROLLA, MO.

VOLUME I: DESIGN AND CONSTRUCTION

PREPARED FOR THE

MISSOURI DEPARTMENT OF TRANSPORTATION

IN COOPERATION WITH THE

UNIVERSITY TRANSPORTATION CENTER

Written by:

Raffaello Fico, Visiting Scholar from University of Naples - Italy

Nestore Galati, Research Engineer at UMR

Andrea Prota, Assistant Professor from University of Naples - Italy

Antonio Nanni, V. & M. Jones Professor of Civil Engineering

CENTER FOR INFRASTRUCTURE ENGINEERING STUDIES

UNIVERSITY OF MISSOURI – ROLLA

Submitted
July 2005

The opinions, findings and conclusions expressed in this report are those of the principal investigators. They are not necessarily those of the Missouri Department of Transportation, U.S. Department of Transportation, Federal Highway Administration. This report does not constitute a standard, specification or regulation.

SOUTHVIEW BRIDGE REHABILITATION IN ROLLA, MO.

VOLUME I: DESIGN AND CONSTRUCTION

EXECUTIVE SUMMARY

A research project was undertaken to evaluate the use of post-tensioned FRP for bridge-deck construction. The type of structure selected for this project is a four-span, continuous concrete slab having GFRP bars for top and bottom mats and CFRP reinforcement for internal post-tensioning of the bridge deck. This bridge is located in Rolla, Missouri (Southview Drive on Carter Creek). One lane of the bridge was already built using a conventional four-cell steel reinforced concrete box culvert. One lane and a sidewalk needed to be added. This additional lane was constructed using FRP bars as internal reinforcement.

The combination of prestressed and non-prestressed FRP reinforcement resulted in an economical solution for a deck system with low deflection and high shear strength at a minimum deck thickness. This study includes the design of the FRP portion of the bridge using existing codes when appropriate, the validation of the FRP technology through a pre-construction investigation conducted on two specimens representing a deck strip, construction, and field evaluation through load testing of the bridge.

The results showed how FRP, in the form of GFRP as passive and CFRP bars as active internal reinforcement, could be a feasible solution replacing the steel reinforcement of concrete slab bridges, specifically enhancing shear capacity of the slab with CFRP prestressing.

ACKNOWLEDGMENTS

The authors would like to acknowledge the following: the City of Rolla for providing this opportunity and Dave Brown for his assistance in the different parts of the project; the financial support of the Missouri Department of Transportation and the University Transportation Center (UTC) at the University of Missouri-Rolla (UMR) for the research component of the project; Hughes Brothers for providing the FRP materials; Jason Cox, whose skills were so critical for this project; and Bill Cochran, whose help and support was very helpful for the execution of the project.

TABLE OF CONTENTS

EXECUTIVE SUMMARY II
TABLE OF CONTENTS IV
LIST OF FIGURES VII
LIST OF TABLES XII
NOTATIONS XIII
1 INTRODUCTION 1
1.1 Background 1
1.2 Objectives 1
1.3 Description of the project 1
1.4 Report Outline 2
2 LITERATURE REVIEW 3
2.1 Load test 3
2.2 Related Literature Review 4
2.2.1 Non-Prestressed FRP Reinforced Bridge Decks 4
2.2.1.1 Bridge Street Bridge, Michigan 4
2.2.2 Prestressed FRP Reinforced Bridge Decks 6
2.2.2.1 Evaluation of FRP Prestressed Panels/Slabs for I-225/Parker Road Project 6
2.2.3 Research works on Shear Behavior of Prestressed FRP 9
2.2.3.1 S.Y. Park and A.E. Naaman (1999) 10
2.2.3.2 P.A. Whitehead and T.J. Ibell (Jan. 2004) 11
2.2.3.3 P. A. Whitehead and T. J. Ibell (Feb. 2004) 12
3 EXPERIMENTAL PROGRAM 14
3.1 Specimens Layout 14
3.2 Material Properties 15
3.3 Specimens Design 15
3.4 Specimens Preparation 17
3.5 Test Setup 22
3.6 Test Results and Discussion 27
3.6.1 Failure Modes 27
3.6.2 Discussion of Test Results 29
3.7 Conclusions 32
4 SOUTHVIEW BRIDGE DESIGN 33
4.1 Introduction 33
4.2 Assumptions 33
4.3 Structural Analysis 34
4.3.1 Load Combinations 34

4.3.2 Design Truck and Design Lanes 34
4.3.3 Deck Analysis 36
4.3.4 Flexural and Shear Analysis 36
4.3.5 Summary of the Analysis 41
4.3.6 Deflections 42
4.3.7 Barrier Analysis 43
4.4 Design 44
4.4.1 Slab Design 45
4.4.1.1 Flexural Design 45
4.4.1.2 Shear Design 47
4.4.1.3 Temperature and Shrinkage Reinforcement 49
4.4.2 Barrier Design 51
4.4.2.1 Flexural Design 51
4.4.2.1 52
4.4.3 Serviceability 52
4.4.3.1 Crack Width 52
4.4.3.2 Long-Term Deflections 54
4.4.3.3 Slab Creep Rupture and Fatigue 54
4.5 Load Rating 55
4.6 Southview Bridge Drawings 57
5 SOUTHVIEW BRIDGE DECK INSTALLATION 61
5.1 Introduction 61
5.2 Pre-construction Meetings 61
5.3 Substructure Construction 62
5.3.1 Footing and Floor Construction 62
5.3.2 Abutments Construction 66
5.3.3 Walls Construction 68
5.4 Slab Construction 70
5.4.1 Bill of Materials 70
5.4.2 Outline of tasks 73
5.4.3 Investigation of the Slab Construction 74
5.4.4 Post-tension of the Slab 81
6 BRIDGE LOAD TESTING 88
7 CONCLUSIONS 93
8 REFERENCES 96
Referenced standards and reports 96
Cited references 96
APPENDIX A: MORE DATA RELATED TO SECTION 2 98
APPENDIX B: LOAD RATING DETAILED CALCULATIONS 113
APPENDIX C: MATERIAL AND CONSTRUCTION SPECIFICATIONS 160

LIST OF FIGURES

Figure 1 - Views of the Former Bridge 2
Figure 2 - Cross Section of the Bridge After the Expansion 2
Figure 3 - Cross-sectional Details of Structure B (dim. in SI units) 4
Figure 4 - Erection of DT Girders at the Bridge Site 5
Figure 5 - Installed DT Girders with External CFCC Post-tensioning Strands 5
Figure 6 - I-225/Parker Road Bridge Under Construction 6
Figure 7 - Installation of Precast Panels 6
Figure 8 - Precast Panels Supported on Two Box Girders 7
Figure 9 - Top Reinforcement 7
Figure 10 - Cast-in-Place Portion of the Deck 8
Figure 11 - Panel and Anchorage Details 9
Figure 12 - Construction of the Panels 9
Figure 13 - Cross-Sectional Dimensions and Helical Reinforcement Shapes 13
Figure 14 - Reinforcement Layout (all dimensions in mm) 14
Figure 15 - CFRP Tendons Trace (all dimensions in mm) 14
Figure 16 - Cage Detail 18
Figure 17 - Strain Gages Detail 18
Figure 18 - Reinforcement Cages 19
Figure 19 - Specimen Curing 19
Figure 20 - Specimens after Removal of the Formwork 20
Figure 21 - Prestressing System 20
Figure 22 - Steel Wedge Anchorage System 21
Figure 23 - Drilling of CFRP Bar after Grout Curing 21
Figure 24 - Static Scheme for the Flexural Specimen 22
Figure 25 - Hyperstatic Scheme 22
Figure 26 - Flexural Plot 24
Figure 27 - Static Scheme for the Shear Specimen 24
Figure 28 - Shear Plot 25
Figure 29 - Steel Plate Detail 26
Figure 30 - Test Setup (all dimensions in mm) 27

Figure 31 - Shear Cracks on the Flexure Specimen 27
Figure 32 - Concrete Crushing in the Compressive Zone 28
Figure 33 - CFRP Bars Rupture Due to Kinking 28
Figure 34 - Failure in the Shear Specimen 29
Figure 35 - $M_{measured}$ Vs. $M_{theoretical}$ 30
Figure 36 - Load deflection Diagram for the Longer Span 31
Figure 37 - Comparison Between Experimental and 32
Figure 38 - Bridge T0530 33
Figure 39 - View of the Existing Bridge 33
Figure 40 - Truck Load on the New Deck 35
Figure 41 - Loading Conditions 35
Figure 42 - Design Truck on the Girder 36
Figure 43 - Design Truck: Possible Loading Conditions 37
Figure 44 - Design Lane: Possible Loading Conditions 38
Figure 45 - Unfactored Bending Moment Diagrams Due to Live Load 38
Figure 46 - Unfactored Bending Moment Diagrams Due to Dead Load 39
Figure 47 - Unfactored Shear Diagrams Due to Live Load 39
Figure 48 - Unfactored Shear Diagrams Due to Dead Load 40
Figure 49 - Unfactored Moment and Shear Diagrams 41
Figure 50 - Bending Moment Envelopes (kN-m/m) 42
Figure 51 - Bridge Deflection Analysis (Live Load) 43
Figure 52 - Bridge Deflection Analysis (Dead Load) 43
Figure 53 - Barrier Analysis 44
Figure 54 - Strength Reduction Factor 46
Figure 55 - Flexural Capacities of the Bridge 46
Figure 56 - Rationale for Proposed Shear Strength 49
Figure 57 - Bridge Internal FRP Reinforcement: Section at Mid-Span 50
Figure 58 - CFRP Prestressing Tendons 51
Figure 59 - Barrier Design 52
Figure 60 - Stress and Strain at Service 54
Figure 61 - Wetting the Basement and Digging the Weeds 63
Figure 62 - Work Area after the Water Filling 63
Figure 63 - Devices to Remove or Avoid the Water 64

Figure 64 - Footing Formwork 64
Figure 65 - Pouring of the Footing 65
Figure 66 - Slump Test and Concrete Cylinders Casting 65
Figure 67 - Footing after Pouring 65
Figure 68 - Floor Reinforcement 66
Figure 69 - Water Overflowing and Casting of the Floor 66
Figure 70 - Laying of Abutments Reinforcement and Formwork 67
Figure 71 - Use of the Steel Ties Gun 67
Figure 72 - Casting of the New Abutments 67
Figure 73 - Reinforcement and Formwork of the First Wall 68
Figure 74 - First Wall 68
Figure 75 - GFRP Anchoring Detail 69
Figure 76 - Laying of the GFRP Rebars 69
Figure 77 - Making of the Notch 69
Figure 78 - Central Wall 70
Figure 79 - Completion of the Preparatory Part of Southview Project 70
Figure 80 - Formwork Hangers Details 74
Figure 81 - Laying of the Formwork 74
Figure 82 - Gluing and Placing of Styrofoam 75
Figure 83 - Neoprene Pads and Plastic Chairs Details 75
Figure 84 - Laying of Bottom Layer of GFRP Rebars 76
Figure 85 - The RTI Team with (from bottom left) Mr. Cochran, ... 76
Figure 86 - Top GFRP Layer 76
Figure 87 - Board Detail 77
Figure 88 - Wooden Board (the wire indicates the position of the tendons) 78
Figure 89 - Slab Section 78
Figure 90 - Plastic Ducts Detail 78
Figure 91 - T Connectors Detail 79
Figure 92 - Attaching of a Strain Gage 79
Figure 93 - Strain Gages Scheme 80
Figure 94 - Pouring Fragments 80
Figure 95 - Concrete Cylinders Execution and Slab Leveling 81
Figure 96 - Poured FRP Bridge Deck 81

Figure 97 - Pulling Machine Before and After the Optimizations 82
Figure 98 - New Pulling Machine Ready for Use 82
Figure 99 - Load Cell and External Chuck Detail 83
Figure 100 - Hammer Detail and Use on the Site 83
Figure 101 - Orange Box 84
Figure 102 - Wedges Insertion and Cutting of the Tendon 84
Figure 103 - Load vs. Time Diagram of Tendon 1 85
Figure 104 - First Set of Pulled Tendons 85
Figure 105 - Grout Injection and Slots Locking 86
Figure 106 - Cutting of the Slab Edge 86
Figure 107 - Southview Bridge-Deck Completed 87
Figure 108 - Bridge after Completion 87
Figure 109 - In-situ Bridge Load Test 88
Figure 110 - Location of the Sensors 89
Figure 111 - Truck Used for the Load Testing 89
Figure 112 - Lateral Location of the Truck During the Load test 90
Figure 113 - FEM Model Geometry 91
Figure 114 – Comparison Between Experimental and Theoretical Results 92
Figure 115 - Buffalo Creek Bridge Construction 98
Figure 116 - Crowchild Trail Bridge Detail 99
Figure 117 - Joffre Bridge in Québec 100
Figure 118 - Pierce Street Bridge Construction 100
Figure 119 - Cut Away View of the Deck 101
Figure 120 - Tailor Bridge in Manitoba 102
Figure 121 - Salem Avenue Bridge, Dayton, OH 102
Figure 122 - Concrete Placement in the GFRP Reinforced Concrete Deck 103
Figure 123 - Bridge Deck Construction 104
Figure 124 - Chatham Bridge Construction 105
Figure 125 - FRP Reinforcement Layout 105
Figure 126 - In Situ Load Test – Walters Street Bridge 106
Figure 127 - Overall View of the Ulenbergstrasse Road Bridge 107
Figure 128 - Technical Data of the Ulenbergstrasse Road Bridge 108
Figure 129 - General View of Concrete Bridge Prestressed with CFRP Strands 109

Figure 130 - General Details of Batigawa-Minami-Bashi Bridge 110
Figure 131 - Schiessbergstrasse Bridge View 110
Figure 132 - Technical Data of the Schiessbergstrasse Bridge..... 111
Figure 133 - Notsch Bridge View..... 111
Figure 134 - Technical Data of the Notsch Bridge 112

LIST OF TABLES

Table 1 - Mechanical Properties of FRP Bars 15
Table 2 – Comparison Experimental Theoretical Results 29
Table 3 – Parameters for Girder Analysis..... 36
Table 4 - Moment and Shear per Unit Strip (Live and Dead Load) 42
Table 5 - Material Properties 44
Table 6 - Slab Geometrical Properties and Internal FRP Reinforcement..... 47
Table 7 - Steel and GFRP Flexural Design of the Deck (No Prestress Used)..... 48
Table 8 - Barrier Geometrical Properties and Internal FRP Reinforcement..... 51
Table 9 - Maximum Shear and Moment due to Live Load..... 56
Table 10 - Rating Factor for the New Slab (Bending Moment) 56
Table 11 - Rating Factor for the New Slab (Shear) 57
Table 12 - Bill of FRP Material 71
Table 13-Examples of Prestressed Concrete Bridges in Japan Using FRP Materials 108

NOTATIONS

A = The effective tension area of concrete, defined as the area of concrete having the same centroid as that of tensile reinforcement, divided by the number of bars

A_1 = Factor for dead loads

A_2 = Factor for live loads

A_f = Area of FRP reinforcement

A_{fp} = Area of post-tensioned FRP reinforcement

$A_{f,ts}$ = Area of shrinkage and temperature FRP reinforcement

A_s = Area of steel reinforcement

b = Web width

c = Distance from extreme compression fiber to the neutral axis

C = Capacity

C_E = Environmental reduction factor

d = Distance from extreme compression fiber to centroid of tension reinforcement

d_c = Thickness of the concrete cover measured from extreme tension fiber to the center of the bar

d_p = Distance from extreme compression fiber to centroid of prestressed reinforcement

D = Dead load

E = Width of the slab

E_c = Modulus of elasticity of concrete

E_f = Guaranteed modulus of elasticity of FRP

E_p = Modulus of elasticity of CFRP

E_s = Guaranteed modulus of elasticity of steel

E_{sl} = Modulus of elasticity of the concrete of the slab

f_c' = Specified compressive strength of concrete

f_f = Stress at service in the FRP

f_{fu} = Design tensile strength of FRP, considering reductions for service environment

f^*_{fu} = Guaranteed tensile strength of an FRP bar

f_{fup} = Design tensile strength of post-tensioned FRP

h = Overall height of the slab

H = Height of the barrier

I = Live load impact

I_{sl} = Moment of inertia of the slab cross section

k_b = Bond-dependant coefficient

ℓ = Slab length

L = Live load

L_1 = Length of the first span of the specimen

L_2 = Length of the second span of the specimen

L_t = Total length of the specimen

M = Flexural moment

M_1 = Flexural moment in $[0;L_1/2]$

M_2 = Flexural moment in $[L_1/2;L_1]$

M_3 = Flexural moment in $[L_1;L_1+ L_2/2]$

M_4 = Flexural moment in $[L_1+ L_2/2;L_t]$

M_{DL} = Moment due to the dead load

M_{LL} = Moment due to the live load

M^{-}_{max} = Maximum negative flexural moment acting on the specimen

M^{+}_{max} = Maximum positive flexural moment acting on the specimen

M_n = Nominal flexural capacity of an FRP reinforced concrete member

M_{pi} = Bending moment to the centroid of the section induced by the post-tensioning of the CFRP bars

M_s = Service moment per unit strip of slab deck

M_u = Factored moment at section

N = Number of bars

N_{pi} = Axial load induced by the post-tensioning of the CFRP bars

P = Concentrated force

P_i = Wheels load

R_1 = Vertical reaction of the first support

R_2 = Vertical reaction of the central support

R_3 = Vertical reaction of the third support

RF = Rating factor

RT = Rating of the bridge

S = Length of the slab

V_1 = Shear in the first part of the specimen

V_2 = Shear in the second part of the specimen

V_3 = Shear in the third part of the specimen

V_4 = Shear in the fourth part of the specimen

V_c = Nominal shear strength provided by concrete with steel flexural reinforcement

$V_{c,f}$ = Nominal shear strength provided by concrete with FRP flexural reinforcement

$V_{\max}^{-}$ = Maximum negative shear acting on the specimen

$V_{\max}^{-}$ = Maximum positive shear acting on the specimen

V_n = Nominal shear strength at section

V_u = Factored shear force at section

w = Crack width

W = Weight of the nominal truck

ω_d = Dead load of the bridge

ω_{LL} = Impact factor

β = Ratio of the distance from the neutral axis to extreme tension fiber to the distance from the neutral axis to the center of tensile reinforcement

β_1 = Factor depending on the concrete strength

β_d = Coefficient given by AASHTO

ε_c = Strain in concrete

ε_f = Strain in FRP reinforcement

ε_{fu} = Design rupture strain of FRP reinforcement

ε^*_{fu} = Guaranteed rupture strain of FRP reinforcement

ε_p = Strain in prestressed CFRP

Δ = Long term deflection

Δ_{LL} = Deflection due to the live load

Δ_{DL} = Deflection due to the dead load

ϕ = Strength reduction factor

λ = Multiplier for additional long-term deflection

ρ_f = FRP reinforcement ratio

ρ_{fb} = FRP reinforcement ratio producing balanced strain conditions

$\rho_{f,ts}$ = Reinforcement ratio for temperature and shrinkage FRP reinforcement

1 INTRODUCTION

1.1 Background

Reinforced and pre-stressed or post-tensioned concrete (RC and PC) structures are facing a worldwide problem—the corrosion of the steel as a result of aging and aggressive environments. Steel corrosion leads to member degradation, endangers structural integrity, and may even cause catastrophic failures. Research has been carried out in an effort to find the solution for this problem. The recent advancements in the field of material science have resulted in the development of new products that can be used in many areas of civil engineering where conventional materials have failed to provide satisfactory service life. Fiber Reinforced Polymers (FRP) have been proposed for use in lieu of steel for RC and PC structures. The promise of FRP materials lies in their strength; light weight; and non-corrosive, non-conducting, and non-magnetic properties. In addition, FRP manufacturing offers a unique opportunity for the development of shapes and forms that would be difficult or impossible with conventional steel materials. FRP can be manufactured in the form of reinforcing bars and tendons for RC and PC structures, sheets, and laminates used for external strengthening of beams, slabs, and masonry walls, wraps, and shells. The materials are then used for confinement of columns.

The interest in the use of FRP composites in PC structures is mainly based on durability issues. Corrosion of steel tendons can cause serious deterioration to infrastructure. Properties such us high tensile strength and high resistance to corrosion make FRP composites good candidates for pre-stressed and post-tensioned tendons.

1.2 Objectives

The scopes of this project can be summarized as follows:

1. Evaluate the feasibility, behavior, and effectiveness of the new deck system; thereby showing how FRP, in the form of GFRP as passive and CFRP bars as active internal reinforcement, could be an excellent solution replacing steel reinforcement.
2. Provide analytical data in support of the enhanced shear capacity of the concrete slab due to the CFRP post-tensioning.

1.3 Description of the project

The City of Rolla in Missouri has made available a bridge (Southview Drive on Carter Creek) to demonstrate the use of FRP bars and tendons in new constructions. One lane of the bridge was already constructed using conventional four-cell steel RC box culvert. It consists of a steel RC slab about 0.25 m (10 in) thick, as depicted in Figure 1. The slab deck is continuous over three intermediate reinforced concrete vertical walls, and the overall length of the bridge is roughly 12 m (40 ft). The new deck was built on three conventional RC walls, the same as

the existing structure. The expansion phase included the removal of the curb from the existing RC deck to allow extending the overall width of the bridge from 3.9 m (12.8 ft) to 11.9 m (39 ft). The curb-to-curb width of the resulting bridge is 9.1 m (30 ft). The two additions consist of a FRP prestressed/reinforced concrete deck and a steel RC deck as shown in Figure 2. The construction of the bridge started on July 2004 and finished in October 2004.

Figure 1 - Views of the Former Bridge

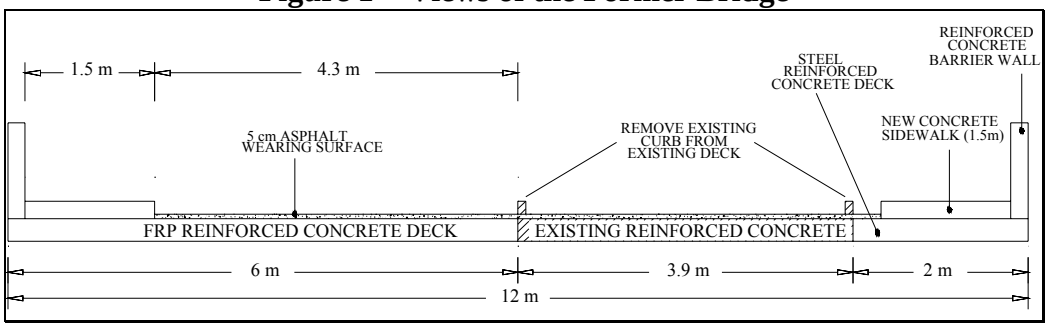

Figure 2 - Cross Section of the Bridge After the Expansion

1.4 Report Outline

This report consists of six sections:

- Section one gives a brief introduction on FRP for bridge applications in civil engineering and introduces the objectives of the research.
- Section two contains information on existing RC and PC FRP bridge decks. It also gives a summary of the main research works on shear behavior of PC FRP structures.
- Section three presents the pre-construction investigations conducted on specimens representing a strip deck 457 mm (18 in) wide and 7 m (23 ft) long, fabricated and tested as continuous slabs over three supports. The testing allowed validating the design calculations both in terms of flexure and shearing capacities.
- Section four focuses on the Southview Bridge design, providing the structural analysis of the new FRP concrete bridge deck based on the AASHTO HS20-44 design truck, and providing calculations for its design.
- Section five details the installation of the Southview Bridge deck, focusing on the post-tensioning of the slab, the most considerable and crucial part of the project.
- Section six gives a brief summary of the steps developed in the previous sections and deepens the results of the research work and installation of the bridge-deck.

2 LITERATURE REVIEW

Only about fifty bridges in the world are using Fiber Reinforced Polymer (FRP) superstructure, as reported by the U.S. Department of Transportation Federal Highway Administration as of July 2002.

The use of FRP bridge decks has been a direct result of technology transfer initiatives lead by the defense industry in late 1980s and early 1990s. In fact, many manufacturers of FRP bridge decks were directly or indirectly related to the aerospace composites industry. Furthermore, in recent years, many state transportation departments, in partnership with the Federal Highway Administration (FHWA), are introducing these new materials to bridge structures with the intention of gaining design and construction experience and long-term performance data on FRP. Thus, FRP deck systems are emerging as a viable alternative to conventional systems, namely RC slabs. Moreover, the research on prestressing with FRP tendons is getting attention mainly because nearly half of the nation's bridges are reported to be in serious disrepair or functionally obsolete.

The use of such systems to replace existing, deteriorated bridge deck systems offers both economic benefits and improved performance. The economic advantages are possible for a number of reasons. Since such composite systems are lighter, considerable savings are realized by reduced transportation costs (*i.e.,* several deck systems can be transported on one truck). Accordingly, erection costs will be less, as relatively light cranes can be used to install the decks. In addition, construction time is reduced, which eliminates long traffic delays. Due to the high resistance of FRP deck systems to environmental effects and corrosion attack, the long-term performance is also expected to improve significantly, leading to lower maintenance and longer service life. In addition to economic advantages, FRP deck systems offer structural advantages as well. For example, higher live loads can be resisted by supporting steel stringers, as the dead load applied by the FRP deck system is about one-fifth of a conventional RC deck.

2.1 Load test

The proposed literature review refers to different topics related to the concrete bridge decks using FRP reinforcement:

- Non-prestressed FRP reinforced bridge decks.
- Prestressed FRP reinforced bridge decks.
- Research works on shear behavior of prestressed FRP.

In this section, some of the main existing internal FRP bridge decks have been presented, so they can be compared with the new deck system that is the subject of this thesis.

Other existing samples are in Appendix A.

2.2 Related Literature Review

2.2.1 Non-Prestressed FRP Reinforced Bridge Decks

2.2.1.1 Bridge Street Bridge, Michigan

The Bridge Street Bridge in Southfield, Michigan, is the first vehicular concrete bridge ever built in the United States that uses CFRP material as the principal structural reinforcement. The project consists of two parallel bridges (Structures A and B) over the Rouge River in the City of Southfield. Both structures use three skewed spans, each over 62 m (204 ft) long, to carry vehicular traffic. Structure A consists of a new substructure as well as a new superstructure and incorporates five equally spaced conventional AASHTO Type III girders in each of its three spans. Its cast-in-place concrete deck slab is placed continuously across the three spans. Structure B consists of four special precast, prestressed, double-tee (DT) girders in each of the three spans configured as simply supported spans. Each DT girder is made of structurally reinforced polymer (CFRP) Leadline^{TM} tendons and post-tensioned carbon fiber composite cable (CFCC)^{TM} strands in both longitudinal and transverse directions. The non-prestressed reinforcement in the girders and deck structure consists of CFCC strands manufactured in bent configurations, straight CFCC reinforcing bars, CFRP NEFMAC^{TM} grid reinforcement, and stainless steel reinforcing bars for stirrups.

The bridge cross section (see Figure 3) consists of four precast DT sections and a minimum 75 mm (3 in) thick, non-continuous deck slab.

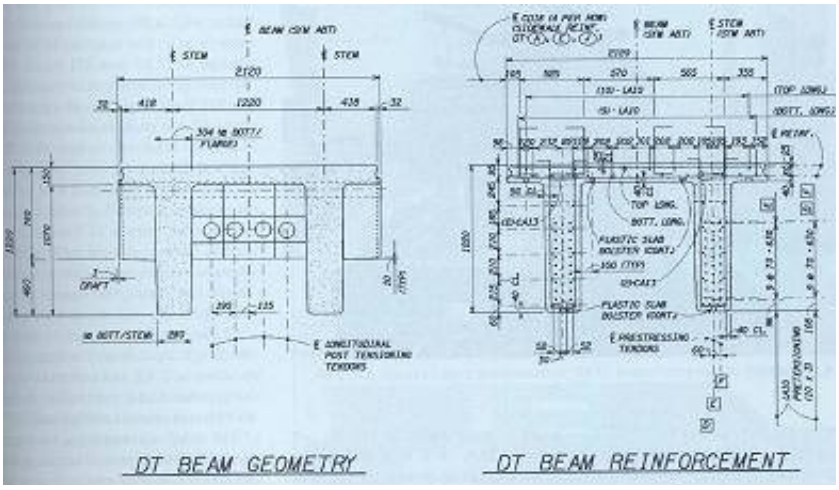

Figure 3 - Cross-sectional Details of Structure B (dim. in SI units)

The composite topping is reinforced with NEFMAC grids. The composite section is also reinforced with four externally draped 40 mm (1.57 in) diameter unbonded CFCC post-tensioning strands.

The transportation of the 12 girders from the precast plant in Windsor, Ontario, to the bridge site in Southfield, Michigan, required a special barging arrangement. The girders were erected using two large capacity cranes at opposite ends of the bridge.

Figure 4 shows the erection of a DT girder for the south span, and Figure 5 shows the installed girders with external post-tensioning strands in place.

Figure 4 - Erection of DT Girders at the Bridge Site

Figure 5 - Installed DT Girders with External CFCC Post-tensioning Strands

The Bridge Street Bridge Deployment Project has served as an extraordinarily successful example of technology transfer from research and development to serviceable structure. The bridge exhibits innovation not only in the material itself, but also in the variety of prestressing methods implemented—pretensioning, post-tensioning, internal, and external.

2.2.2 Prestressed FRP Reinforced Bridge Decks

2.2.2.1 Evaluation of FRP Prestressed Panels/Slabs for I-225/Parker Road Project

Under the Innovative Bridge Research and Construction (IBRC) program of the Federal Highway Administration (FHWA), in 2001 the Colorado Department of Transportation (CDOT) introduced FRP reinforcement in a bridge project at I-225/Parker Road. Precast, prestressed concrete panels were used as stay-in-place forms for a bridge deck. Figure 6 shows the bridge during construction.

Figure 6 - I-225/Parker Road Bridge Under Construction

Some of these panels were prestressed with CFRP tendons and the rest with regular seven-wire steel strands. The primary objective of this project was to demonstrate the feasibility of using CFRP tendons in place of seven-wire steel strands for prestressed concrete panels. It was the first time CFRP bars were used in such fashion. The precast panels were supported on two cast-in-place, post-tensioned concrete box girders (Figure 7 and Figure 8). A topping slab was added to the panels to form a composite bridge deck to carry the traffic.

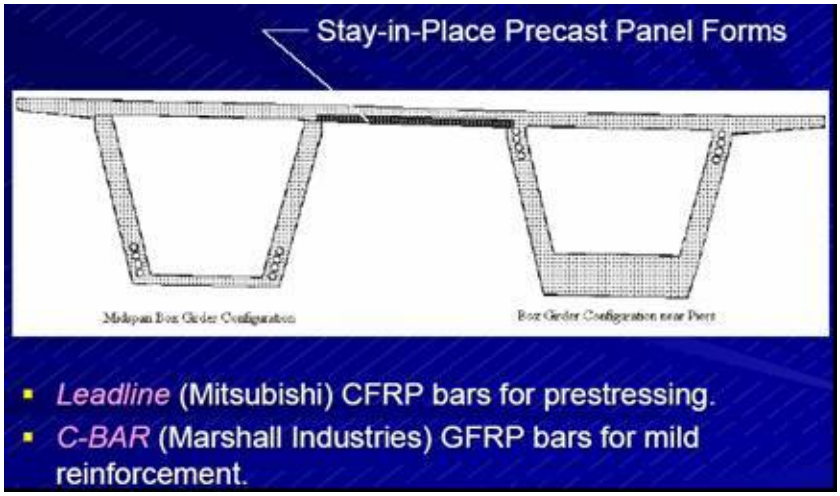

Figure 7 - Installation of Precast Panels

Figure 8 - Precast Panels Supported on Two Box Girders

Furthermore, the applicability of current AASHTO provisions to CFRP prestressed panels was investigated. In addition to the experimental investigation, a new rational design methodology for bridge decks was proposed and investigated (Borlin 2001) in this project. Most highway bridges in the United States have slab-on-girder decks, in which steel or precast concrete girders support a RC slab. The two components are tied together with shear connectors to allow for composite action. The main reinforcement in the deck slabs is placed perpendicular to the direction of traffic. For these decks, both the AASHTO Standard Specifications for Highway Bridges (AASHTO 1996) and the conventional method in the AASHTO LRFD Bridge Design Specifications (AASHTO 1998) resulted in two dense reinforcement mats, one in the top of the slab and one in the bottom (Figure 9 and Figure 10).

Figure 9 - Top Reinforcement

Figure 10 - Cast-in-Place Portion of the Deck

Pullout tests conducted in this study showed that Leadline CFRP prestressing tendons and C-BAR GFRP reinforcing bars had higher bond strengths than seven-wire steel strands and regular steel reinforcing bars, respectively.

Load tests were first performed on two panels, one prestressed and reinforced with FRP and the other prestressed and reinforced with steel. Both panels were designed to barely satisfy the AASHTO specifications. An additional panel that was prestressed and reinforced with FRP and brought from the I-225/Parker Road project was tested as well. This panel was conservatively designed with a significant reserve capacity compared to the first two. Load tests were also performed on steel and FRP prestressed panels that had a 125 mm (5 in.) composite topping slab (see Figure 11 and Figure 12). All test results showed the feasibility of using CFRP tendons for prestressing and GFRP bars for temperature and distribution reinforcement in precast bridge panel construction. The GFRP reinforcement was selected according to the recommendation for temperature reinforcement in the ACI 440H draft report. Load distribution data were taken during the composite slab tests to validate the adequacy of the Equivalent Width Strip method used in AASHTO LRFD Specifications. The method was found to be conservative for both steel and FRP reinforced composite slabs.

However, results showed that the steel reinforced slab better distributed the loading in the transverse direction than the FRP reinforced slab. This suggests that the recommendation for temperature reinforcement in the ACI 440H draft report may not be adequate for distribution reinforcement.

Figure 11 - Panel and Anchorage Details

Figure 12 - Construction of the Panels

2.2.3 Research works on Shear Behavior of Prestressed FRP

The majority of research on concrete structures using FRP reinforcement has been on members that are not critical in shear tests. At present, the shear behavior of prestressed concrete members using FRP reinforcement is not well understood. Unlike flexural behavior, shear behavior is quite complex itself, even in ordinary reinforced or prestressed concrete members.

Structures are usually conservatively designed and rely on plasticity theory for safety. This design ensures that if a set of internal forces exists that is in

equilibrium with the applied load and since steel is known to be ductile, the lower bound (or 'Safe Load') theorem can be used to assert that the structure is safe.

When advanced composites are used, however, the theoretical justification is much less sound; many of the basic assumptions no longer hold. Composites are generally less stiff than steel, so when the concrete cracks, a composite is carrying less force than steel would be. Cracks will be wider, so less concrete-concrete interaction will occur across the crack; thus, less 'aggregate interlock' will occur. Composites also delaminate when placed across shear cracks, so 'dowel action' will be lower, and some problems will be caused by the bends in the bars.

Finally, and most importantly, although composites have high strain capacities, they do not behave plastically, so the Safe Load theorem cannot be used to hide the lack of knowledge about the deflections.

Taken together, these results mean that care must be taken when producing design guidelines for shear in compositely reinforced structures. Clearly, much work needs to be done in this field; a model is needed that satisfies all three of the basic principles of structural mechanics—equilibrium, compatibility, and the material stress-strain behavior (C.J. Burgoyne, August 2001).

Here a summary of the main research works on this topic is given.

2.2.3.1 S.Y. Park and A.E. Naaman (1999)

The authors conducted an experimental program on two series of tests (two sets of beams). The first series comprised nine prestressed concrete beams fabricated without stirrups. Five beams were prestressed using CFRP tendons, and for comparison, four beams were prestressed using conventional steel tendons.

The main objective of this first series of tests was to experimentally confirm the shear-tendon rupture failure mode in prestressed concrete beams with FRP tendons and to compare it with other failure modes in prestressed concrete beams with steel tendons.

The second series of the experimental program comprised 7 FRP prestressed concrete beams and 1 non-prestressed concrete beam shear reinforced with steel stirrups (7 beams) or steel fibers (1 beam). The test parameters were the pretensioning ratio, the shear span-to-depth ratio, shear reinforcement ratio, the use of steel fibers, the compressive strength of concrete, and the type of reinforcement.

The main goal of the second series was to evaluate the parameters affecting the shear strength and ductility of concrete beams prestressed with FRP tendons.

On the basis of this experimental investigation, the following conclusions were drawn:

1. The shear-tendon rupture failure is a unique mode of failure, which, unless properly designed for, is likely to occur in concrete beams prestressed with FRP tendons. This premature failure is due to tendon rupture by dowel shear at the shear-cracking plane. The failure is attributed to the poor resistance of FRP tendons in the transverse direction and their brittle behavior.

2. The ultimate shear resisting capacity of beams prestressed with FRP tendons was about 15 percent less than that of beams prestressed with steel tendons, regardless of shear failure mode.
3. The shear-tendon rupture failure occurred at the flexural shear-cracking plane in beams with FRP tendons, even when the effective prestress ratio was low (about 40 percent), and the required amount of steel stirrups was provided according to the ACI Code.
4. Adding steel fibers is a possible way to improve the shear resistance of concrete beams prestressed with FRP tendons by avoiding or delaying shear-tendon rupture failure.
5. Differences in the properties of FRP and steel tendons appear to have no significant effect on the initial portion of load-deflection response of prestressed concrete beams subjected to a center point loading with a shear span-to-depth ratio of 2.5.
6. The ultimate shear displacement and crack width of prestressed beams that failed by shear-tendon rupture were about one-third and one-half, respectively, of those of similar beams with steel tendons.
7. The following observations were made for beams prestressed with FRP tendons:
    - Increasing the shear span-to-depth ratio from 1.5 to 3.5 led to a decrease in shear resistance but an increase in shear ductility (displacement).
    - Adding stirrups in sufficient quantity changes the failure mode from shear-tension to shear-tendon rupture in beams with a low effective prestress ratio of about 40 percent.
    - Increasing the compressive strength of concrete slightly increases the shear strength and considerably increases the corresponding deflection.

2.2.3.2 P.A. Whitehead and T.J. Ibell (Jan. 2004)

The authors developed a model incorporating force equilibrium and compatibility of strains, so the elastic properties of FRP could be included rationally.

Fifteen specimens from the experimental program and four case-study specimens (all of which failed in shear) were used to assess the accuracy of predictions from the most prevalent codes and design guides currently in use in the UK and the US, namely BS8110 (1997), BD44 (1995), EC2 (1992), and ACI-440.1R-03 (2003). ACI-440.1R-03 is specifically intended for FRP-reinforced concrete. However, predictions obtained using modified versions of the other three standard codes were also provided. These modifications were termed the Strain Approach and the Sheffield Approach (Guadagnini et al., 2001).

The following conclusions were drawn:

1. The analytical shear predictions developed by the authors predicted the experimental results with a better accuracy when compared to the existing building codes.
2. Using either the Strain or Sheffield modification suggestions in tandem with BS8110, BD44, and EC2 results in reasonable predictions for all the

reinforced (AFRP and GFRP) specimen capacities. ACI-440.1R-03 provides more conservative predictions for the FRP-reinforced specimens.
3. The presence of prestress was found to be significant in increasing shear capacity of such specimens, due to the significant crack-closing influence of the prestress. The unfactored code evaluations are more conservative for the prestressed specimens, implying that the presence of prestress aids the FRP-reinforced concrete beams to a greater extent than it does steel-reinforced concrete.

2.2.3.3 P. A. Whitehead and T. J. Ibell (Feb. 2004)

A novel FRP shear reinforcement strategy, in which both the concrete and FRP are employed to maximum advantage, was conceived by the authors.

They presented the findings of research conducted into the shear behavior of FRP-reinforced and prestressed concrete beams containing continuous FRP helical transverse reinforcement. Twelve tests were conducted on ordinarily reinforced beams and fifteen on FRP-prestressed concrete beams.

Tests on FRP-reinforced concrete beams were conducted initially, thereby allowing rapid assessment of the influence of various shear reinforcement strategies, which could later be investigated under prestressed conditions. Accordingly, the more effective forms of shear reinforcement were taken forward and re-examined under prestressed conditions while the non-responsive forms were discarded. Furthermore, to make direct comparisons between FRP-reinforced and prestressed beams, the effective depth was kept the same for both sets of tests.

Ibell and Burgoyne suggested that geometry and bond (including the locality of bond) are of paramount importance in the performance of FRP shear reinforcement. Therefore, to examine these aspects, the following FRP shear reinforcement strategies were employed within the FRP-reinforced and prestressed rectangular concrete beams:

1. Circular helix, fully bonded or entirely unbonded, placed along the top of the beam within the flexural compression zone (see Figure 13-a).
2. Circular helix, fully bonded or entirely unbonded, angled in the shear zones, following the lines of principal compression (see Figure 13-b).
3. Continuous rectangular draped helix, fully bonded, intermittently bonded or entirely unbonded, placed over the full depth of the section (see Figure 13-c).
4. Two interlocking rectangular draped helices, entirely unbonded, placed over the full depth of the section (see Figure 13-d).

The following conclusions were made regarding shear behavior:

1. The presence of prestress was significant in increasing shear capacity of such specimens.
2. When used to resist shear, fully unbonded circular and rectangular helices had to be spaced at a closer pitch in comparison with fully bonded or intermittently bonded rectangular helices to provide a similar increase in failure capacity. The fully unbonded rectangular helices appeared to have

been about 50 percent as effective as fully or intermittently bonded rectangular helices in resisting shear.

3. Of the arrangements considered, the best technically seemed to involve the use of a fully bonded circular helix and a fully bonded rectangular helix in the constant-moment region, coupled with an intermittently bonded rectangular helix in the shear zones. This configuration led to considerable deformability and ductility and produced high shear capacity and genuine plastic-based ductility during shear collapse.
4. FRP reinforcement need not simply be treated as a direct substitute for steel reinforcement, but rather its inherent advantages should be exploited using rational design approaches.

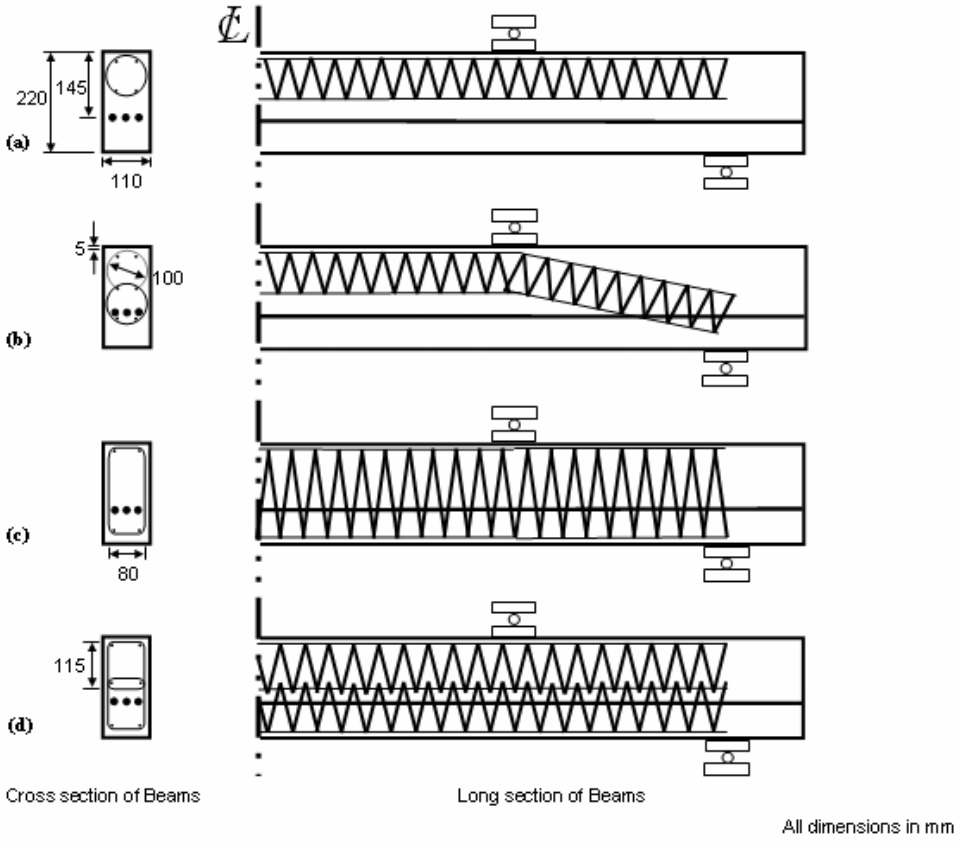

Figure 13 - Cross-Sectional Dimensions and Helical Reinforcement Shapes for (a) Specimens containing a circular helix placed along the top of the beam, (b) Specimens containing a circular helix angled in the shear zone, (c) Specimens containing a continuous draped rectangular helix, and (d) A specimen containing two interlocking rectangular helices

3 EXPERIMENTAL PROGRAM

This section presents the pre-construction investigations conducted on two specimens representing a deck strip 457 mm (18 in.) wide, 254 mm (10 in.) deep, and 7 m (23 ft) long, fabricated and tested. The specimens were constructed by the contractor peculiar for the project allowing for his familiarization with the use of non-conventional materials. The testing of the specimens as continuous slabs over three supports validated the design calculations in terms of flexure and shear capacities.

3.1 Specimens Layout

Two specimens having the same geometry and amount of reinforcement were built and tested, one to investigate the flexural behavior, the other one the shear behavior. The specimens were reinforced using 3 ϕ19 (6/8 in) GFRP bars as top and bottom mat and 2 ϕ9 (3/8 in) CFRP bars as prestressed tendons. The position of the prestressed tendons was varied along the slab to match the moment demand. In addition, to reproduce the actual field conditions, ϕ13 (4/8 in) GFRP bars spaced 305 mm (12 in) on center were placed in the transversal direction as temperature and shrinkage reinforcement. Figure 14 shows a detailed layout of the reinforcement, while Figure 15 shows the position of the CFRP tendons.

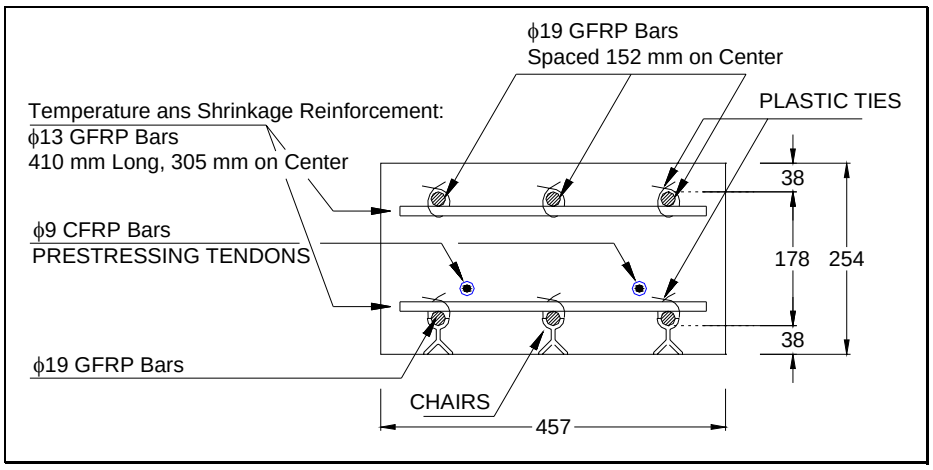

Figure 14 - Reinforcement Layout (all dimensions in mm)

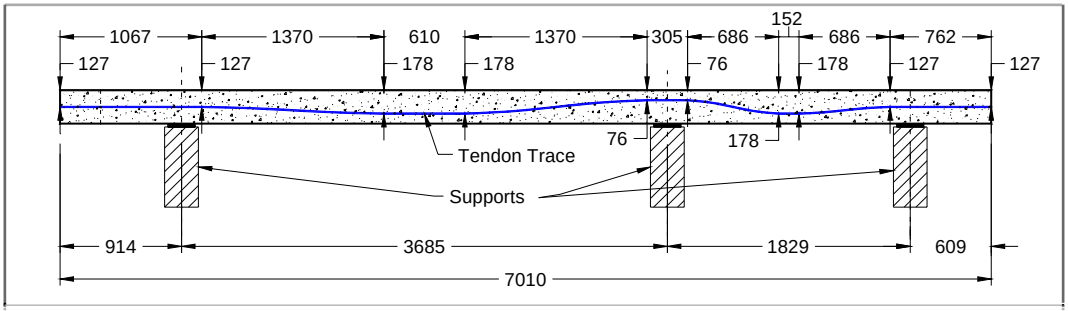

Figure 15 - CFRP Tendons Trace (all dimensions in mm)

3.2 Material Properties

Tests were performed to characterize the mechanical properties of the materials used in this investigation.

The designed concrete compressive strength was equal to 41.4 MPa (6000 psi). Water to cement ratio for the concrete mixture was 0.45. The components in the concrete mixture were proportioned by weight as follows: 19 percent portland cement, 40 percent crushed limestone, 33 percent sand, and 8 percent water.

The actual compressive strength of the concrete was checked on three 100 x 200 mm (4 x 8 in) cylinders per slab. The cylinders were tested in compliance with ASTM C39/C39M. The average compressive strength at the time of the test was found equal to 48.6 MPa (7040 psi) and 45.4 MPa (6585 psi) for the flexural and shear specimens, respectively.

The compressive strength of the high performance cementitious grout was determined on 3 cylinders 100 x 200 mm (4 x 8 in), and it was found to be 21.7 MPa (3150 psi) after 1 day, 36.5 MPa (5300 psi) after 3 days, 49.3 MPa (7150 psi) after 7 days, and 58.9 MPa (8550 psi) after 28 days. In addition, splitting tensile tests in compliance with ASTM C496 were performed on the same type of cylinders (three repetitions). The splitting tensile strength was found to be 1.5 MPa (218 psi) after 1 day, 2.8 MPa (406 psi) after 3 days, 3.58 MPa (520 psi) after 7 days, and 5.59 MPa (810 psi) after 28 days.

Tensile tests were performed on FRP bars to determine their mechanical properties related to fiber content. The average tensile strength, ultimate strain, and modulus of elasticity obtained from the testing of the specimens (ASTM D3039) are presented in Table 1.

Table 1 - Mechanical Properties of FRP Bars

Bar Type	Nominal Diameter of the Bar mm (in)	Average Max. Strain %	Average Max. Stress MPa (ksi)	Average Elastic Modulus GPa (ksi)
GFRP Bar	12.7 (0.5)	1.68	689.5 (100.0)	40.80 (5920)
GFRP Bar	19.1 (0.75)	1.52	620.5 (90.0)	40.80 (5920)
CFRP Bar	9.5 (0.375)	1.67	2124.2 (308.1)	142.7 (20702)

3.3 Specimens Design

The theoretical moment and shear capacities have been computed according to ACI 440.1R-03 provisions. As an alternative method to compute the shear capacity of the specimens, the equation developed by Tureyen A. K. and Frosh R. J. and now under consideration for adoption by ACI Committee 440, was used.

According to ACI 440.1R-03, the nominal flexural capacity of an FRP reinforced concrete member can be computed as shown in Equation 3.1:

$$M_n = A_f f_{fu}(d - \frac{\beta_1 c}{2}) + A_{fp} f_{fup}(d_p - \frac{\beta_1 c}{2}) \quad \text{Equation Section 3}(3.1)$$

where

A_f = area of FRP reinforcement

f_{fu} = design tensile strength of FRP, considering reductions for service environment

d = distance from extreme compression fiber to centroid of tension reinforcement

β_1 = factor depending on the concrete strength, $f_c^{'}$, equal to 0.75 for $f_c^{'}$ = 41.4 MPa (6000 psi)

c = distance from extreme compression fiber to the neutral axis

The second term symbols represent the same factors but refer to the prestressed reinforcement.

The theoretical moment capacity is 97.9 kN-m (72.2 kip-ft). If no post-tensioning is provided, the corresponding moment capacity would be just the same, being the strain in the GFRP controlling.

According to ACI 440.1R-03, the concrete shear capacity $V_{c,f}$ of flexural members using FRP as main reinforcement can be evaluated as shown below in Equation 3.2. The proposed equation accounts for the axial stiffness of the FRP reinforcement (A_fE_f) as compared to that of the steel reinforcement (A_sE_s).

$$V_{c,f} = \frac{A_f E_f}{A_s E_s} V_c \qquad (3.2)$$

V_c as computed in Equation 3.3 is the nominal shear strength provided by concrete with steel flexural reinforcement for members with effective prestress force not less than 40 percent of the tensile strength of flexural reinforcement, according to ACI 318R-99:

$$V_c = (0.6\sqrt{f_c^{'}} + 700\frac{V_u d_p}{M_u})bd_p \qquad (3.3)$$

where

$f_c^{'}$ = specified compressive strength of concrete

V_u = factored shear force at section

d_p = distance from extreme compression fiber to centroid of prestressed reinforcement (but needs to be not less than 0.80h for circular sections and prestressed members)

M_u = factored moment at section

b = web width

When assuming the C_E (environmental reduction factor) equal to 1, the theoretical shear capacity will be 69.8 kN (15.7 kip).

According to Tureyen A. K. and Frosh R. J., the shear capacity can be derived from the following Equation 3.4:

$$V_{c,f} = 5\sqrt{f_c^{`}}bc \qquad (3.4)$$

where

c = the position of the neutral axis at the service conditions

b = the width of the specimens

$f_c^{`}$ = compressive strength of the concrete

The shear capacity computed according to this approach is 97.4 kN (21.9 kip).

Indeed, using the neutral axis at the service conditions may not be correct when the member is approaching its flexural capacity; hence, assuming c corresponding to the ultimate conditions of the section, the shear capacity will be 54.7 kN (12.3 kip).

The prestressing was primarily used to increase the shear capacity of the slabs rather than the flexural one. In fact, the shear capacity of the slabs without any prestressing load would have been 30.7 kN (6.9 kip) using ACI and 33.8 kN (7.6 kip) using Tureyen A. K. and Frosh R. J., while the post-tensioned load would have been 69.8 kN and 97.4 kN, respectively. As for flexure, since the failure mode is controlled by the rupture of the mild reinforcement, the post-tensioning does not influence the moment capacity, but the shear more than doubles.

3.4 Specimens Preparation

The specimens were built in the way to reproduce the same characteristics of the bridge deck that would be constructed in the field.

The CFRP tendons were housed inside a plastic duct to allow the post-tensioning operations. Plastic T joints were used to connect the duct housing the tendons with the duct going out of the specimen to inject the grout.

Plastic chairs and ties were used to lay the bars and the tendons to have a completely “steel free” structure, in compliance with the requirements of the Southview bridge project. Figure 16 shows the cage details of both specimens.

Figure 16 - Cage Detail

A total of 21 Electrical Strain Gages (ESG) were used to monitor the strain at the most critical sections. They were placed on each GFRP bar (see Figure 17) and on the compressive face of the slab. Figure 18 shows the two specimens ready for pouring.

Figure 17 - Strain Gages Detail

Figure 18 - Reinforcement Cages

The prestressing of the tendons was executed 28 days after the pouring of the concrete. Figure 19 and Figure 20 show the specimens while curing and after the removal of the formwork, respectively.

Figure 19 - Specimen Curing

Figure 20 - Specimens after Removal of the Formwork

The CFRP bars were prestressed by applying a force of 98 kN (22 kip) using hydraulic jacks at both ends. This level of prestressing corresponds to 65 percent of the ultimate capacity of the CFRP bars. Such pre-stressing level was chosen to respect, after the initial strain losses (supposed to be 35 percent of the initial strain of prestress reinforcement), the creep rupture limits dictated for GFRP bars according to ACI 440.1R-03 (*0.20* times the ultimate guaranteed tensile strength for prestress CFRP reinforcement), as underlined in the next section.

Initially the prestressing load was applied only to one end of the slab, causing the breaking of the FRP tendons from the high eccentricity of the active reinforcement and the friction between ductwork and tendons. This problem was solved by applying the prestressing load in steps of 31 kN (7 kip) from both ends by means of two hydraulic jacks (See Figure 21). The prestressing load was monitored using two load cells, one for each end of the slab, while the strain was measured using two electrical strain gages attached on the bar. This solution was suitable because the increased losses after the release of the tendons induced by the new pre-stressing system (30 percent) were less than the ones assumed for design (35 percent).

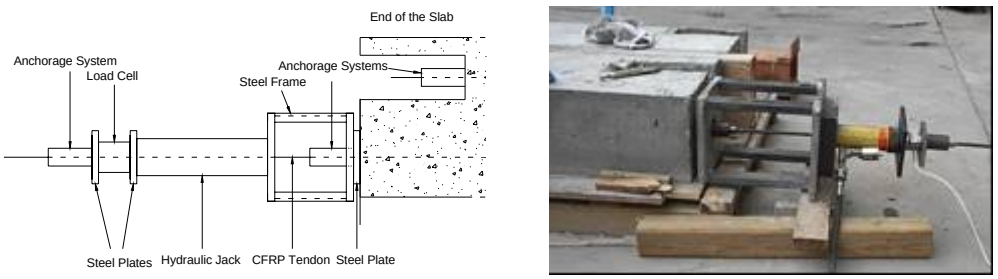

a) System Detail *b) Field Assembly*

Figure 21 - Prestressing System

The steel wedge anchorage system used to anchor the CFRP bar and to react against the hydraulic jack was a resin-free, three-part system developed at the University of Waterloo, Canada. It included an outer steel cylinder, a four-piece wedge, and an inner sleeve (see Figure 22). The inner sleeve was made out of copper/steel and it was deformable. The four-piece wedge was placed evenly around the inner sleeve and inserted into the outer steel cylinder. The anchorage system was later secured by tapping the inner sleeve and four-piece wedge into the outer steel cylinder with a hammer.

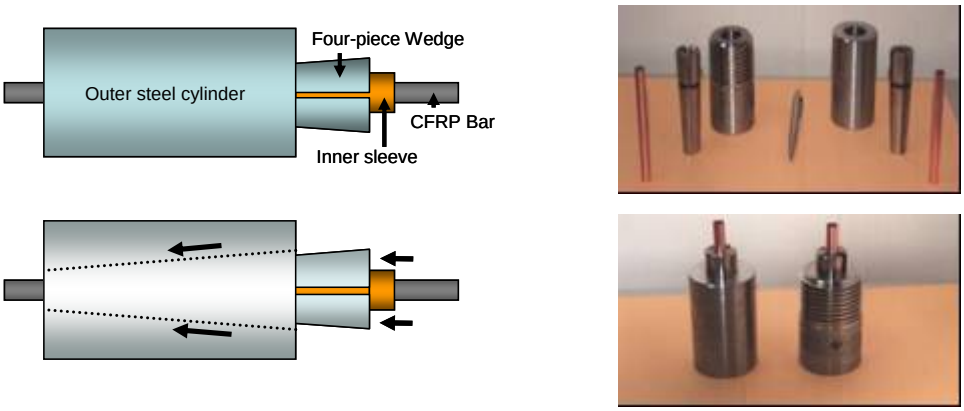

Figure 22 - Steel Wedge Anchorage System

The prestressing of the CFRP bars was followed by grouting using a high performance cementitious grout. The cementitious grout was allowed to cure for seven days after which the anchoring of the tendons was removed by drilling the CFRP bar inside the barrel (see Figure 23). The strain in the slab was monitored during and for 48 hours after the cutting of the anchoring system. During this time no loss of compressive strain in the specimens was recorded.

Figure 23 - Drilling of CFRP Bar after Grout Curing

3.5 Test Setup

Each slab was tested as a continuous member on three supports, comprising of 3.6 m (12 ft) and 1.8 m (6 ft) spans. The positions of the two loading points were chosen to force flexural and shear failure for the flexural and shear specimens, respectively.

The slabs were placed at the mid-span for the flexural specimen (see Figure 24).

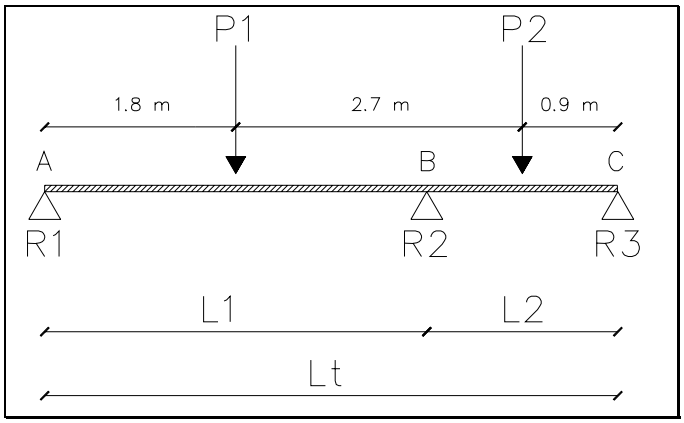

Figure 24 - Static Scheme for the Flexural Specimen

Given the following:

$L_1 = 3.6m\,(12\,ft)$ Length of the first span

$L_2 = 1.8m\,(6\,ft)$ Length of the second span

$P_1 = 165kN(37kip)$ First live load

$P_2 = 100kN(23kip)$ Second live load (higher than the theoretic value)

By solving the hyperstatic scheme (see Figure 25), one can derive the flexural moment acting on the central support (assigned as hyperstatic unknown).

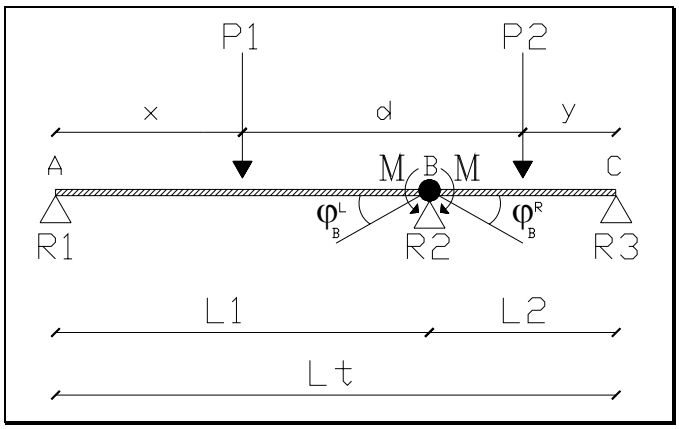

Figure 25 - Hyperstatic Scheme

$$\varphi_B{}^L = \varphi_B{}^R$$

$$M = -\frac{3}{16} * \frac{(P_1 * L_1^2 + P_2 * L_2^2)}{L_1 + L_2} \quad (3.5)$$

Hence, the reactions of each support can be derived by the following equations:

$$R_1 = \frac{P_1}{2} - \frac{M}{L_1} = 13.2kip \quad (3.6)$$

$$R_2 = \frac{P_1}{2} + \frac{M}{L_1} + \frac{P_2}{2} + \frac{M}{L_2} = 46kip \quad (3.7)$$

$$R_3 = \frac{P_2}{2} - \frac{M}{L_2} = 0.8kip \quad (3.8)$$

Finally, the equation of flexural moment and its plot (see Figure 26) depending on z can be derived:

$$M_1(z) = R_1 * z \quad (3.9) \quad \text{when} \quad z \in \left[0; \frac{L_1}{2}\right]$$

$$M_2(z) = M_1(z) - P_1 * (z - x) \quad (3.10) \quad \text{when} \quad z \in \left[\frac{L_1}{2}; L_1\right]$$

$$M_3(z) = M_2(z) + R_2 * (z - L_1) \quad (3.11) \quad \text{when} \quad z \in \left[L_1; L_1 + \frac{L_2}{2}\right]$$

$$M_4(z) = M_3(z) - P_2 * [z - (L_t - y)] \quad (3.12) \quad \text{when} \quad z \in \left[L_1 + \frac{L_2}{2}; L_t\right]$$

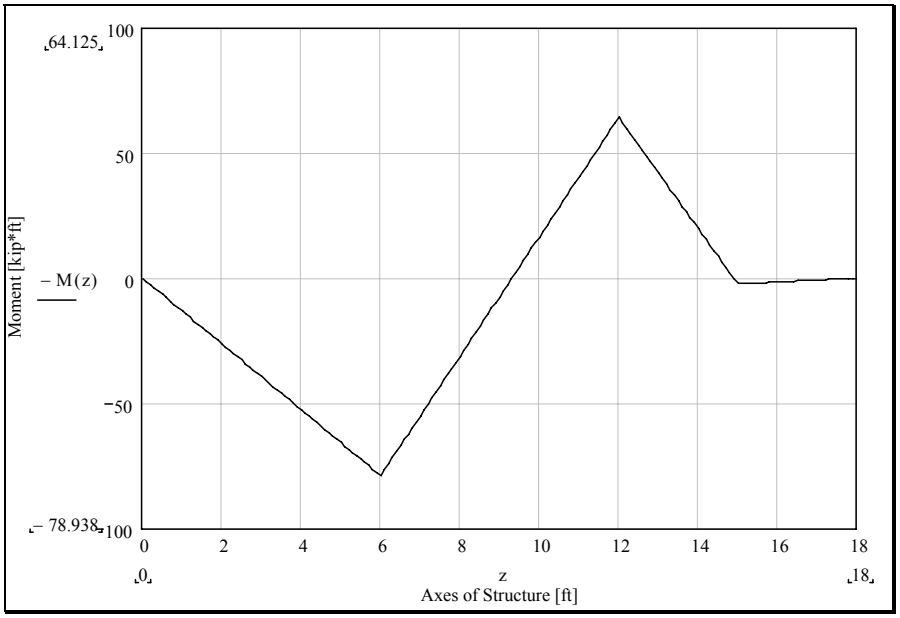

Figure 26 - Flexural Plot

$M^{-}_{\max}(z) = -86.9kN*m(-64.1kip*ft)$

$M^{+}_{\max}(z) = 107kN*m(78.9kip*ft)$

Regarding the shear test, the loading points were placed 0.9 m (3 ft) away from the central support, and the distance was determined by performing the following calculations (See Figure 27):

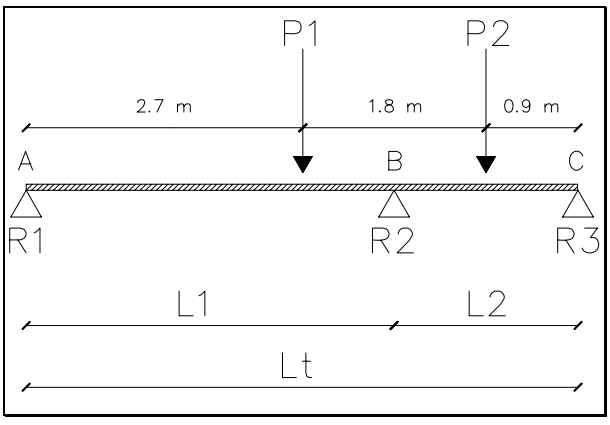

Figure 27 - Static Scheme for the Shear Specimen

According to the same procedure used to solve the flexural scheme and given the following:

$P_1 = 222kN(50kip)$ First live load

$P_2 = 222kN(50kip)$ Second live load

the shear equations depending on z and the corresponding plot (see Figure 28) were derived:

$V_1 = R_1$ (3.13) when $z \in [0; 2.7m]$

$V_2 = V_1 - P_1$ (3.14) when $z \in [2.7m, L_1]$

$V_3 = V_2 + R_2$ (3.15) when $z \in [L_1; L_1 + 0.9m]$

$V_4 = V_3 - P_2$ (3.16) when $z \in [L_1 + 0.9m, L_t]$

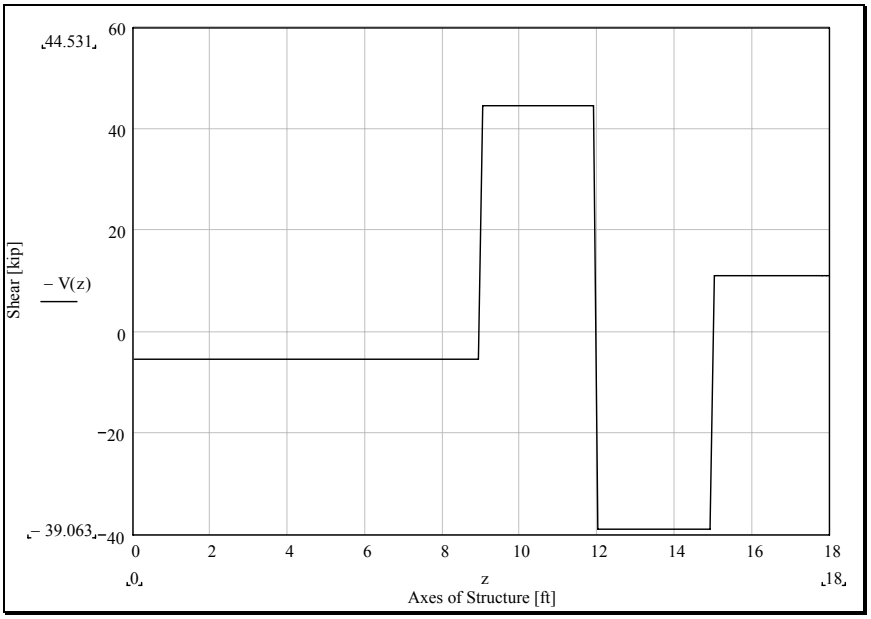

Figure 28 - Shear Plot

$V_{\max}^{-}(z) = -198kN(-44.5kip)$

$V_{\max}^{+}(z) = 173.5kN(39kip)$

The load was applied in cycles of loading and unloading. An initial cycle for a low load was performed on each specimen to verify that both the mechanical and electronic equipment was working properly.

Loads were applied to 102 x 457 x 25 mm (4 x 18 x 1 in) steel plates resisting on the slab to prevent the structure from touching the edge of the support in the case of large deflections (see Figure 29).

The flexural specimen (See Figure 30 –a) was instrumented using three load cells. Two of them were placed under the loading points while the third one was placed under one of the supports to determine the end reaction, and therefore, the actual distribution of moments in the slab.

Figure 29 - Steel Plate Detail

The loads were applied by means of 30 ton (66 kip) hydraulic jacks reacting against a steel frame. The loading rate was the same for the two spans until reaching 85 kN (19 kip). After that, the load in the shorter span was kept constant while the one in the longer span was increased up to failure. This solution was adopted to avoid shear failure at the central support. Linear Variable Displacement Transducers (LVDTs) were positioned at the loading points (two for each loading point) and at the supports to record maximum displacements and support settlements. The strain gages were placed on each GFRP bar at the location of the loading points and of the central support. In addition, at the same locations, an additional strain gage was attached on the compressive face of the slab to have an additional backup point while determining the experimental moment-curvature response of the slab.

For the shear specimen, the number of load cells was reduced to two. The loads were applied to 102 x 457 x 25 mm (4 x 18 x 1 in) steel plates using a 100 ton (220 kip) hydraulic jack (see Figure 30 –b). Two additional LVDTs were inserted to measure also the maximum displacement, which in this case, was not at the loading points.

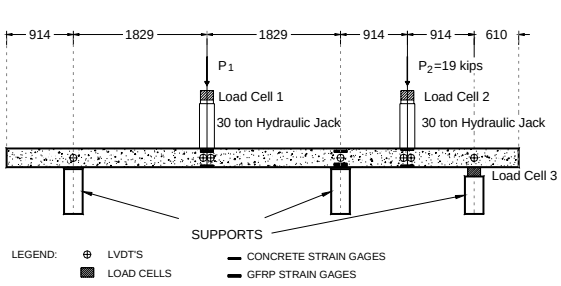

a) Test Setup to Determine the Flexural Capacity

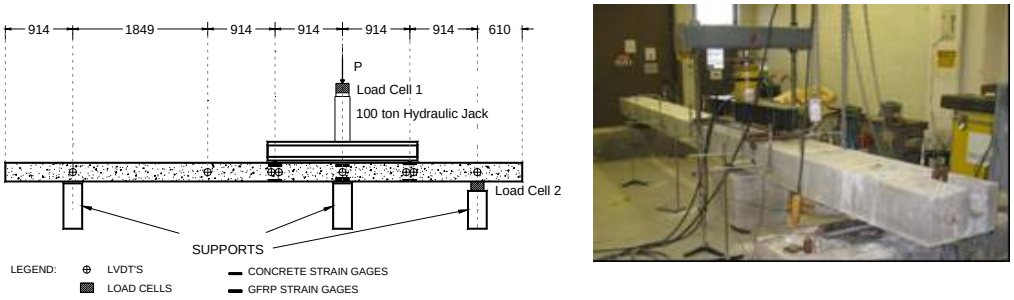

b) Test Setup to Determine the Shear Capacity

Figure 30 - Test Setup (all dimensions in mm)

3.6 Test Results and Discussion

3.6.1 Failure Modes

For the "flexural" specimen, the first flexural crack was observed on the longer span when the load was approximately 66 kN (15 kip) on both spans. As the loads were increased, some of the cracks started to extend diagonally to form shear cracks (see Figure 31).

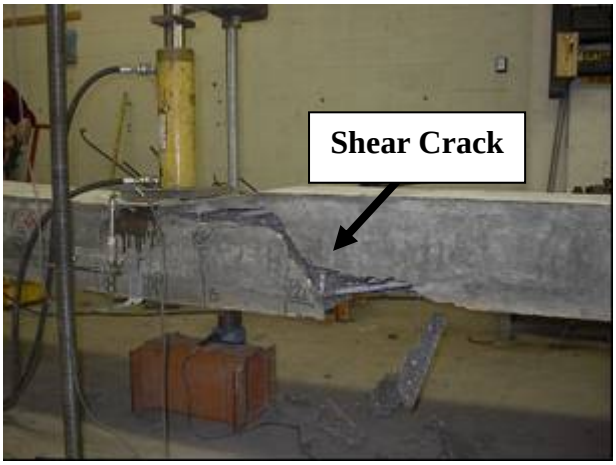

Figure 31 - Shear Cracks on the Flexure Specimen

The maximum forces, 163 kN (37 kip) and 100 kN (23 kip) on long and short spans, respectively, represented the maximum load-determining concrete crushing on the top of the longer span, indicating brittle flexural failure (see Figure 32).

Figure 32 - Concrete Crushing in the Compressive Zone

This crushing was immediately followed by a sudden shear failure, which also caused the rupture of the CFRP bars due to kinking (see Figure 33).

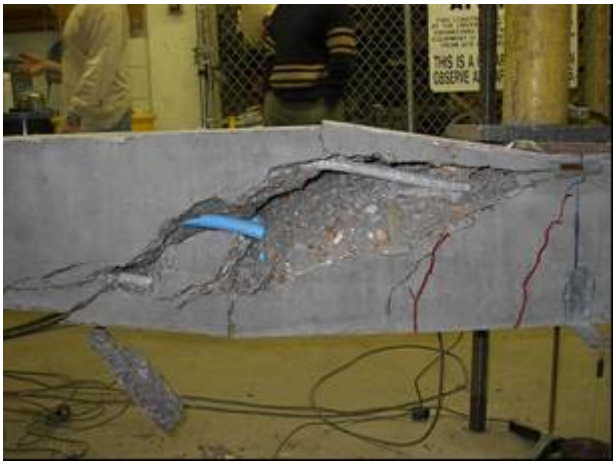

Figure 33 - CFRP Bars Rupture Due to Kinking

Regarding the "shear" specimen, the first crack was observed at a load of approximately 89 kN (20 kip) in correspondence with the central support where the moment was maximum (see Figure 34). As the load was increased, the newly formed cracks between the central support and the loading point on the central span started to extend diagonally to form a shear crack. The failure of the specimen occurred for an applied load equal to 273 kN (61 kip) due to diagonal tension shear.

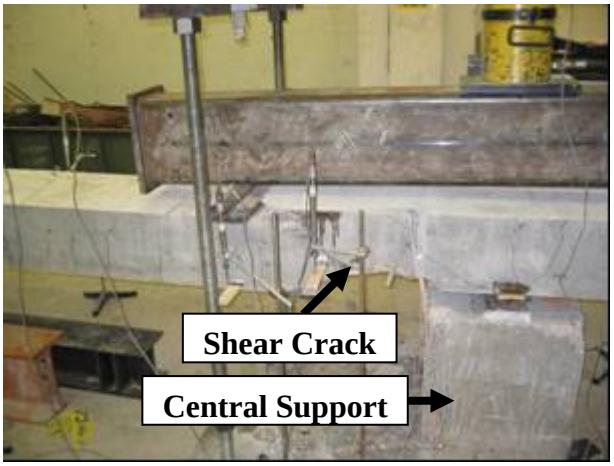

Figure 34 - Failure in the Shear Specimen

3.6.2 Discussion of Test Results

Table 2 compares the experimental results with the theoretical moment and shear capacities of the slabs computed according to ACI 440 provisions and to the equation developed by Tureyen A. K. and Frosh R. J.

Table 2 – Comparison Experimental Theoretical Results

Specimen	Experimental		Theoretical			
	Maximum Bending Moment kN-m (kip-ft)	Maximum Shear Force kN (kip)	Moment Capacity kN-m (kip-ft)	Shear Capacity[1] kN (kip)	Shear Capacity [2] kN (kip)	Shear Capacity[3] kN (kip)
Flexure	101.87 (73.7)	99.7 (22.4)	97.9 (72.2)	69.8 (15.7)	97.4 (21.9)	54.7 (12.3)
Shear	70.2 (51.8)	142.3 (32.0)				

[1] Computed according to ACI 440 provisions

[2] Computed according to Tureyen A. K. and Frosh R. J.

[3] Computed with a modified Tureyen A. K. and Frosh R. J. considering c at ultimate

Table 2 shows that for the flexural specimen, the experimental shear results largely overcame the theoretical shear capacities of the specimen when calculated according to ACI 440. For the same specimen, the Tureyen A. K. and Frosh R. J. approach overestimated the shear capacity when using the neutral axis at the service conditions. By removing such assumption and taking *c* corresponding to the ultimate conditions of the section, a more conservative approach can be attained as shown in the last column of Table 2.

The shear specimen presented a shear capacity larger than the theoretical, demonstrating again the safe approach of ACI 440. For this specimen, the maximum theoretical bending moment determined from the Tureyen A. K. and

Frosh R. J. approach was only half of the ultimate moment capacity found by the experimental test.

Figure 35 shows the different trend of measured moment compared to the theoretical one derived by solving the hyperstatic sheme (worked out in the

Test Setup), both related to the central support reaction, R_2.

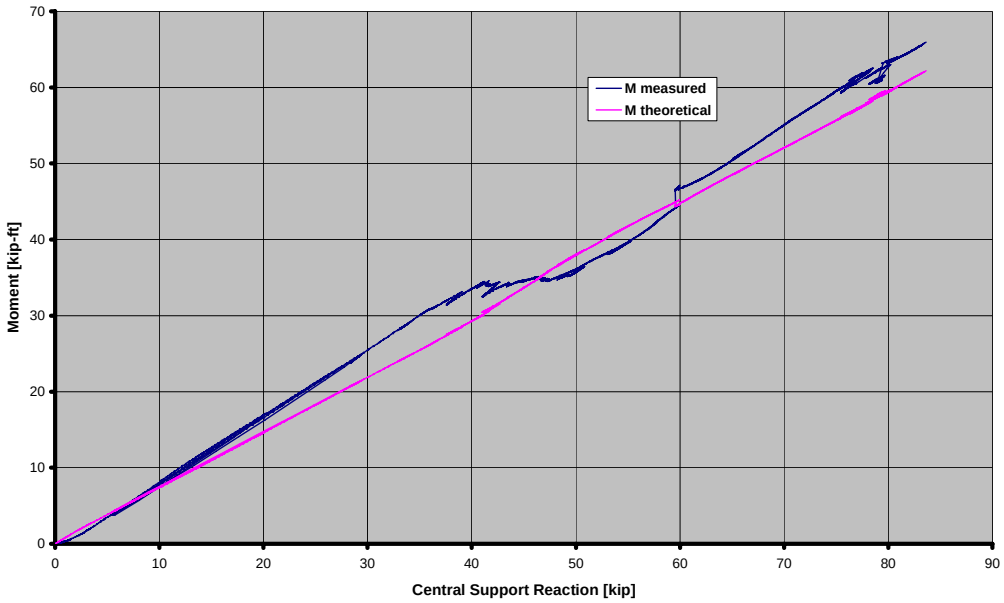

Figure 35 - $M_{measured}$ Vs. $M_{theoretical}$

Figure 36 shows the load deflection diagram. The change of slope in the diagram corresponds to the cracking of the specimen.

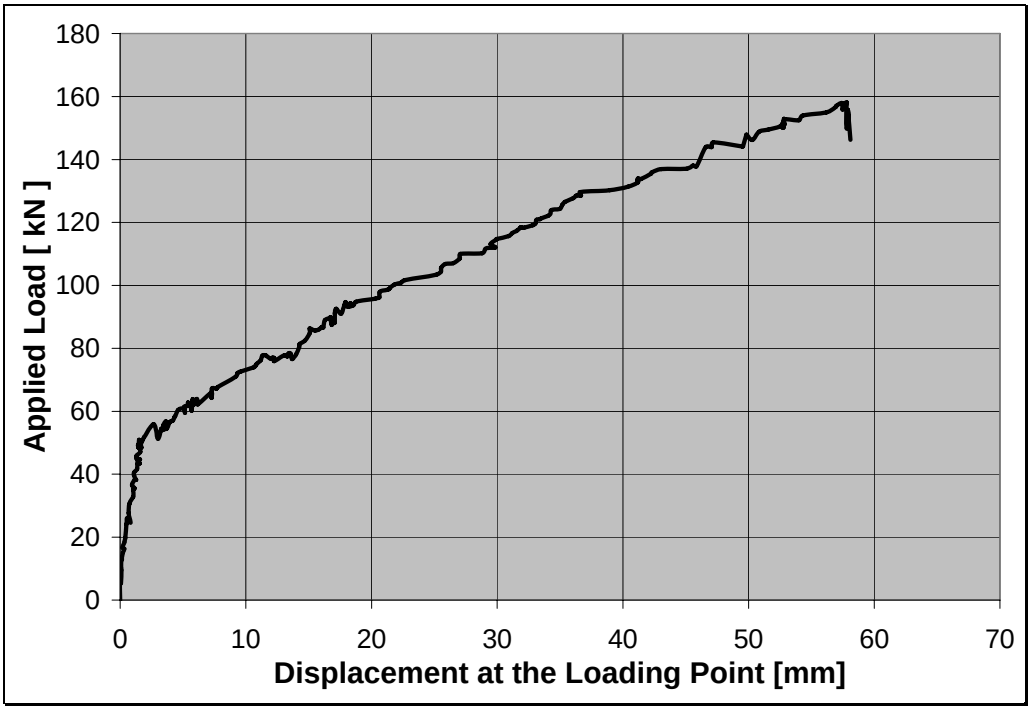

Figure 36 - Load deflection Diagram for the Longer Span of the Flexural Specimen

The same change can be observed, for the same specimen at the same location, in the diagram of Figure 37, which shows a comparison between the experimental and the theoretical moment curvature diagrams for the "flexure" specimen. The experimental diagram was determined on the longer span in correspondence with the maximum bending moment. Compared with the experimental curve, the theoretical moment curvature diagram showed a lower slope, leading to an overestimate for the deflection of the bridge.

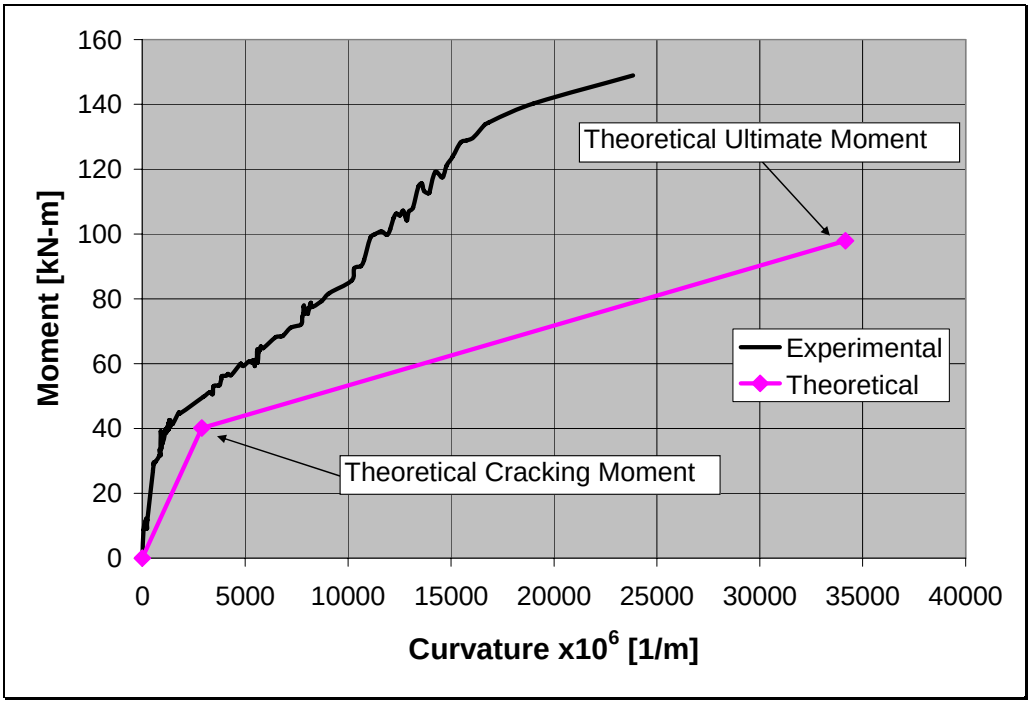

Figure 37 - Comparison Between Experimental and Theoretical Moment-Curvature Diagrams

3.7 Conclusions

On the basis of the experimental investigation, it can be concluded that GFRP bars as passive and CFRP bars as active internal reinforcement could represent a feasible solution replacing the steel reinforcement of concrete slab bridges. The prestressing material is mostly needed for shear purposes rather than for flexure.

According to ACI 440, the shear capacity increases from 30.7 kN (6.9 kip) with mild reinforcement to 69.8 kN (15.7 kip) with post-tensioned reinforcement, while the flexural capacity increases from 76.0 kN-m (55 kip-ft) to 97.9 kN-m (72.2 kip-ft).

Finally, the tools provided by ACI 440 provide a safe design at both service and ultimate conditions.

4 SOUTHVIEW BRIDGE DESIGN

4.1 Introduction

In the following section, the analytical procedures used in the widening of the Southview Bridge, located in Rolla, Phelps County, MO, are summarized. The expansion phase included the removal of the existing curb from the existing RC deck to allow the construction of two new structures adjacent to the original deck, so the width of the bridge can be extended from *3.9 m* (*13 ft)* to *11.9 m* (*39 ft)*. The curb-to-curb width of the resulting bridge is *9.1 m* (*30 ft)*. The two new structures consist of a FRP prestressed/reinforced concrete deck and a steel RC deck as shown in Figure 38.

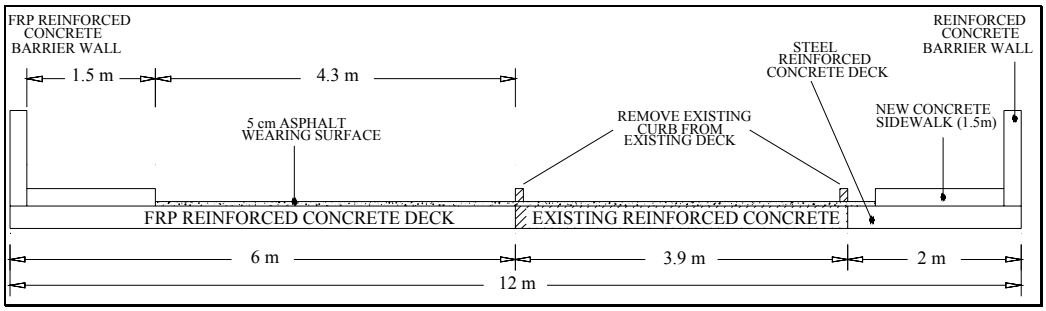

Figure 38 - Bridge T0530

The new structure is a box culvert. It consists of a steel reinforced concrete slab about *0.25 m (10 in.)* thick, as depicted in Figure 39. The slab deck is continuous over three intermediate RC vertical walls, and the overall length of the bridge is roughly *12 m* (*40 ft)*. The new deck was built on conventional RC walls. The new number of walls is identical to the existing number of walls.

Figure 39 - View of the Existing Bridge

The objective of this section is to provide the structural analysis of the new FRP concrete bridge deck based on the AASHTO HS20-44 design truck (a detailed analysis is presented in APPENDIX B) and provide calculations for its design using a combination of non-traditional corrosion-resistant composites materials.

4.2 Assumptions

The following assumptions are made:

a) Nominal properties for FRP reinforcing material are taken from the manufacturer published data and considered as initial guaranteed values to be further reduced to take into account the environmental reduction factors as given in ACI 440.1R-03 (ACI 440 in the following sections).
b) Load configurations are consistent with AASHTO Specifications.
c) Design carried out according to ACI 440.
d) Effects due to the skew are neglected..

4.3 Structural Analysis

4.3.1 Load Combinations

For the structural analysis of the bridge, the definitions of the design truck and design lane are necessary. These specifications will be addressed in the next paragraph.

Ultimate values of bending moment and shear force are obtained (in the following Summary of the Analysis) by multiplying their nominal values by the dead and live load factors and by the impact factor according to AASHTO Specifications as shown in Eq. (4.1):

$$\omega_u = 1.3\left[\beta_d D + 1.67(L+I)\right] \qquad \text{Equation Section 4}(4.1)$$

where D is the dead load, L is the live load, $\beta_d=1.0$ as per AASHTO TEquation Section 3able 3.22.1A, I is the live load impact calculated as follows:

$$I = \frac{50}{L+125} = \frac{50}{10+125} = 0.37 > 0.30 \quad \text{Equation Section 4} \quad (4.2)$$

and $L=3.0\ m\ (10\ ft)$ represents the span length from center to center of support. The impact factor should not be larger than 0.30, and therefore, the latter value is assumed for the design.

4.3.2 Design Truck and Design Lanes

The analysis of the bridge is carried out for an HS20-44 design truck load having geometrical characteristics and weight properties as shown in Figure 40.

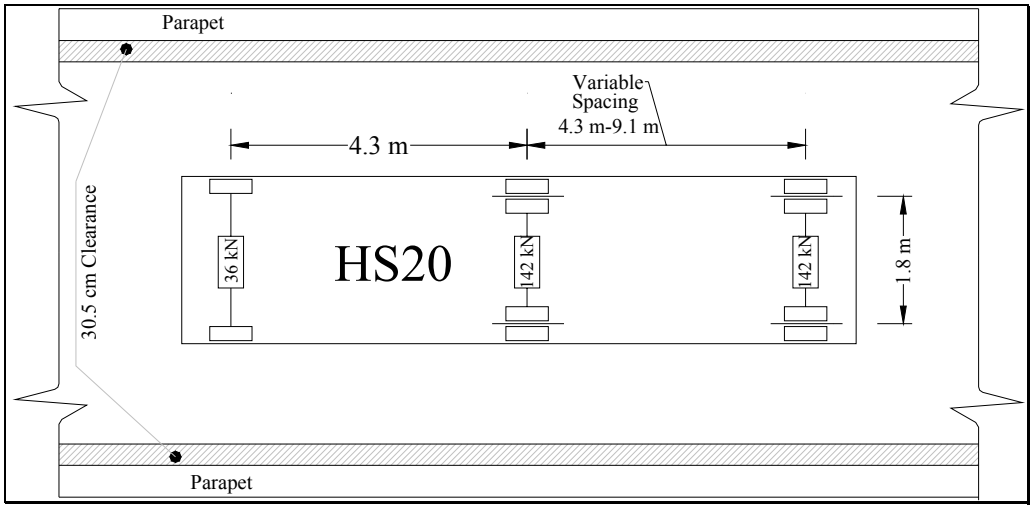

Figure 40 - Truck Load on the New Deck

Two loading conditions are required to be checked as depicted in Figure 41. The HS20-44 design truck load (Figure 41-*a*) has a front axle load of *35.6 kN (8.0 kips)*, a second axle load, located *4.3 m (14.0 ft)* behind the drive axle, of *142.3 kN (32.0 kips)*, and a rear axle load also of *142.3 kN (32.0 kips)*. The rear axle load is positioned at a variable distance, ranging between *4.3 m (14.0 ft)* and *9.1 m (30.0 ft)*. Given the specific bridge geometry, the worst loading scenario is obtained for the minimum spacing of *4.3 m (14.0 ft)* between the two rear axles. The design lane loading condition consists of a load of *9.3 kN/m (640 lbs/ft)*, uniformly distributed in the longitudinal direction with concentrated loads so placed on the span as to produce maximum stress. The concentrated load and uniform load are considered to be applied over a *3.0 m (10ft)* width on a line normal to the center line of the lane. The intensity of the concentrated load is represented in Figure 41-*b* for both bending moments and shear forces. This load shall be placed in such positions within the design lane as to produce the maximum stress in the member.

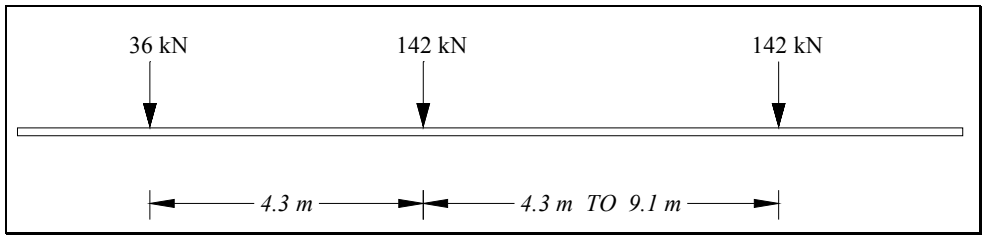

a) Design Truck (HS20-44)

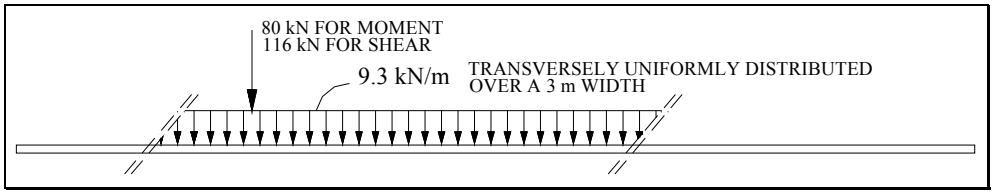

b) Design Lane

Figure 41 - Loading Conditions

4.3.3 Deck Analysis

The deck slab is considered to be a one-way slab system. The width of the slab, *E*, to be used in the analysis is provided by AASHTO (Section 3.24.3.2) as follows:

$$E = 4 + 0.06S = 4 + 0.06(10\ ft) = 1.4m(= 4.6\ ft) \qquad (4.2)$$

where *S* represents the slab length assumed equal to *3.0 m (10 ft)*.

4.3.4 Flexural and Shear Analysis

Figure 42 shows a lateral view of the bridge deck when an HS20-44 design truck moves from the right to the left as the value of x_1 increases from *0* to *L,* where *L* represents the total bridge length.

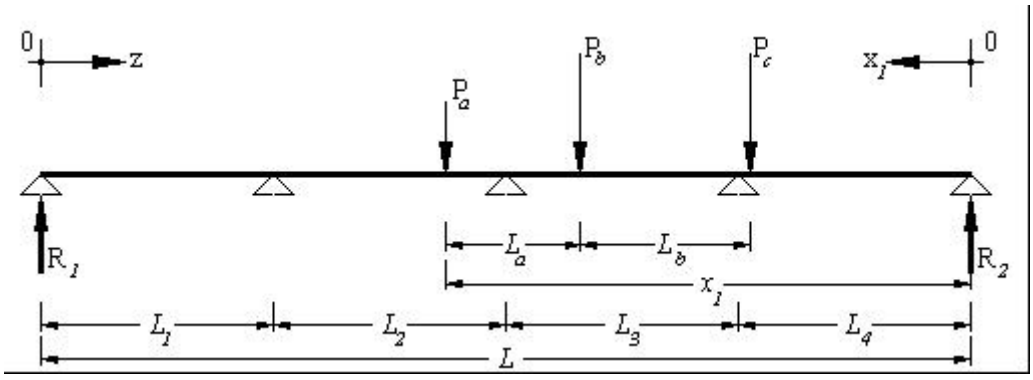

Figure 42 - Design Truck on the Girder

The values of P_i *(i=a,b,c)* represent the wheel load as defined by AASHTO (*~18, 71,* and *71 kN,* namely *4, 16,* and *16 kips*, respectively).

Table 3 summarizes values reported in Figure 42 and reports parameters used in the calculation of the moment and shear due to dead load. The analysis and design are carried out for a unit-width strip *(~30 cm, 12 in)* of slab deck.

Table 3 – Parameters for Girder Analysis

First Span Length, L_1	2.89 m (9.49 ft)
Second Span Length, L_2	3.38 m (11.10 ft)
Third Span Length, L_3	3.30 m (10.82 ft)
Fourth Span Length, L_4	2.85 m (9.35 ft)
First Load, P_a	17.8 kN (4 kip)

Second Load, P_b	71.2 kN (16 kip)
Third Load, P_c	71.2 kN (16 kip)
Concrete Unit Weight, γ_c	24 kN/m^3 (150 p/f^3)
Asphalt Unit Weight, γ_a	17.3 kN/m^3 (108 p/f^3)
Slab Unit-Width, b	30.5 cm (12 in)
Slab Height, h	25.4 cm (10 in)
Asphalt Thickness, t	15.2 cm (6 in)

As the design truck moves from the right to the left side of the bridge, fourteen different loading conditions are defined, as shown in Figure 43.

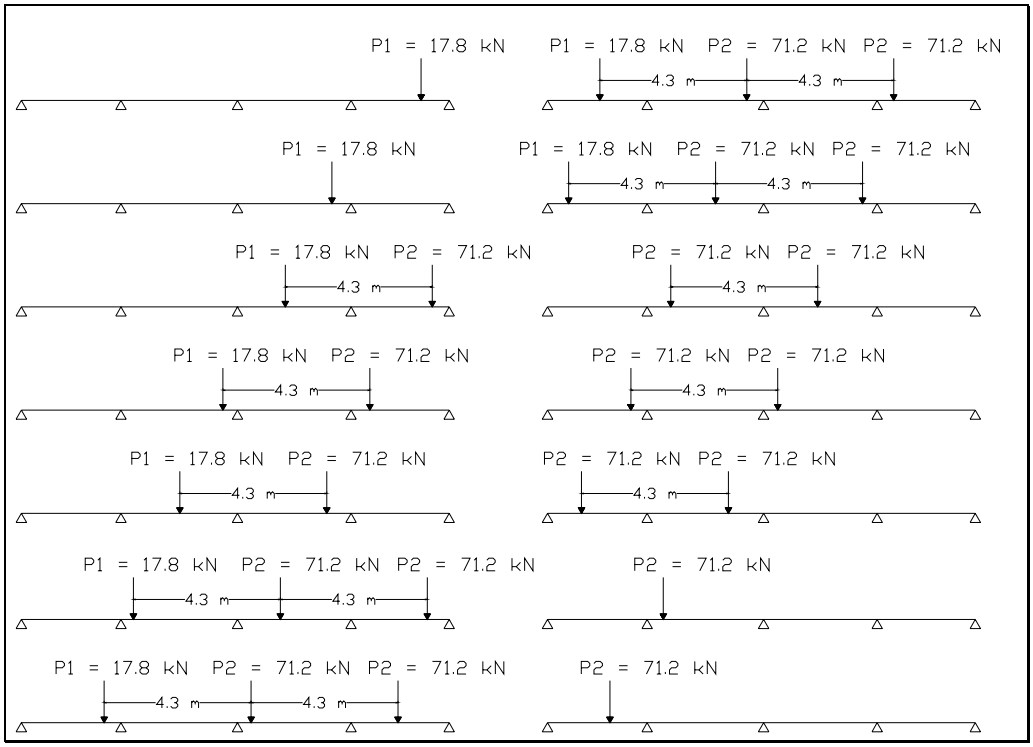

Figure 43 - Design Truck: Possible Loading Conditions

Three more loading conditions related to the design lane will be analyzed as reported in Figure 44. The first loading condition is related to the maximum positive moment, the second one to the maximum negative moment, and the third one to the maximum shear.

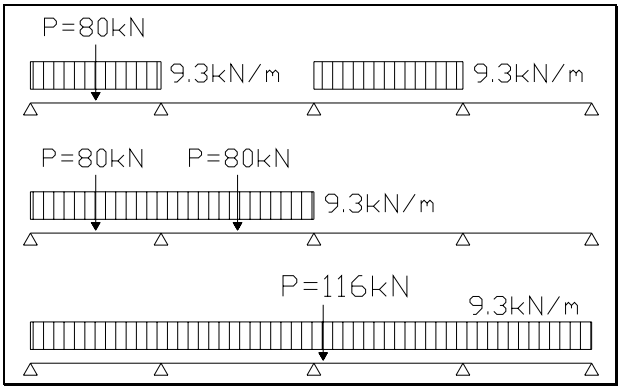

Figure 44 - Design Lane: Possible Loading Conditions

Figure 45 shows the moment diagram as the design truck moves on the bridge following the fourteen loading phases highlighted in Figure 43. Figure 46 shows the moment diagram due to the slab and asphalt layer self-load. Both diagrams are drawn for a *~30 cm (12 in)* strip-width.

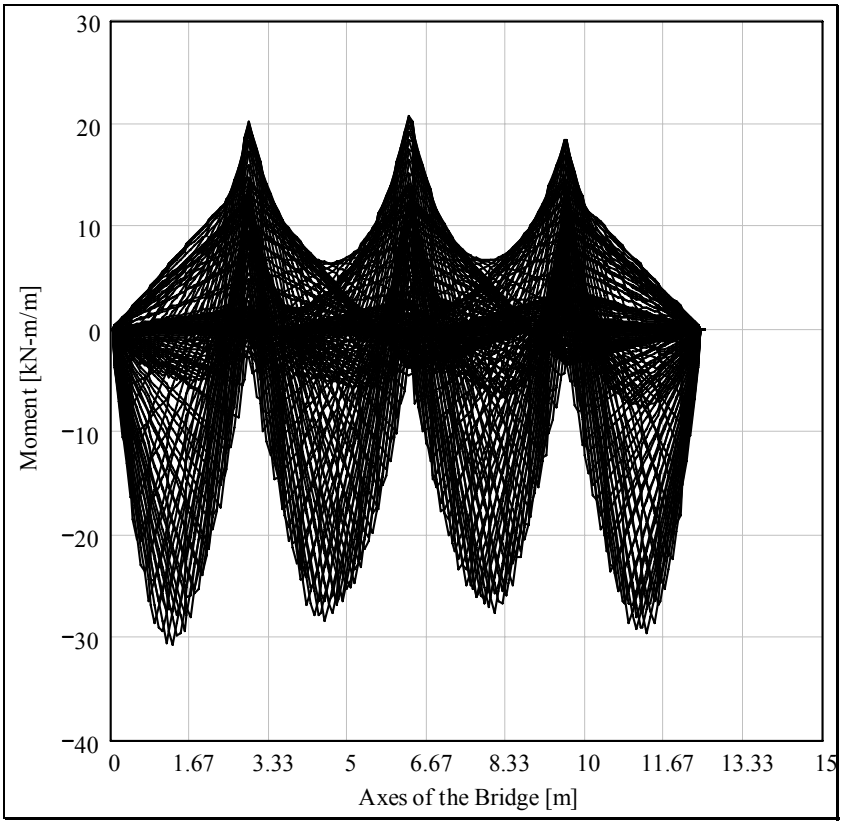

Figure 45 - Unfactored Bending Moment Diagrams Due to Live Load

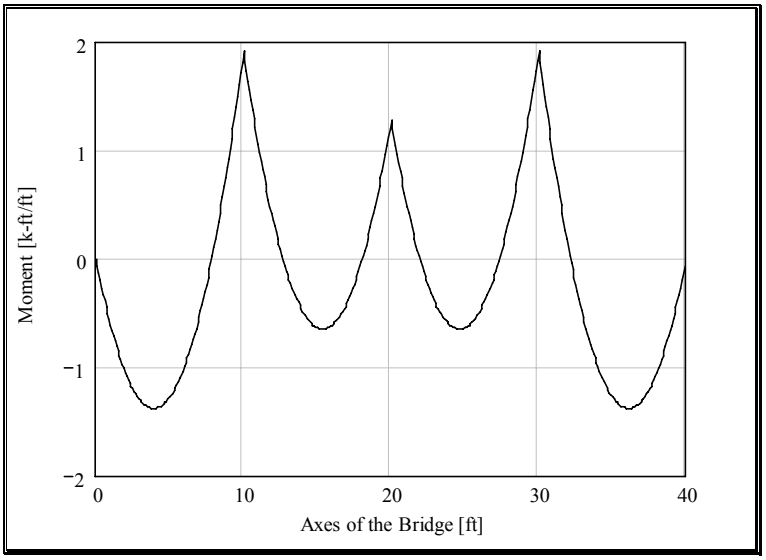

Figure 46 - Unfactored Bending Moment Diagrams Due to Dead Load

Ultimate values are obtained by taking into account the maximum positive and negative moment from Figure 45 with the load factors summarized in Eq.(4.1), and by adding the corresponding moment due to the dead load (Figure 46) with the load factors taken from the same equation.

The same diagrams can be drawn for shear as reported in Figure 47 and Figure 48 for live and dead load, respectively, and for a *~30 cm (12 in)* wide unit-strip.

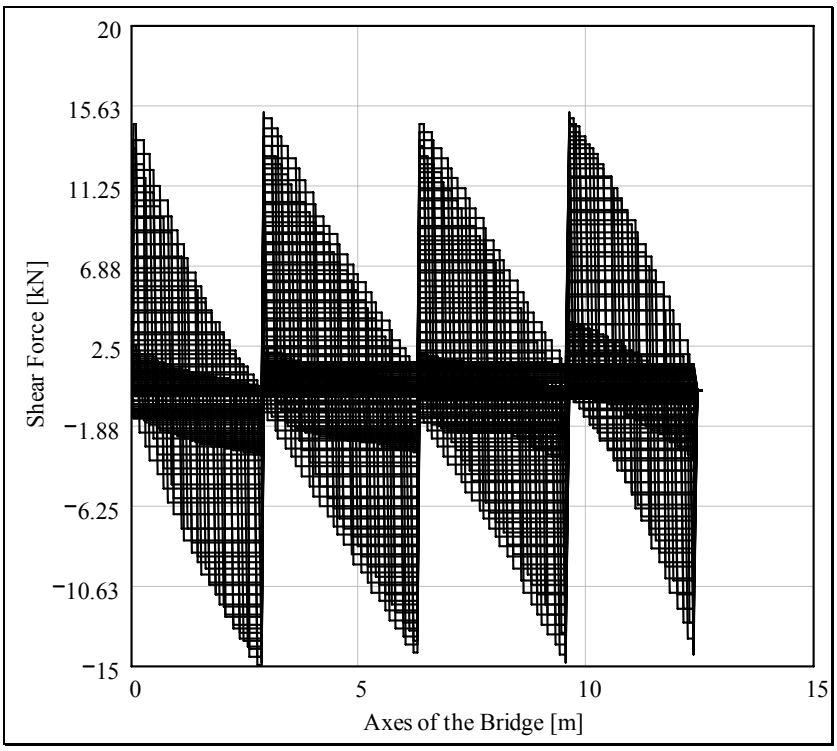

Figure 47 - Unfactored Shear Diagrams Due to Live Load

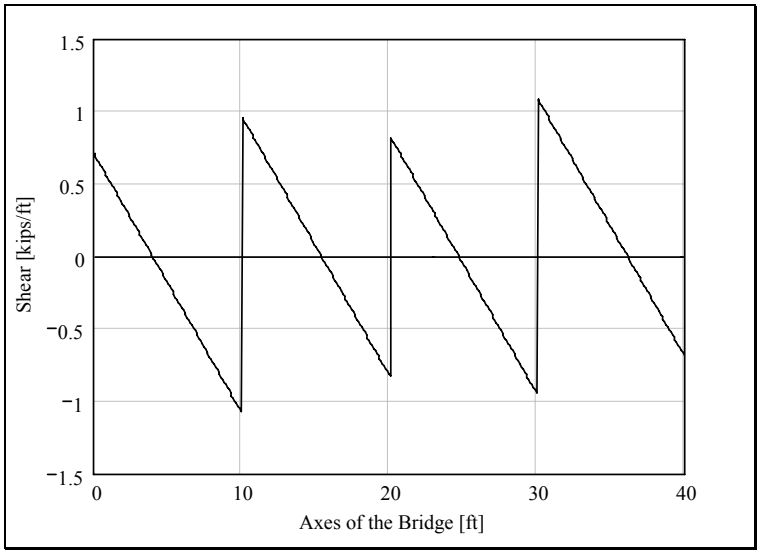

Figure 48 - Unfactored Shear Diagrams Due to Dead Load

Please note that both moment and shear diagrams due to the dead load have been calculated using a simplified structure where the distances between supports were assumed to be equal to *3.0 m (10 ft)*.

Similarly, moment and shear diagrams related to the design lane loading condition can be found as depicted in Figure 49 for the three structures shown in Figure 44. The design has been performed for a *~30 cm (12 in)* unit strip.

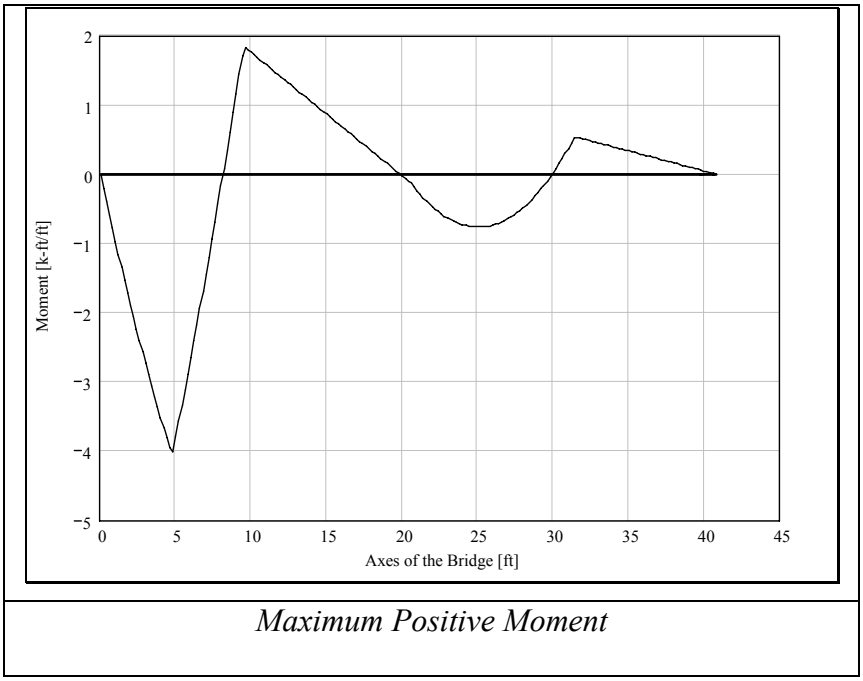

Maximum Positive Moment

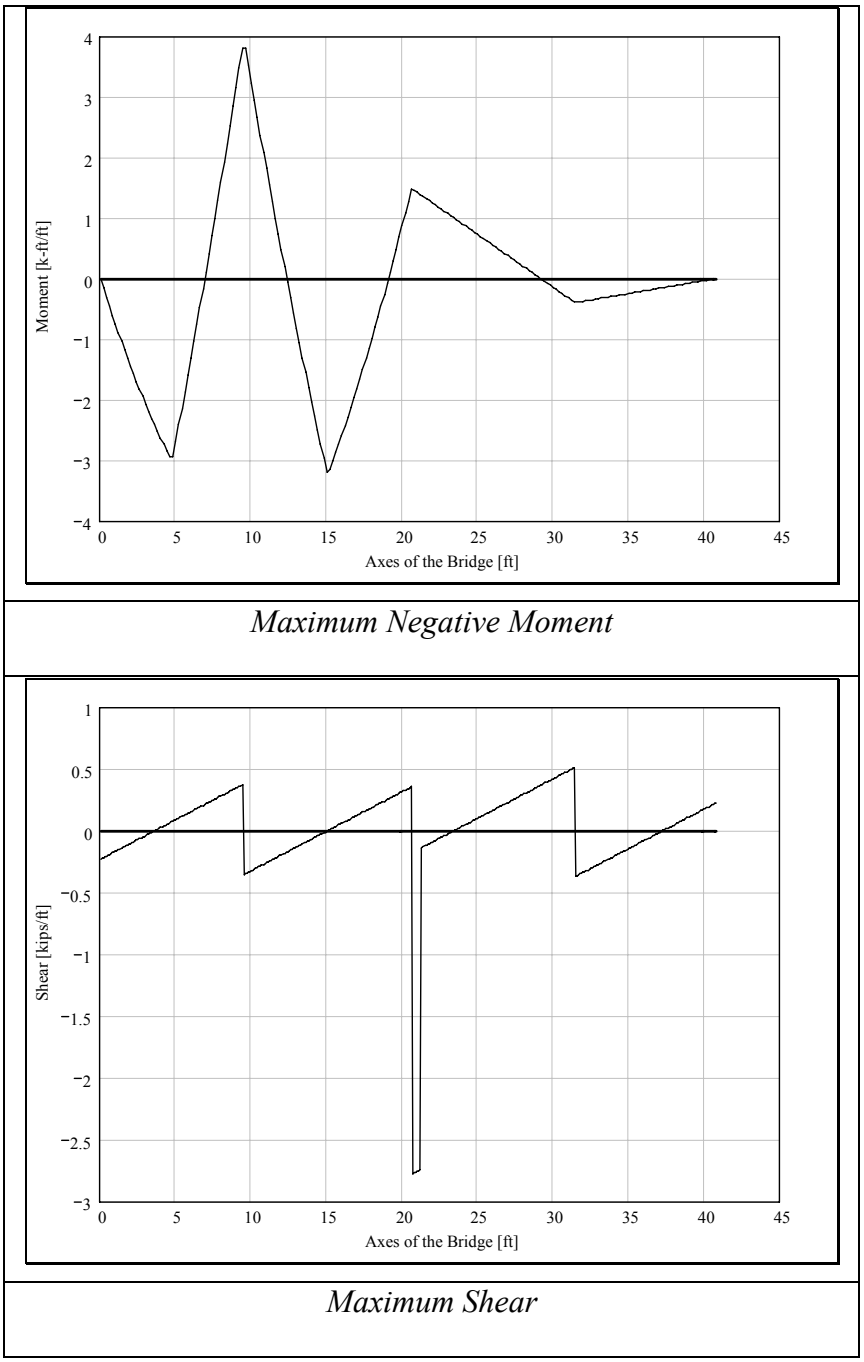

Figure 49 - Unfactored Moment and Shear Diagrams Due to Design Lane Analysis

4.3.5 Summary of the Analysis

Bending moments and shear forces are summarized in Table 4. Columns (1) and (3) represent the factored coefficient to be applied to dead and live load, respectively. Columns (2) and (4) show both unfactored dead and live load moment and shear, respectively, as taken from the previous figures.

Table 4 - Moment and Shear per Unit Strip (Live and Dead Load)

Loading Conditions	Moment and Shear	Dead Load		Live Load		Ultimate
		(1)	(2)	(3)	(4)	(5)=(1)(2)+(3)(4)
Design Truck	M^+ [kN-m/m]	(1.3)	6.27 (1.38 k-ft/ft)	(1.3)(1.67)(1.3)	29.69 (6.55 k-ft/ft)	92.09 (20.3 k-ft/ft)
	M^- [kN-m/m]		8.69 (1.92 k-ft/ft)		23.52 (5.19 k-ft/ft)	77.56 (17.1 k-ft/ft)
	Shear [kN /m]		4.92 (1.09 kip/ft)		15.42 (3.40 kip/ft)	160.53 (11.0 kip/ft)
Design Lane	M^+ [kN-m/m]		6.27 (1.38 k-ft/ft)		18.21 (4.01 k-ft/ft)	59.41 (13.1 k-ft/ft)
	M^- [kN-m/m]		8.69 (1.92 k-ft/ft)		17.29 (3.81 k-ft/ft)	59.88 (13.2 k-ft/ft)
	Shear [kN /m]		4.92 (1.09 kip/ft)		12.47 (2.75 kip/ft)	134.25 (9.2 kip/ft)

Since the design truck analysis produces the highest stresses on the slab, only moment and shear related to this analysis will be considered.

Figure 50 shows the envelope of the bending moment diagram obtained when the truck travels on the bridge following all the loading conditions summarized in Figure 43.

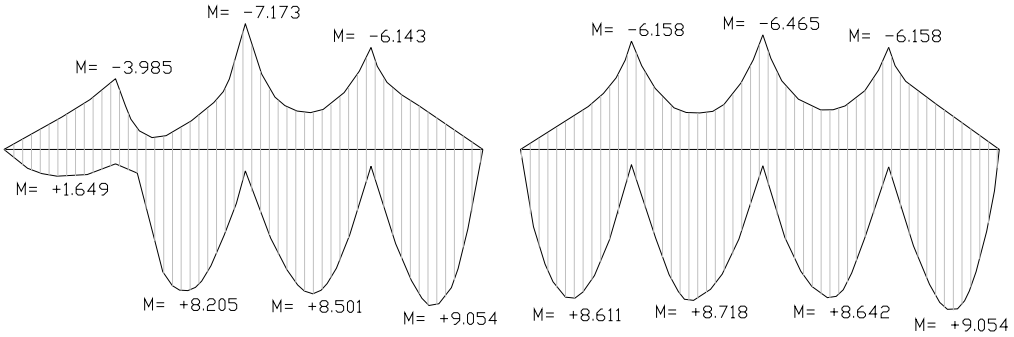

Figure 50 - Bending Moment Envelopes (kN-m/m)

4.3.6 Deflections

The worst loading condition scenario for calculating the slab deck deflections is reported in Figure 51. Two concentrated loads simulating the truck wheels are applied at mid-span of the second and fourth span. For this analysis, the span lengths have been assumed equal to *30 m (10 ft)*. To further simplify the analysis, the fourth span of Figure 51-*a* could be separately analyzed as depicted in Figure 51-*b*. Only the latter approach is presented here, and the obtained results need to be considered as an upper bound limit.

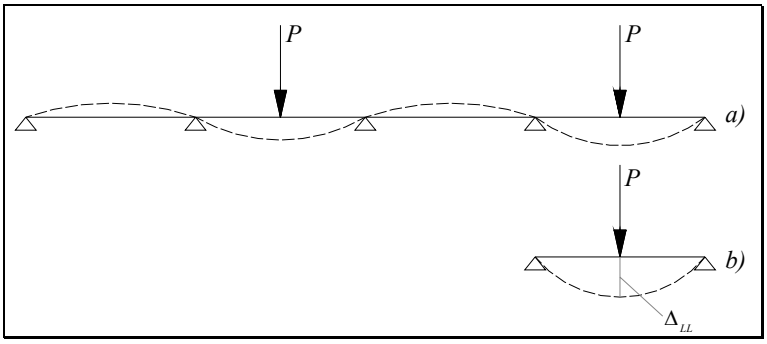

Figure 51 - Bridge Deflection Analysis (Live Load)

The deflection due to the dead load (as depicted in Figure 52) needs to be added to the live load deflections of Figure 51.

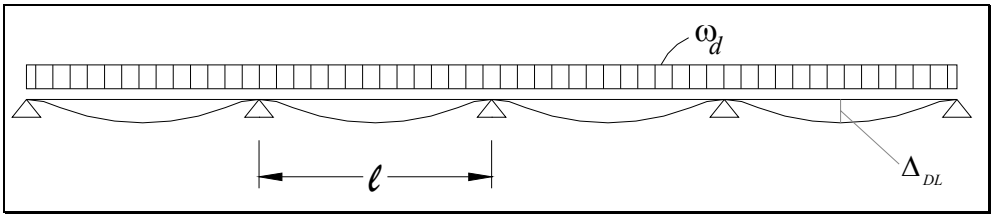

Figure 52 - Bridge Deflection Analysis (Dead Load)

The two settlements can be written as follows:

$$\Delta_{LL} = \frac{8}{384}\frac{P\ell^3}{E_s I_s}$$
$$\Delta_{DL} = 0.0065\frac{\omega_d \ell^4}{E_s I_s} \qquad (4.3)$$

where *P= 1.3* 71.2 kN (1.3*16 kips)* is the wheel load increased by the impact factor, ω_d *~2.6 kN/m (0.179 k/ft)* represents the dead load of the bridge, and E_s and I_s are the modulus of elasticity of the concrete and the moment of inertia of the cross-section of the slab, respectively. The value of the moment of inertia will change depending on whether the cross-section can be considered cracked or uncracked.

4.3.7 Barrier Analysis

The barrier analysis is conducted considering the parapet as a cantilever beam fixed at the intersection point with the deck. A concentrated force *P*, distributed over a longitudinal length of *~1.5 m* (*5 ft)* (AASHTO Section 2.7.1.3.6), is applied at the top of the barrier simulating an impacting vehicle. The maximum intensity of the concentrated force *P* needs to be taken as no larger than *~44.5 kN* (*10 kip)*

as specified in AASHTO Section 2.7.1.3.1. Figure 53 shows a sketch of the structure being studied.

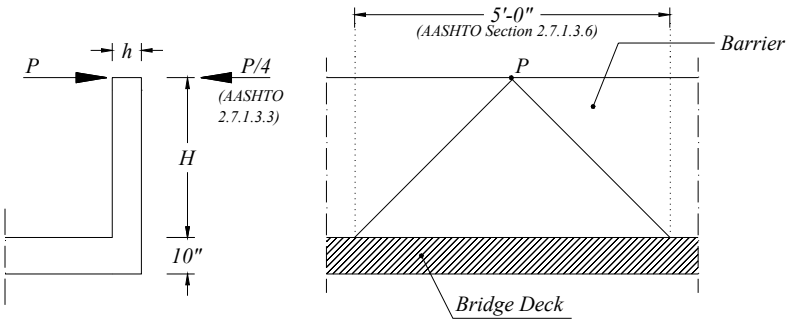

Figure 53 - Barrier Analysis

The maximum bending moment can be written as follows:

$$M = PH = \left(\frac{10^k}{5'}\right)\left(\frac{44"}{12}\right) = 32.5kN - m/m(7.3 \quad k - ft/ft) \tag{4.4}$$

where *H ~1.1 m (3'-8")*.

4.4 Design

The design of the internal FRP reinforcement is carried out according to the principles of ACI 440. The properties of concrete, steel, and FRP bars used in the design are summarized in Table 5. The reported FRP properties are guaranteed values.

Table 5 - Material Properties

Concrete Compressive Strength f'_c (MPa)	FRP Internal Reinforcement Type	FRP Bar Size	FRP Tensile Strength f^*_{fu} (MPa)	FRP Tensile Strain ε^*_{fu}	FRP Modulus of Elasticity E_f (GPa)
41.4 (Deck) (6,000 psi) 27.8 (Barrier) (4,000 psi)	GFRP	ϕ9 (#3)	758 (110 ksi)	0.018	40.8 (5,920 ksi)
		ϕ13 (#4)	689 (100 ksi)	0.017	40.8 (5,920 ksi)
		ϕ19 (#6)	621 (90 ksi)	0.015	40.8 (5,920 ksi)
		ϕ22 (#7)	586 (85 ksi)	0.014	40.8 (5,920 ksi)
	CFRP	ϕ19 (#3)	2068 (300 ksi)	0.017	124.1 (18,000 ksi)

Material properties of the FRP reinforcement reported by manufacturers, such as the ultimate tensile strength, typically do not consider long-term exposure to environmental conditions and should be considered as initial properties. FRP properties to be used in all design equations are given as follows (ACI 440):

$$f_{fu} = C_E f^*_{fu} \qquad \varepsilon_{fu} = C_E \varepsilon^*_{fu} \qquad (4.5)$$

where f_{fu} and ε_{fu} are the FRP design tensile strength and ultimate strain considering the environmental reduction factor (C_E) as given in Table 7.1 (ACI 440), and f^*_{fu} and ε^*_{fu} represent the FRP guaranteed tensile strength and ultimate strain as reported by the manufacturer (see Table 5). The FRP design modulus of elasticity is the average value as reported by the manufacturer.

4.4.1 Slab Design

4.4.1.1 Flexural Design

The flexural design of a FRP reinforced concrete member is similar to the design of a steel RC member. The main difference is that both concrete crushing and FRP rupture are potential mechanisms of failure. As an FRP reinforced concrete member is usually less ductile than the correspondent steel RC member, the strength reduction factor, ϕ, needs to be revisited according to Eq. (4.6) (ACI 440):

$$\phi = \begin{cases} 0.50 & if \quad \rho_f \le \rho_{fb} \\ \dfrac{\rho_f}{2\rho_{fb}} & if \quad \rho_{fb} < \rho_f < 1.4\rho_{fb} \\ 0.70 & if \quad \rho_f \ge 1.4\rho_{fb} \end{cases} \qquad (4.6)$$

where ρ_f is the FRP reinforcement ratio and ρ_{fb} represents the FRP reinforcement ratio producing balanced failure condition.

Figure 54 shows the trend of the strength reduction factor as a function of both concrete compressive strength and the number of GFRP bars used.

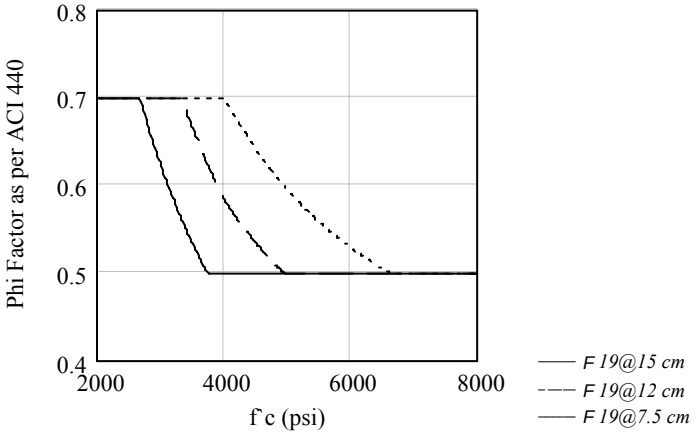

Figure 54 - Strength Reduction Factor

By increasing the concrete compressive strength, the value of the ϕ factor changes from *0.7* to *0.5* as the failure mode moves from concrete crushing to FRP rupture.

Figure 55 shows the nominal and factored flexural capacities of the bridge deck as a function of the concrete compressive strength and the number of FRP bars installed (same legend of Figure 54).

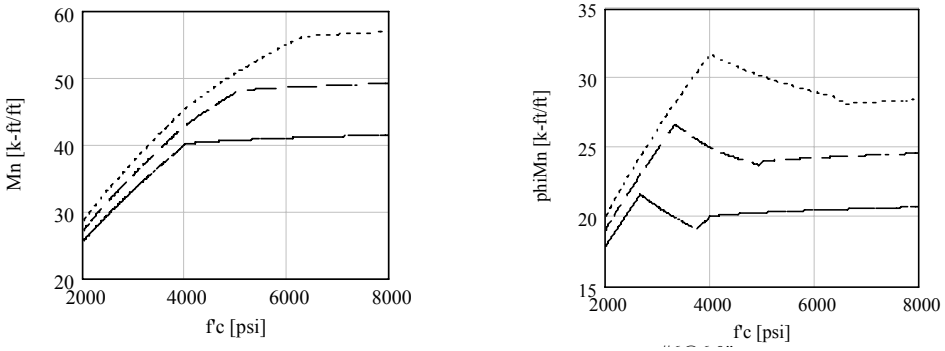

a) Nominal *b) Factored*

Figure 55 - Flexural Capacities of the Bridge

Table 6 summarizes the properties and the flexural capacity of the bridge deck corresponding to a cross section with a ϕ19 (#6) Aslan 100 GFRP as mild reinforcement at *~15 cm (6 in)* center-to-center. Prestressing FRP tendons made out of ϕ9 (#3) Aslan 200 CFRP bars are installed at *~23 cm (9 in)* center-to-center and post-tensioned after the concrete deck is cured. Calculations are carried out for a *~30 cm (12 in)* unit strip.

Table 6 - Slab Geometrical Properties and Internal FRP Reinforcement

Overall Height of the Slab, h *[cm]*	Area of Tension GFRP Reinforcement, A_f *[cm²/m]*	GFRP Effective Depth, d *[cm]*	Area of Prestressed CFRP Tendons, A_p *[cm²/m]*	CFRP Effective Depth, d_p *[cm]*	Flexural Capacity ϕM_n *[kN-m/m]*
25.4 (10 in)	19.39 (0.916 in²/ft)	20.6 (8.125 in)	2.13 (0.101 in²/ft)	17.8 (7.0 in)	92.8 (20.5 k-ft/ft)

The above flexural capacity is related to both positive and negative moment regions, and it is larger than the required demand previously shown in Table 4.

The prestress strain in the tendons is equal to 65 percent of the ultimate strain. All CFRP losses are assumed to be 30 percent of the initial prestressing strain.

4.4.1.2 Shear Design

The shear capacity of FRP reinforced concrete sections is calculated following the principles of ACI 440. Particularly, the concrete contribution to the shear capacity, $V_{c,f}$, can be expressed as follows:

$$V_{c,f} = \frac{A_f E_f}{A_s E_s} V_c \qquad (4.7)$$

where the ratio $(A_f E_f / A_s E_s)$ takes into account the axial stiffness of the FRP reinforcement as compared to that of steel reinforcement, and V_c is given as follows (ACI 318-99):

$$V_c = (0.6\sqrt{f_c'} + 700\frac{V_u d_p}{M_u})bd_p \qquad (4.8)$$

A_s reported in Eq. (4.7) can be found by determining the area of steel reinforcement required to match the factored FRP flexural capacity, ϕM_n. Table 7 summarizes the steel and GFRP design and the assumed value of A_s.

The concrete contribution to the shear capacity of the member yields the following:

$$V_c = \left(0.6\sqrt{6000} + 700\frac{11.0(7/12)}{17.1}\right)(12)(7) = 379.4kN/m (= 26.0\ \ kips/ft) \qquad (4.9)$$

and from Eq. (4.7):

$$V_{c,f} = \frac{(1.195)(5,920)}{(0.528)(29,000)} 26.0 = 175 kN/m (= 12.0 \ kips/ft) \quad (4.10)$$

Table 7 - Steel and GFRP Flexural Design of the Deck (No Prestress Used)

Description	Steel Design	GFRP Design
Deck Slab, *h*	25.4 cm (10 in)	25.4 (10 in)
Deck Width, *b*	30.5 cm (12 in)	30.5 (12 in)
Effective Depth, *d*	20.6 cm (8.125 in)	20.6 (8.125 in)
Reinforcement Area	ϕ13@25cm=11.2cm^2/m (#4@10"=0.528 in^2/ft)	ϕ19@11cm=25.3 cm^2/m (#6@4.5"=1.195 in^2/ft)
Factored Flexural Capacity,ϕM$_n$	94.3 kN-m/m (20.8 k-ft/ft)	93.0 kN-m/m (20.5 k-ft/ft)

Finally, the factored shear capacity is $\phi V_n = \phi V_{c,f} = 0.85*175 = 148.9$ *kN/m (=10.2 kips/ft)*. This value is slightly smaller than the shear demand $V_u = 160.5$ *kN/m (=11.0 kips/ft,* see Table 4). The value can be accepted because the analysis has been performed on the centerline of the support, while it is allowed to evaluate both V_u and M_u at a cross section flush with the vertical wall representing the support. In this case, V_u will not change substantially, while M_u will have an appreciable lower value. Therefore (while keeping $V_u d_p / M_u < 1$), V_c expressed by Eq. **Error! Reference source not found.** will be *162 kN/m,* which is higher than the shear demand.

Consistent with section 3, note that the prestressing force is most needed for shear purposes rather than flexure. In fact, if the prestressing action was not considered, the concrete contribution to the shear capacity would have been $V_c = 220.4$ *kN/m (=15.1 kips/ft)*, and the final factored shear capacity of the bridge would have been equal to $\phi V_n = 86.09$ *kN/m* << *148.9 kN/m* ($\phi V_n = 5.9$ *kips/ft* << *10.2 kips/ft)*; therefore, the post-tensioning allowed the increase of the slab's shear capacity more than 70 percent.

As an alternative approach to the shear capacity of the bridge deck, the following equation (Tureyen A. K. and Frosh R. J., 2003), now under consideration for adoption by ACI Committee 440, could be used:

$$V_{c,f} = 5\sqrt{f_c^{`}} bc \quad (4.11)$$

where *c* is the position of the neutral axis at service. This approach is justified by the parametric analysis laid out in the next Figure 56.

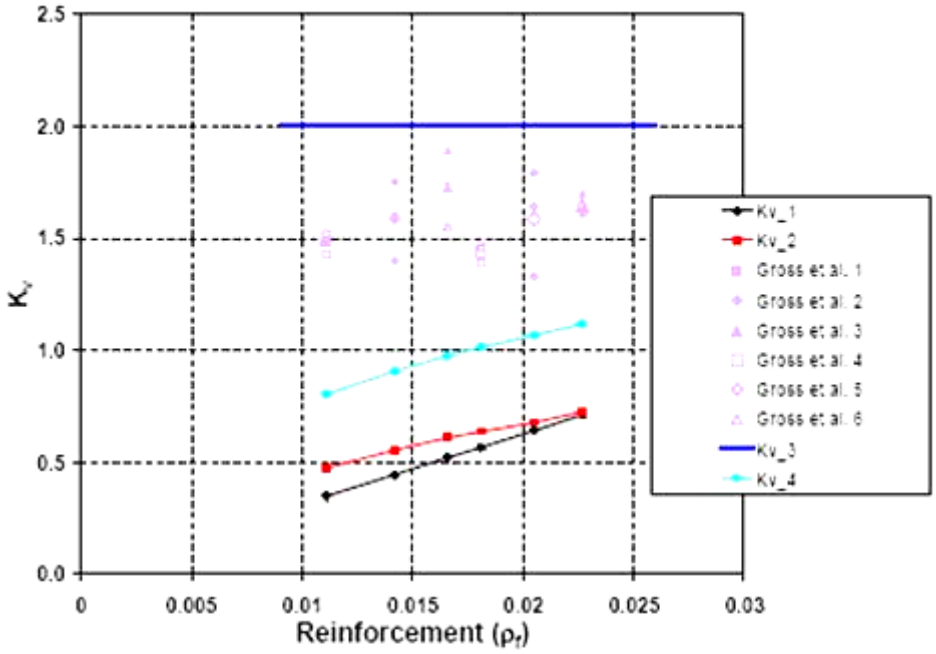

$$V_c = K_v \sqrt{f'_c}\, bd$$

$$K_{v_1} = 2\frac{\rho_f E_f}{90\beta_1 f'_c}$$

$$K_{v_2} = 2\frac{\rho_f E_f}{\rho_s A}$$

$$K_{v_3} = 2$$

$$K_{v_4} = 5\frac{c}{d}$$

Figure 56 - Rationale for Proposed Shear Strength

The values of *c* can be determinate using the approach shown in paragraph 4.4.3.1:

$$V_c = 5 \cdot \sqrt{6000} \cdot 12 \cdot 3.295 = 68.10\text{kN}(=15.31\text{ kip}) \qquad (4.12)$$

Finally, the factored shear capacity is $\phi V_n = \phi V_{c,f} = 0.85(213.2) = 189.9$ *kN/m (0.85(14.61)=13.01 kip/ft)* larger than $V_u = 160.5$ *kN/m (11.0 kip/ft)*.

4.4.1.3 Temperature and Shrinkage Reinforcement

GFRP reinforcement perpendicular to the main flexural reinforcement is required to control both crack width and shrinkage of the concrete. The equation adopted by ACI 440 can be written as follows:

$$\rho_{f,ts} = 0.0018 \frac{60,000}{f_{fu}} \frac{E_s}{E_f} \leq 0.0036 \qquad (4.13)$$

where f_{fu} *(psi)* is defined in Eq.(4.5), and E_s an E_f are the elastic moduli of steel and GFRP, respectively. The area of GFRP reinforcement deemed necessary for temperature and shrinkage can be expressed as follows:

$$A_{f,ts} = \rho_{f,ts} bh \qquad (4.14)$$

and it is subdivided in two layers, each close to one of the concrete surfaces. In the previous equation, *b* and *h* represent unit width and height of the cross-section, respectively (*b=30.5 cm, 12 in*, and *h=25.4 cm, 10 in)*.

It is suggested to use a ϕ13 (#4) Aslan 100 GFRP bar spaced at *~30 cm (12 in)* center-to-center, as depicted in Figure 57 representing a cross sectional view of the bridge deck.

Figure 58 shows a longitudinal view of the prestressing CFRP tendons.

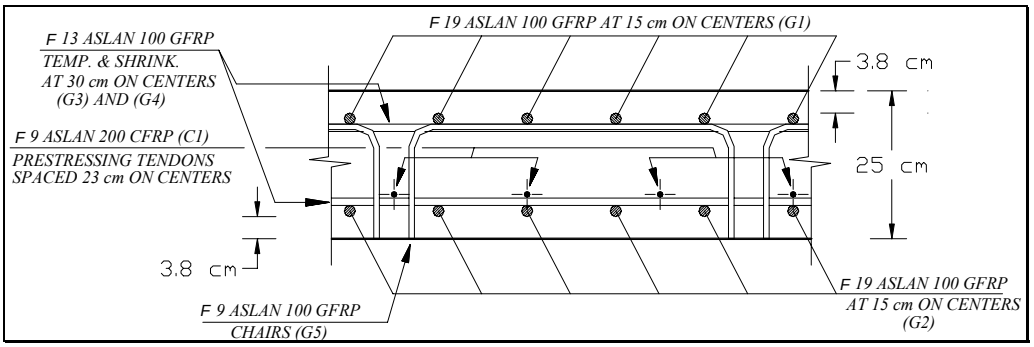

Figure 57 - Bridge Internal FRP Reinforcement: Section at Mid-Span

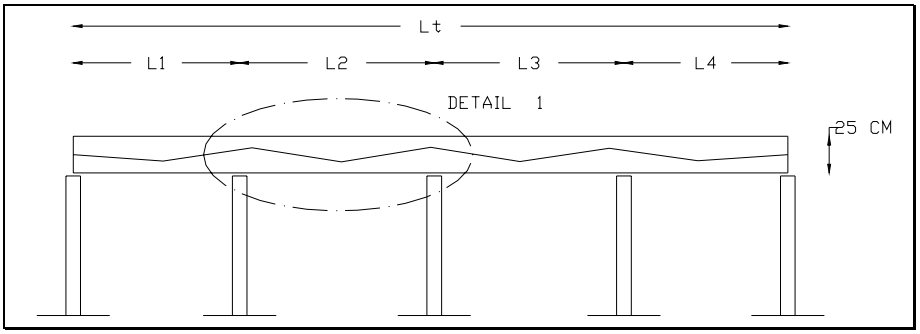

a) Longitudinal View

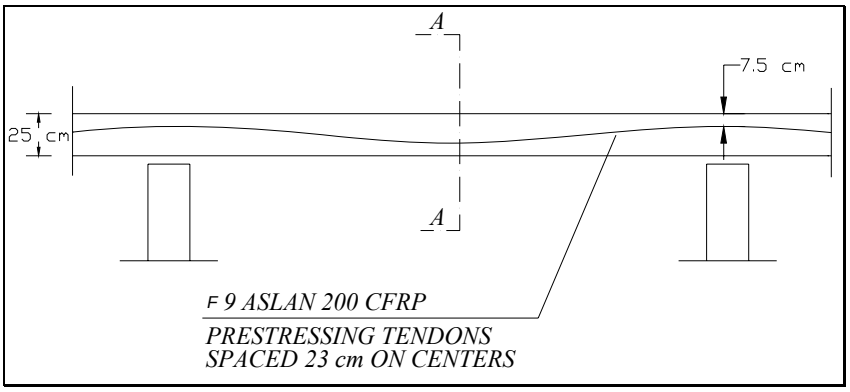

b) Detail

Figure 58 - CFRP Prestressing Tendons

4.4.2 Barrier Design

4.4.2.1 Flexural Design

Table 8 summarizes the flexural capacity of the barrier. Calculations are carried out for a *30.5 cm* (*12 in)* unit strip.

Table 8 - Barrier Geometrical Properties and Internal FRP Reinforcement

Overall Height of the Barrier, *h* *[cm]*	Area of Tension GFRP Reinforcement, A_f *[cm²/m]*	GFRP Effective Depth, *d* *[cm]*	Flexural Capacity, ϕM_n *[kN-m/m]*
20.3 (8 in)	ϕ13@30.5 cm=4.76 (#4@12"=0.225 in²/ft)	15.9 (6.25 in)	17.3 (3.9 k-ft/ft)
20.3 (8 in)	ϕ19@30.5 cm=9,69 (#6@12"=0.458 in²/ft)	15.6 (6.1 in)	30.7 (6.9 k-ft/ft)
20.3 (8 in)	ϕ22@30.5 cm=12.55 (#7@12"=0.593 in²/ft)	15.4 (6.06 in)	36.9 (8.3 k-ft/ft)

Coforce suggests using a ϕ22 (#7) ASLAN 100 GFRP bar at *30.5 cm* (*12 in)*. center-to-center as main flexural reinforcement of the barrier.

On the external side of the barrier a ϕ13 (#4) ASLAN 100 GFRP bar at *30.5 cm (12 in)* center-to-center is required. The obtained flexural capacity *(17.3 kN-m/m, 3.9 k-ft/ft)* is larger than the demand since the applied moment is *M=32.5/4~8kN-m/m (1.8 k-ft/ft)*, as previously recognized in Figure 53 and Eq. (4.4).

A sketch of the GFRP reinforced concrete barrier is shown in Figure 59

4.4.2.1

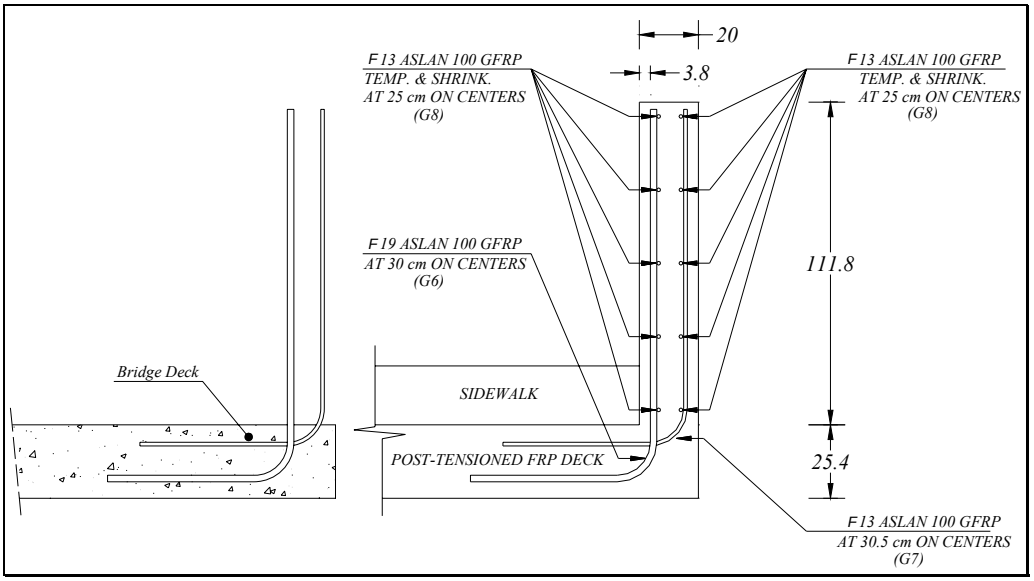

Figure 59 - Barrier Design

4.4.3 Serviceability

Unlike steel reinforced concrete sections, members reinforced with FRP bars have relatively small stiffness after cracking. Therefore, serviceability requirements like crack width and long-term deflection need to be specifically tailored for composite structures as highlighted in ACI 440. In the following two sections, both crack width and long-term deflection checks will be presented.

4.4.3.1 Crack Width

The service moment per unit strip of slab deck can be calculated starting from the data of Table 4 as follows:

$$M_s = M_{DL} + 1.3M_{LL} = 1.381 + (1.3)(6.549) = 44kN - m/m (= 9.9\ \ k - ft/ft) \quad (4.15)$$

where M_{DL} and M_{LL} represent moment due to dead and live load, respectively.

Crack width of FRP reinforced flexural members can be expressed as suggested by ACI 440 as follows:

$$w = \frac{2200}{E_f}\beta k_b f_f \sqrt[3]{d_c A} \qquad (4.16)$$

where β is the ratio of the distance between the neutral axis and the extreme tension fiber to the distance between the neutral axis and the center of tensile reinforcement, k_b is a bond-dependant coefficient equal to *1.2*, f_f represents the stress at service in the FRP, d_c is the thickness of the concrete cover measured from extreme tension fiber to the center of the bar, A is the effective tension area of concrete defined as the area of concrete having the same centroid as that of tensile reinforcement divided by the number of bars *(N=2)*, and E_f is the modulus of elasticity of FRP. The above mentioned terms can be written as follows:

$$\begin{aligned} \beta &= \frac{\beta_1 h - c}{\beta_1 d - c} \\ d_c &= h - d \\ A &= \frac{2 d_c b}{N} \end{aligned} \qquad (4.17)$$

Assuming a cracked concrete cross-section at service as shown in Figure 60, the stress in the GFRP, $f_f = E_f \varepsilon_f$, can be calculated by solving the following system of equations:

$$\begin{cases} \frac{1}{2}\mathrm{E_c}\varepsilon_\mathrm{c}\mathrm{bc} - \mathrm{A_p}\mathrm{E_p}\varepsilon_\mathrm{p} - \mathrm{A_f}\mathrm{E_f}\varepsilon_\mathrm{f} = \mathrm{N_{pi}} \\ \frac{1}{2}\mathrm{E_c}\varepsilon_\mathrm{c}\mathrm{bc}\left(\frac{\mathrm{h}}{2} - \frac{\mathrm{c}}{3}\right) + \mathrm{A_p}\mathrm{E_p}\varepsilon_\mathrm{p}\left(\mathrm{d_p} - \frac{\mathrm{h}}{2}\right) + \mathrm{A_f}\mathrm{E_f}\varepsilon_\mathrm{f}\left(\mathrm{d} - \frac{\mathrm{h}}{2}\right) = \mathrm{M_s} - \mathrm{M_{pi}} \\ \frac{\varepsilon_\mathrm{c}}{\mathrm{c}} = \frac{\varepsilon_\mathrm{p}}{\mathrm{d_p} - \mathrm{c}} \\ \frac{\varepsilon_\mathrm{c}}{\mathrm{c}} = \frac{\varepsilon_\mathrm{f}}{\mathrm{d} - \mathrm{c}} \end{cases} \qquad (4.18)$$

where M_{pi} and N_{pi} represent the axial load and the bending moment to the centroid of the section, induced by the post-tensioning of the CFRP bars.

By solving Eq. (4.18) and finding the unknown ε_f, the following value for the stress in the GFRP can be evaluated as follows:

$$\mathrm{f_f} = \mathrm{E_f}\varepsilon_\mathrm{f} = 13.58\mathrm{MPa}(= 1.97\ \mathrm{ksi}) \qquad (4.19)$$

The crack width calculated with Eq. (4.16) yields *w=0.086mm (0.0034 in),* which is smaller than the allowed values suggested by ACI 440 and equal to *0.51mm (0.02 in)*.

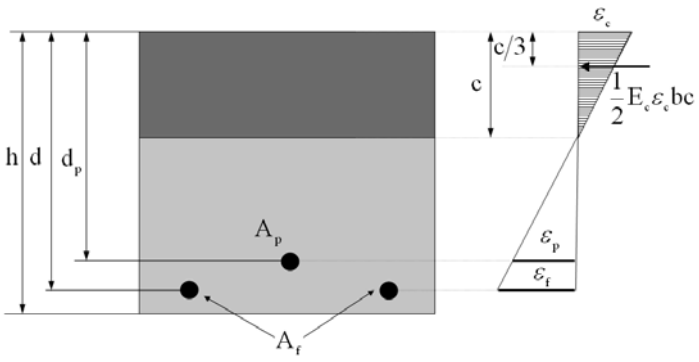

Figure 60 - Stress and Strain at Service

4.4.3.2 Long-Term Deflections

Based on the conservative deflection analysis carried out on Section B.3.3, the long-term deflection can be calculated as suggested by ACI 440 as follows:

$$\Delta = \Delta_{LL} + \lambda(\Delta_{DL} + 0.2\Delta_{LL}) \qquad (4.20)$$

where $\lambda=1.2$ represents the multiplier for additional long-term deflection as recommended in ACI 440. Assuming the concrete cross-section uncracked because of the presence of the prestressing tendons, both concrete modulus of elasticity and moment of inertia can be expressed as follows:

$$E = 57000\sqrt{f_c'}$$
$$I = \frac{bh^3}{12} \qquad (4.21)$$

where *b~30 cm (=12 in)* for dead load analysis, and *b=E=1.4 m (4.6 ft)* for live load analysis. Eq. (4.20) yields to Δ*=1.30 mm (0.051 in)* smaller than the suggested AASHTO value of $\ell/800$*=3.81mm (0.15 in).*

4.4.3.3 Slab Creep Rupture and Fatigue

To avoid creep rupture of the FRP reinforcement under sustained loads, the stress level in the FRP bar should be limited to the value suggested in ACI 440. Specifically, when GFRP reinforcement is used, the stress limit has been set to be equal to $0.20\,f_{fu}$ *~87 MPa (12.6 ksi).* The stress at service in the FRP can be found as follows:

$$f_f = \frac{M_s}{A_f\left(d - \frac{c}{3}\right)} = \frac{(9.9)(12)}{0.916\left(8.125 - \frac{0.943}{3}\right)} = 114.5MPa(=16.6\ ksi) \qquad (4.22)$$

Once again, because the bridge is mostly uncracked at service because of the prestress, the above findings are conservative, and the value obtained from Eq. (4.22) can be considered acceptable.

4.5 Load Rating

Bridge load rating calculations provide a basis for determining the safe load carrying capacity of a bridge. According to the Missouri Department of Transportation (MoDOT), anytime a bridge is built, rehabilitated, or reevaluated for any reason, inventory and operating ratings are required using the Load Factor rating. All bridges should be rated at two load levels, the maximum load level called the operating rating and a lower load level called the inventory rating. The operating rating is the maximum permissible load that should be allowed on the bridge. Exceeding this level could damage the bridge. The inventory rating is the load level the bridge can carry on a daily basis without damaging the bridge.

The operating rating is based on the appropriate ultimate capacity using current AASHTO specifications (AASHTO, 1996). The inventory rating is taken as 60 percent of the operating rating.

The vehicle used for the live load calculations in the Load Factor Method is the HS20 truck. If the stress levels produced by this vehicle configuration are exceeded, load posting may be required.

The tables below show the rating factor and load rating for this bridge. The method for determining the rating factor is that outlined by AASHTO in the Manual for Condition Evaluation of Bridges (AASHTO, 1994). Equation (4.23) was used to find the rating factor:

$$RF = \frac{C - A_1 D}{A_2 L(1 + I)} \qquad (4.23)$$

where RF is the rating factor, C is the capacity of the member, D is the dead load effect on the member, L is the live load effect on the member, I is the impact factor to be used with the live load effect, A_1 is the factor for dead loads, and A_2 is the factor for live loads. Since the load factor method is being used, A_1 is taken as 1.3, and A_2 varies depending on the desired rating level. For inventory rating, A_2 = 2.17, and for operating rating, A_2 = 1.3.

Equation (4.24) was used to determine the rating (RT) of the bridge:

$$RT = (RF)W \qquad (4.24)$$

In the above equation, W is the weight of the nominal truck used to determine the live load effect.

For the Southview Bridge, the load rating was calculated for a number of different trucks—HS20, H20, 3S2, and MO5. The different ratings are used for different purposes by the bridge owner. For each of the different loading conditions, the maximum shear and maximum moment were calculated. Impact factors are also taken into account for load ratings. This value is 30 percent for the Southview Bridge. The shear and moment values for the deck are shown in below in Table 9.

Table 9 - Maximum Shear and Moment due to Live Load

Truck	Maximum Shear (kN)	Maximum Moment (kN-m)	Maximum Shear with Impact (kN)	Maximum Moment with Impact (kN-m)
HS20	15.1 (3.40 kips)	9.06 (6.55 k-ft)	19.66 (4.42 kips)	11.78 (8.52 k-ft)
MO5	14.7 (3.30 kips)	6.47 (4.68 k-ft)	19.66 (4.29 kips)	8.41 (6.08 k-ft)
H20	12.7 (2.86 kips)	5.93 (4.29 k-ft)	14.55 (3.72 kips)	7.70 (5.57 k-ft)
3S2	13.0 (2.93 kips)	5.89 (4.26 k-ft)	16.95 (3.81 kips)	7.66 (5.54 k-ft)

Table 10 below gives the results of the Load Rating pertaining to moment, and Table 11 shows the results for shear. All calculations for the load rating are located in Appendix B.

Since the RF factors are greater than one, the bridge does not need to be load posted. In addition, from Table 10 and Table 11, the maximum operating and inventory load can be found as 64.5T and 38.7T, respectively.

Table 10 - Rating Factor for the New Slab (Bending Moment)

Truck	Rating Factor (RF)	Rating (RT) (Tons)	Rating Type
HS20	1.793	64.5	Operating
HS20	1.074	38.7	Inventory
MO5	2.482	89.4	Operating
H20	2.330	46.6	Posting
3S2	2.345	85.9	Posting

Table 11 - Rating Factor for the New Slab (Shear)

Truck	Rating Factor (RF)	Rating (RT) (Tons)	Rating Type
HS20	2.152	77.5	Operating
HS20	1.289	46.4	Inventory
MO5	2.217	81.2	Operating
H20	2.202	44.0	Posting
3S2	2.148	78.7	Posting

4.6 Southview Bridge Drawings

The following drawings show the main characteristics of the Southview bridge deck, consistent with the previously tested specimens and with the design presented in this section.

Drawing 1 and Drawing 2 show a plan strip view with the transverse and longitudinal sections of the deck, respectively. Drawing 3 details profile, section, top, and bottom views of the slab; FRP reinforcement details at the midspan and at the supports are also shown.

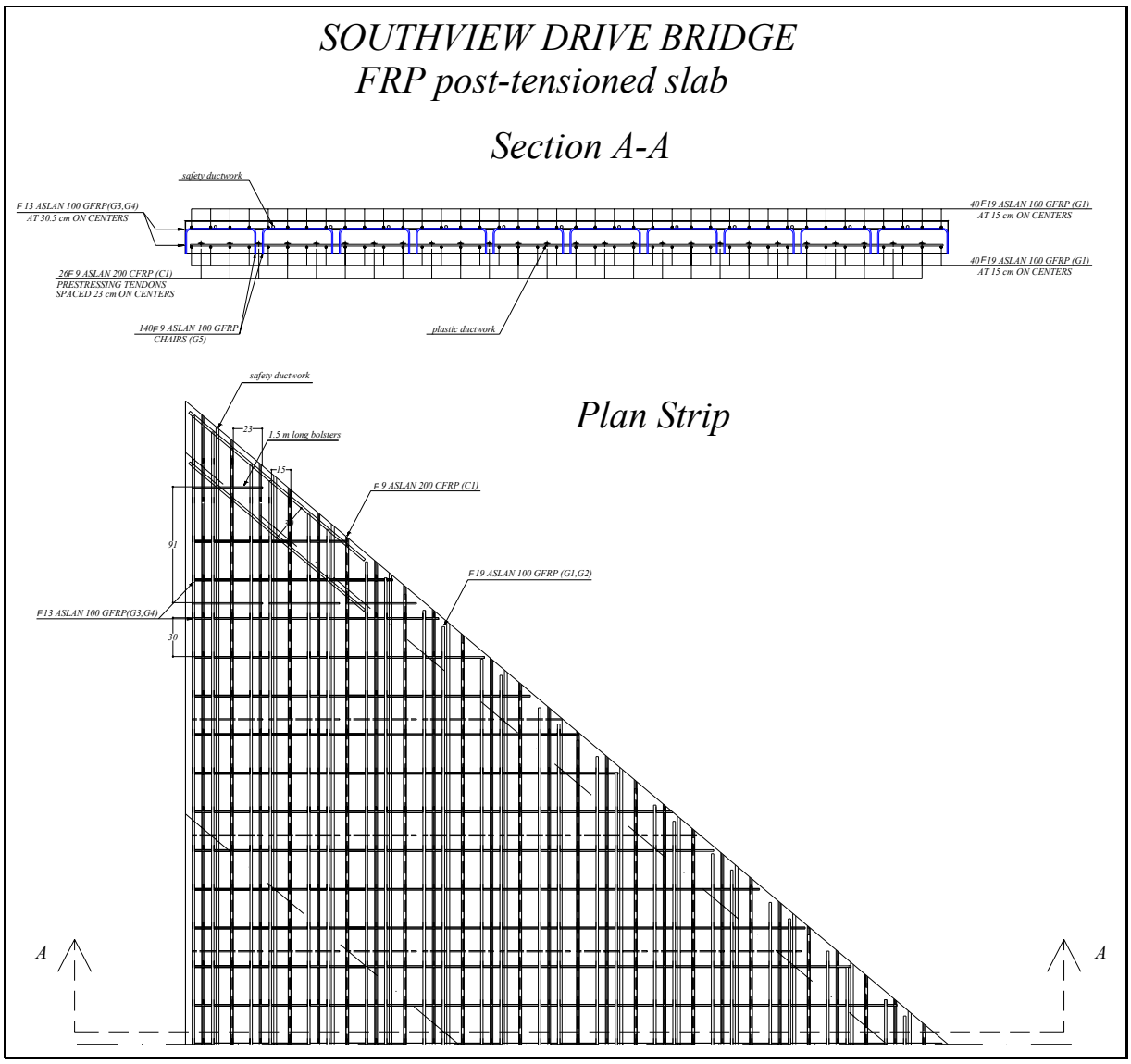

Drawing 1 - Section A-A

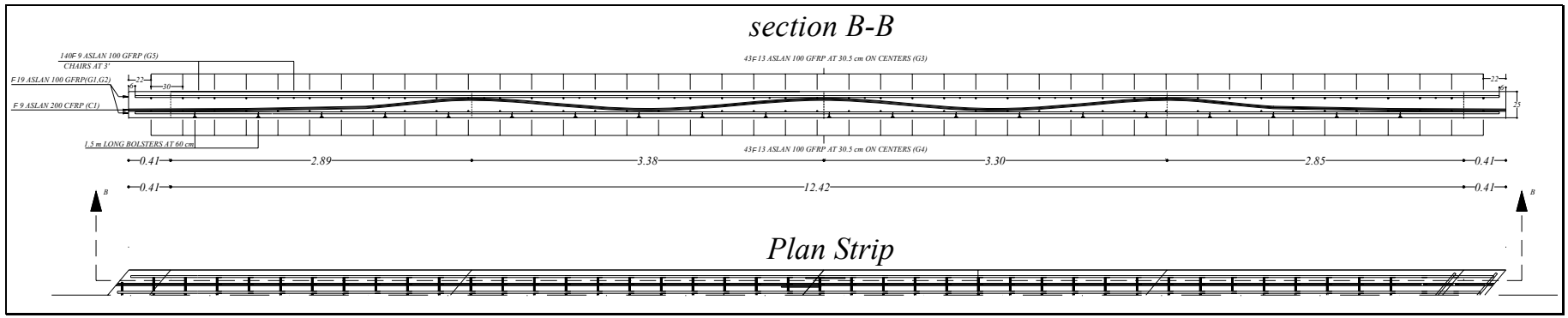

Drawing 2 - Section B-B

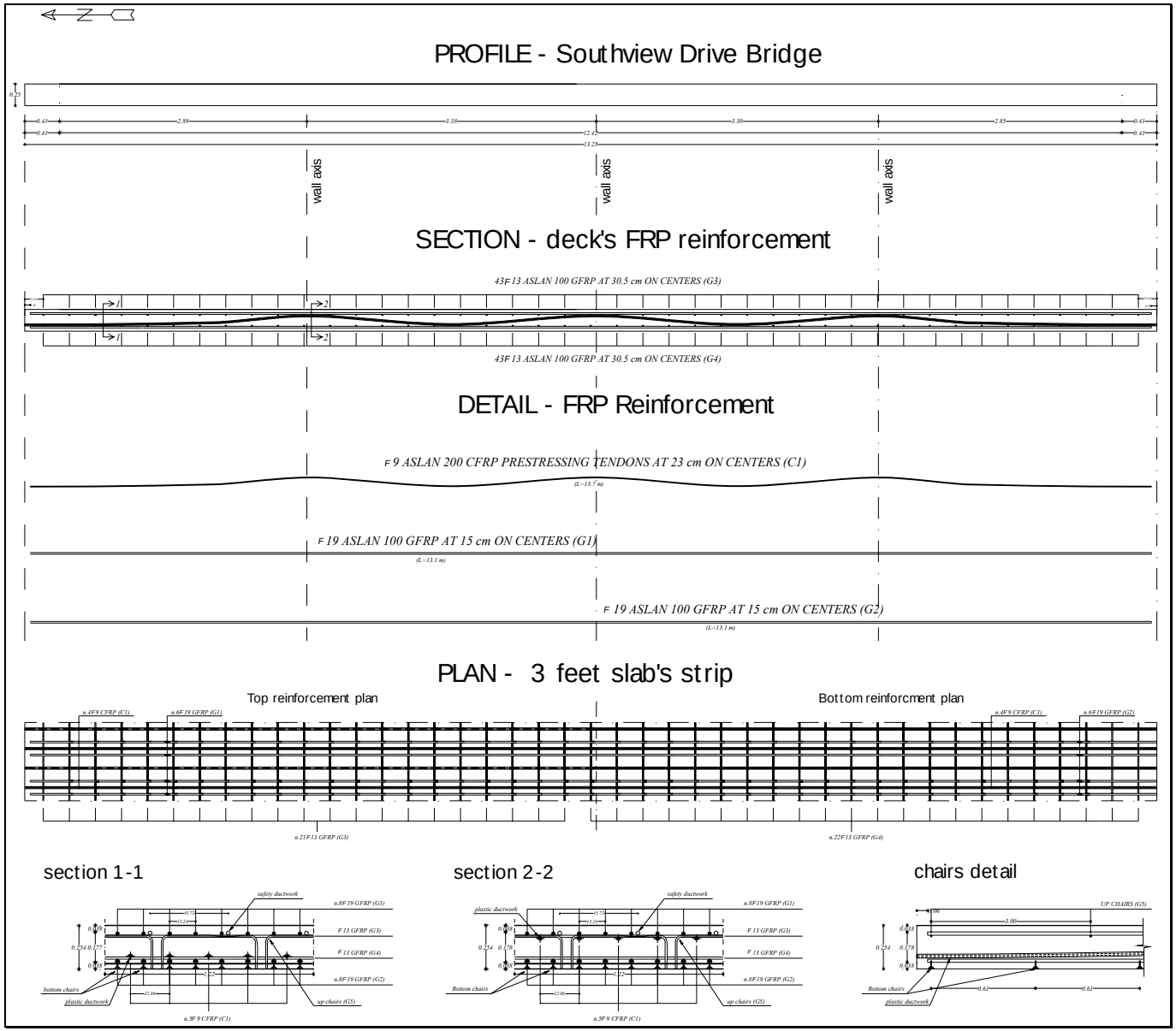

Drawing 3 - Ultimate Design

5 SOUTHVIEW BRIDGE DECK INSTALLATION

5.1 Introduction

This section details the installation of the Southview bridge deck, conducted by Master Contractors LLC, overseen and documented by the author as part of this thesis.

As outlined in the first section, the slab is 25 cm (10 in) thick, 12 m (40 ft) long, and 6 m (19.83 ft) wide. It is supported by three intermediate RC vertical walls. The four span lengths are, from north to south, 2.89 m (9.49 ft), 3.38 m (11.10 ft), 3.30 m (10.82 ft), and 2.35 m (9.35 ft), on centers.

The material and construction specifications are detailed in Appendix C.

5.2 Pre-construction Meetings

In order to ensure a successful completion of the project, extensive planning and collaboration was required between the different entities involved in the construction. The City of Rolla was in charge of the construction of walls and abutments expansion and of the post-tensioning system, which was optimized for the particular field application as part of a cooperation between University of Missouri-Rolla (UMR) and the Rolla Technical Institute (RTI) in the person of Mr. Max Vath.

A first meeting was held on Tuesday, July 27, 2004, in the City of Rolla. This meeting was attended by representatives of the city; the engineer, Mr. David Brown, and the construction foreman, Mr. Bill Cochran; the contractor in charge of the construction of the slab, Mr. Jason Cox from Master Contractors LLC; and Dr. Antonio Nanni and the author from UMR.

The three main topics discussed at this meeting were concerning issues of constructability, materials, and structural concerns.

- Constructability issues dealt with the schedule of construction and access to the bridge deck during construction. The existing lane of the bridge was the only access that could be used to reach the construction site; therefore, caution had to be taken with the trucks that continuously passed on the bridge in order to create a safe environment for the workers.
- Material issues dealt with quality assurance testing. The University of Missouri-Rolla volunteered to test the concrete samples extracted during the pouring and to test the steel rebar.
- Structural issues dealt with specific details regarding construction. For example, GFRP bars should be placed on the central wall to create a connection between slab and walls, the walls should have different heights due to the presence of Neoprene pads only on two

of the three walls, and the construction of the formwork supporting the slab should be done by the City of Rolla.

The second pre-construction meeting was held at the construction site on Thursday, August 12, 2004. The meeting was attended by the same people present at the first one, with the addition of one the bridge deck designers, Dr. Nestore Galati from UMR.

The main topics pertained to the concrete, formwork, and barrier.

- Concrete: Issues dealt with quality and required characteristics of concrete to be used for the construction of the deck. A high slump value was determined to be necessary, which required the addition of super-plasticizers to make sure the matching of adequate strength in a short period of time. The City of Rolla was in charge of providing the concrete.
- Formwork: In order to facilitate the post-tensioning, a formwork longer than the slab itself had to be built on both sides of the bridge (see Figure 80). This extending part of the formwork would have to be cut after the post-tensioning operations, so as to not affect the construction of two more box cells, which was scheduled to occur after the installation of the deck.
- Barrier: During the construction of the walls, the decision was made to build the barrier on the "FRP side" of the bridge using GFRP rebars instead of steel rebars. Such decision would in fact allow the comparison between the durability of the FRP and the steel barrier to be built on the opposite side of the bridge, as already discussed and shown before.

5.3 Substructure Construction

5.3.1 Footing and Floor Construction

As highlighted before, the erection of the substructure and the extension of the existing abutments and walls were performed by the City of Rolla employees prior to the slab construction.

On July 21, 2004, the work started with removing the guardrail, wetting the basement, and digging the weeds on the "FRP side," as shown in Figure 61.

Figure 61 - Wetting the Basement and Digging the Weeds

In the days following the excavation of the bridge site and the moving of soil, the suction of the water overflowing from the creek was the main operation to deal with. The area where the footing had to be built (see Figure 62) was often and very easily filled with water either from rain or from a mizzle. To remove the stagnant water, different devices were utilized, such as electric pumps or a pipe allowing the water to flow from the creek, over the basin, to the opposite side of the stream (see Figure 63).

Figure 62 - Work Area after the Water Filling

Figure 63 - Devices to Remove or Avoid the Water

On July 27, 2004, the formwork and the steel reinforcement for the footing were placed (see Figure 64). The following day, after removing the remaining water, the footing was poured (see Figure 65). The concrete slump was found to be 10 cm (4in).

Figure 64 - Footing Formwork

Figure 65 - Pouring of the Footing

Figure 66 shows the slump test and the casting of concrete cylinders used to determine the concrete strength. The footing was built by the end of the working day (see Figure 67).

Figure 66 - Slump Test and Concrete Cylinders Casting

Figure 67 - Footing after Pouring

On July 29, 2004, the floor reinforcement was placed, after filling the voids between the footing beams with gravel (see Figure 68).

Figure 68 - Floor Reinforcement

As highlighted before, several delays were caused by bad weather conditions. Figure 69 shows the site conditions after a thunderstorm. The casting of the floor was completed on August 3, 2004.

Figure 69 - Water Overflowing and Casting of the Floor

5.3.2 Abutments Construction

The abutments construction started after the former abutments caps were replaced, since the existing ones were in very bad condition. The formwork and the reinforcement of the abutments were then placed quickly (see Figure 70). Figure 71 shows the device used to tie the steel reinforcement together.

On August 5, 2004, the new abutments were cast (see Figure 72).

Figure 70 - Laying of Abutments Reinforcement and Formwork

Figure 71 - Use of the Steel Ties Gun

Figure 72 - Casting of the New Abutments

5.3.3 Walls Construction

Prior to the walls construction and during the curing of the new abutments, the dowels for the walls were fixed on the existing floor; thus, the first wall reinforcement and formwork were placed (as shown in Figure 73).

The following Monday, August 9, 2004, the first wall was cast (see Figure 74).

Figure 73 - Reinforcement and Formwork of the First Wall

Figure 74 - First Wall

The second wall to be built was the one close to the other abutment, thereby making it possible to reuse the first wall formwork. The central wall formwork had to be lower than the others to allow the insertion of the GFRP bars anchoring the slab to that wall.

The construction of the central wall was complicated by the lack of room and the short distance between the vertical steel rebars, on which the GFRP rebars had to be tied (see Figure 75 and Figure 76). In addition, a central groove on the top of the wall was made to strengthen the connection between wall and slab (see Figure 77).

The preparatory part of the project was completed on August 12, 2004 (see Figure 78 and Figure 79).

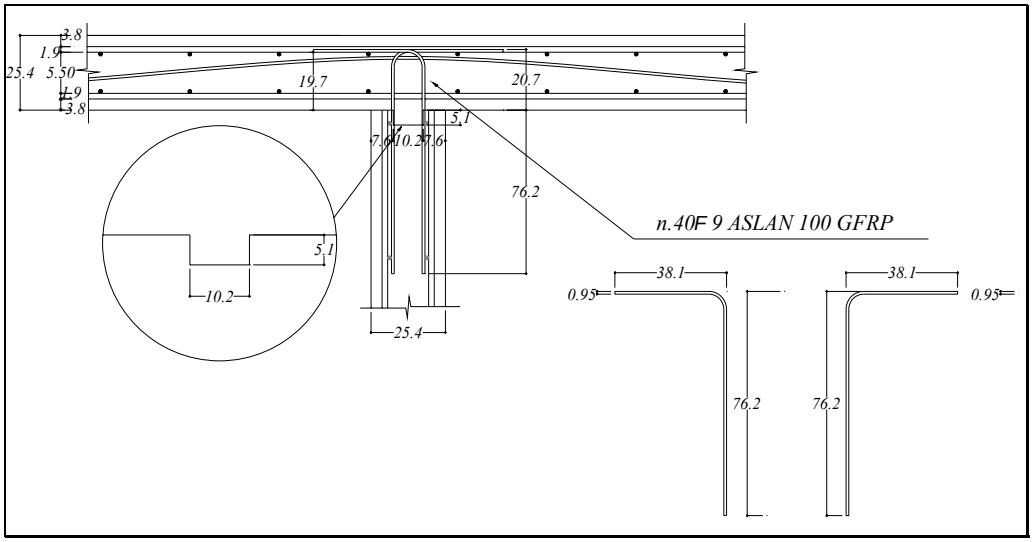

Figure 75 - GFRP Anchoring Detail

Figure 76 - Laying of the GFRP Rebars

Figure 77 - Making of the Notch

Figure 78 - Central Wall

Figure 79 - Completion of the Preparatory Part of Southview Project

5.4 Slab Construction

Prior to the construction of the slab, all the material needed was computed. The bill of materials and equipment used for the installation of the slab is reported in the following section.

5.4.1 Bill of Materials

Table 12 summarizes the amount of FRP reinforcement needed.

Table 12 - Bill of FRP Material

No.	Size	Length	Mark	Location	Fiber Type	Bending Sketches
26	ϕ9 #3	16.15 m (53'-0")	C1	Deck	Carbon	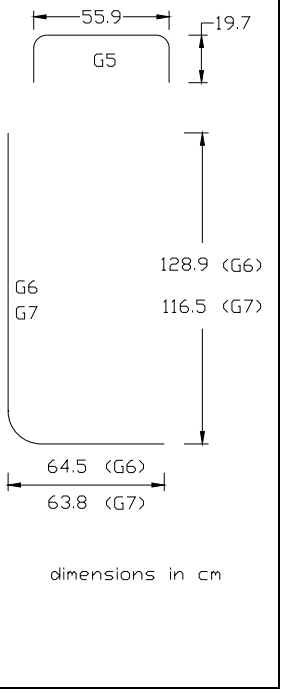
40	ϕ19 #6	13.11 m (43'-0")	G1	Deck	Glass	
40	ϕ19 #6	13.11 m (43'-0")	G2	Deck	Glass	
43	ϕ13 #4	5.79 m (19'-0")	G3	Deck	Glass	
43	ϕ13 #4	5.79 m (19'-0")	G4	Deck	Glass	
140	ϕ9 #3	0.97 m (3'-2")	G5	Deck	Glass	
43	ϕ19 #6	1.95 m (6' -1")	G6	Barrier	Glass	
43	ϕ13 #4	1.85 m (5' -9")	G7	Barrier	Glass	
10	ϕ13 #4	13.11 m (43'-0")	G8	Barrier	Glass	
40	ϕ19 #6	1.70 m (5' -7")	G9	Deck	Glass	
40	ϕ9 #3	1.24 m (3'-9")	G10	Deck-Wall	Glass	

Moreover, the following materials were used:

1. **Neoprene pads**: NEWLON 60 durometer molded neoprene for load-bearing applications. Considering ~15x10 cm^2 (6x4 in^2) pads, 1.3 cm (1/2 in) thick, ~15 cm (6 in) from each other, each wall needed 24 pads. Since only two of the three walls needed the pads and accounting also for the two abutments, a total of 96 pads were needed (~1.5 m^2, about 2300 in^2).
2. **Styrofoam**: ~6.6 m^2 (71 ft^2) of styrofoam were required to place around the pads.

3. **Chairs**: ~1.5 m (5 ft) long bolsters at ~60 cm (2 ft) spacing were deemed necessary to support the bottom longitudinal GFRP bars, considering ~6 m (20 ft) of width and ~12 m (40 ft) of the length of the slab; therefore, 4 sets of 20 chairs, (80 chairs total) were ordered.
4. **Ties**: 5000 plastic zip ties were used to tie the bars and the duct to have a complete "steel free" structure.
5. **Plastic duct**: The bridge is ~13 m (43 ft) long, so a ~13.7 m (45 ft) long duct was necessary for each tendon, plus three ~1.5 m (5 feet) long pieces of duct coming out from the deck and inserted through a T connector to the previous duct in the way to inject the grout. Hence, the needed amount was about ~18 m (60 ft) of ~2.3 cm (9/10 in) diameter plastic duct for each tendon, for a total amount of ~400 m (1300 ft). Adding thirteen ~13.7 m (45 ft) long safety ducts (plus two ~1.5 m long coming out pieces), plus a supply, the overall duct length was ~700 m (2300 ft).
6. **T connectors**: Three T connectors of ~2.5 cm (1 in) internal diameter for each tendon trace were provided, so as to create a straight duct with a 3rd piece coming out in the way to inject the grout. Twenty-six tendons require 78 T connectors, plus 26 T connectors for the safety duct, equals 104 T connectors, with supplies; hence, 110 T connectors were needed overall.
7. **Injection grout**: The Sikadur 300 PT is the grout for injection that was used for the bridge. Every bag is about ½ cubic foot, thus considering 39 per ~13.7 m (45 ft) long duct, ~2.3 cm (9/10 in) in diameter with a ϕ9 (#3) tendon inside, ~0.26 m^3 (9.35 ft^3) of grout was ordered, and 20 bags of Sikadur 300 PT were provided.
8. **Concrete**: The ~12*6*0.25 m^3 (40*20*0.83 ft^3) slab required ~21 m^3 (750 ft^3) of concrete, with supplies.

In addition, the following tools were used to pull the CFRP tendons:

1. **Stereophone packs**: Two ~37*25*25 cm^3 (12*10*10 in^3) stereophone packs were assembled to house the tendons, at the same time providing enough room to push the wedges inside the chucks before cutting the post-tensioned bars. More details will be itemized later.
2. **Chucks**: Pulling 13 tendons per time, 2 chucks for each tendon and 2 more after the 2 hydraulic jacks when the load was applied were deemed needful. Therefore, 28 chucks

were requested overall. Each chuck includes an outer steel cylinder, a four-piece steel wedge, and an inner copper sleeve (the same type used for the specimens load test; see section 3).

3. **Steel Plates**: Each tendon needed two steel plates between the edges of the slab and the pulling machine. Thus, 26 ~(10*10*1.3) cm^3 (4*4*1/2 in^3) steel plates were required. All the steel plates had a 1.9 cm (0.75 in) inner hole to avoid excessive transversal movement of the tendons.

Additionally the following equipment was used for the prestressing operations:

- 2 hydraulic jacks (40 tons) to pull the tendons from each side of the slab.
- 2 load cells (~222 kN, i.e. 50 kips each) to monitor the applied load.
- 1 injection pump to inject the grout inside the duct.
- 4 wedges hammers to push the wedges inside the chucks.
- Orange box, an easily transportable system that records the load, the strains, and the deflections.
- Wooden boards to build a surface suitable for the post-tensioning, given the skewness of the slab.

5.4.2 Outline of tasks

The installation of the deck proceeded based on the following tasks:

- Partial embedding of anchoring GFRP bars into the central wall, already described before.
- Laying of neoprene pads on the two external walls and on the abutments.
- Setting of the formwork.
- Installation of bottom chairs, bottom longitudinal and transversal GFRP bars.
- Installation of top chairs, top longitudinal and transversal GFRP bars.
- Placing of the GFRP reinforcement for the barrier.
- Placing of ductwork, T connectors, and CFRP bars inside the ductwork; setting of the safety ductwork.
- Pouring and curing of concrete.
- Post-tensioning of CFRP tendons.
- Injection of grout inside the ductwork.

- Cutting of the tendons outside of the slab after the curing of the grout.
- Cutting of the slab's edges.

5.4.3 Investigation of the Slab Construction

On August 13, 2004, the installation work started, but given the lack of some hangers (see details in Figure 80 and Figure 81), the activities could begin again on August 17, 2004.

Figure 80 - Formwork Hangers Details

Figure 81 - Laying of the Formwork

After the installation of the formwork, on August 18, 2004, the following operation of gluing the Styrofoam on the two abutments and on the two walls that didn't have the GFRP anchoring rebars was performed (see Figure 82).

Figure 82 - Gluing and Placing of Styrofoam

Hence, the Neoprene pads were placed in the space created in the Styrofoam as shown in Figure 83. The Neoprene pads were used to avoid horizontally restraining the slab, thereby effectively post-tensioning it.

Figure 83 also shows the plastic chairs that supported the bottom layer of GFRP mild reinforcement.

Figure 83 - Neoprene Pads and Plastic Chairs Details

The placing of the FRP reinforcement was sped up thanks to the presence of many students from RTI, lead by Mr. Harold Martin, who envisioned this as an opportunity to teach his students new technologies (see Figure 84 and Figure 85).

Figure 84 - Laying of Bottom Layer of GFRP Rebars

Figure 85 - The RTI Team with (from bottom left) Mr. Cochran, the author, and Mr. Cox

On August 21, 2004, the top layer was also laid after placing all the GFRP top chairs. Furthermore, according to the design reported in Figure 59, the GFRP rebars for the barrier were also placed.

Figure 86 - Top GFRP Layer

A wooden board was built to make the slab surface perpendicular to the tendons. This operation was performed to ease the post-tensioning phase. An alternative solution would have been to build a skewed slab, but that solution would have required the development of a more sophisticated tool to pull the tendons. The position of the wooden triangles was designed to have the two tendons full centering each board. After the post-tensioning, the slab portion coming out of the abutments had to be cut (see Figure 87 and Figure 88).

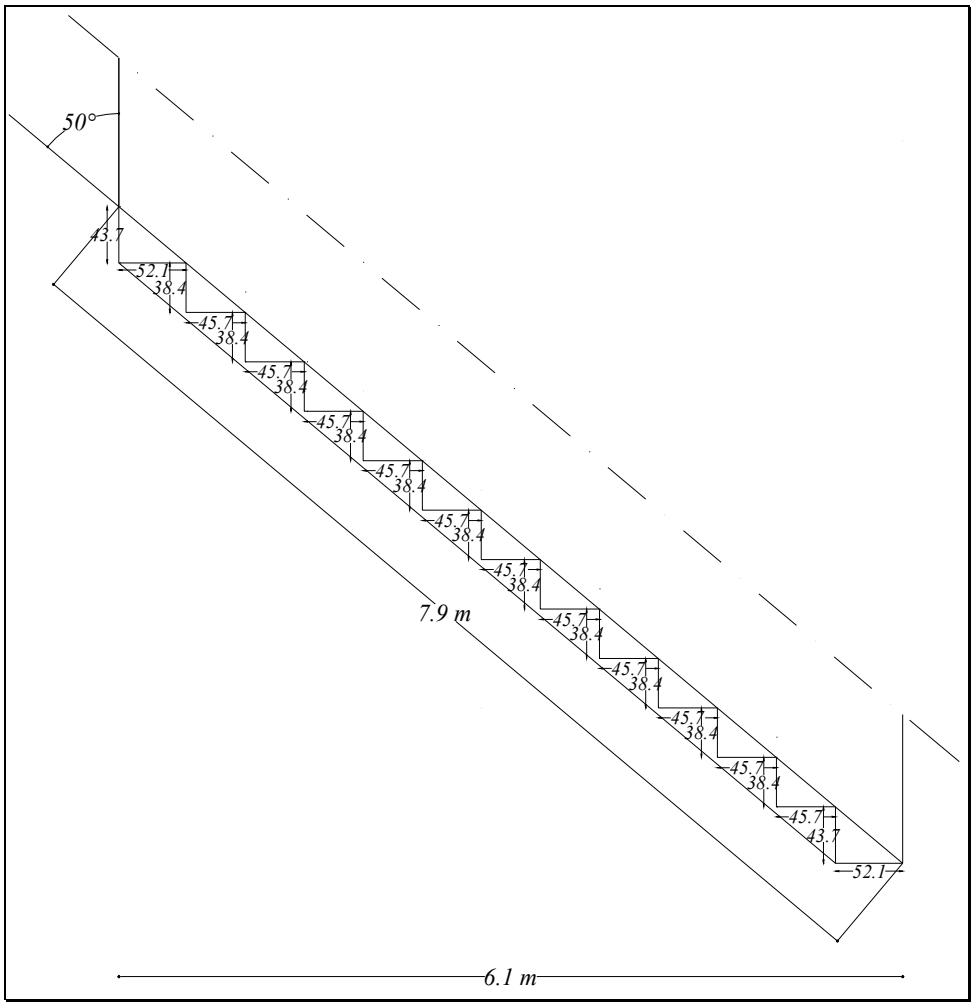

Figure 87 - Board Detail

Figure 88 - Wooden Board (the wire indicates the position of the tendons)

On August 23, 2004, the plastic ducts were placed and tied to the GFRP rebars as prescribed in the design specifications. Thirteen additional safety ducts were placed (as shown in Figure 89 and Figure 90) straight and carefully tied to avoid their floating on the liquid concrete during the pouring.

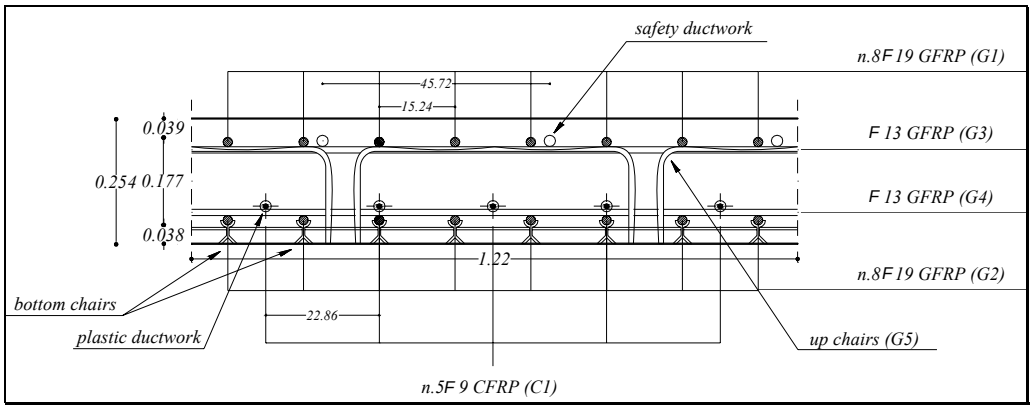

Figure 89 - Slab Section

Figure 90 - Plastic Ducts Detail

T connectors were used on each end (see Figure 91) to allow the injection of the grout as specified in the construction specifications in Appendix D.

Figure 91 - T Connectors Detail

Strain gages were also attached on the GFRP bars (see Figure 92), and they were positioned as shown in Figure 93.

Figure 92 - Attaching of a Strain Gage

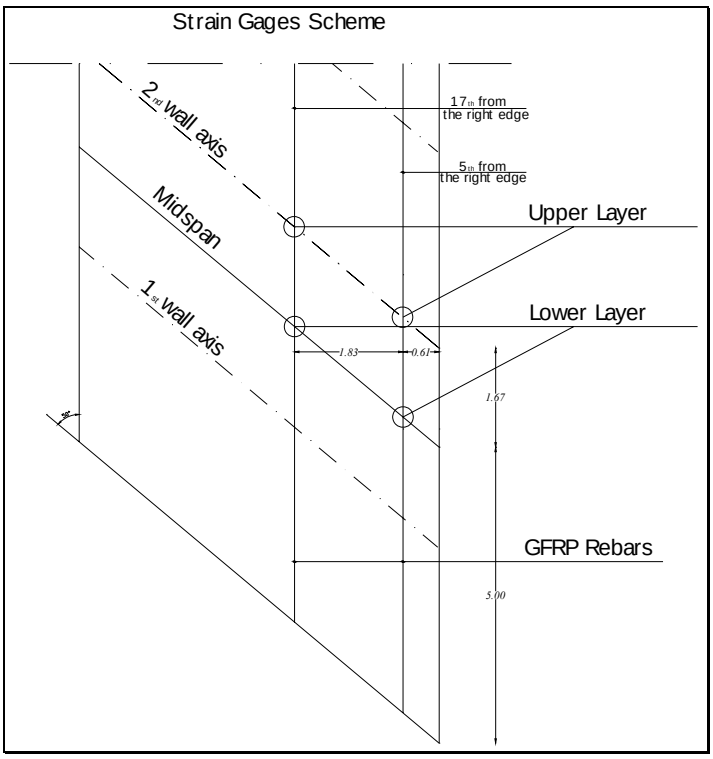

Figure 93 - Strain Gages Scheme

The bridge deck was poured by the city workers on August 25, 2004. The pour began at 7:30 a.m. and was finished at 9:30 a.m. (see Figure 94).

Figure 94 - Pouring Fragments

To let the concrete fill all the voids inside the FRP cage, a more liquid concrete was used (Slump Test = 9 cm, ~4.5 in.), with the addition of super-plasticizers that increase the slump without detrimental effects on the concrete strength. A total of 16 concrete cylinders were also prepared (see Figure 95). Figure 96 shows the just-poured slab.

Figure 95 - Concrete Cylinders Execution and Slab Leveling

Figure 96 - Poured FRP Bridge Deck

5.4.4 Post-tension of the Slab

After a week of curing the slab, on September 1, 2004, the CFRP tendons were post-tensioned. The pulling was achieved by means of the machine already used for the two test specimens. Modifications were required afterward to decrease its weight and improve its functionality. These improvements were accomplished with the help of Mr. Max Vath, a Rolla Technical Institute instructor. Moreover, some handles were joined to better and more easily transport it from one tendon to another (see Figure 97).

Figure 97 - Pulling Machine Before and After the Optimizations

Figure 98 shows the modified pulling device. The device is comprised of an open steel box having enough room to push the wedges inside the chuck after pulling the tendon, a hydraulic jack to apply the pulling force, a round steel plate, a load cell to measure the load, a second plate, and a second chuck. Figure 99 details the terminal part of the pulling machine.

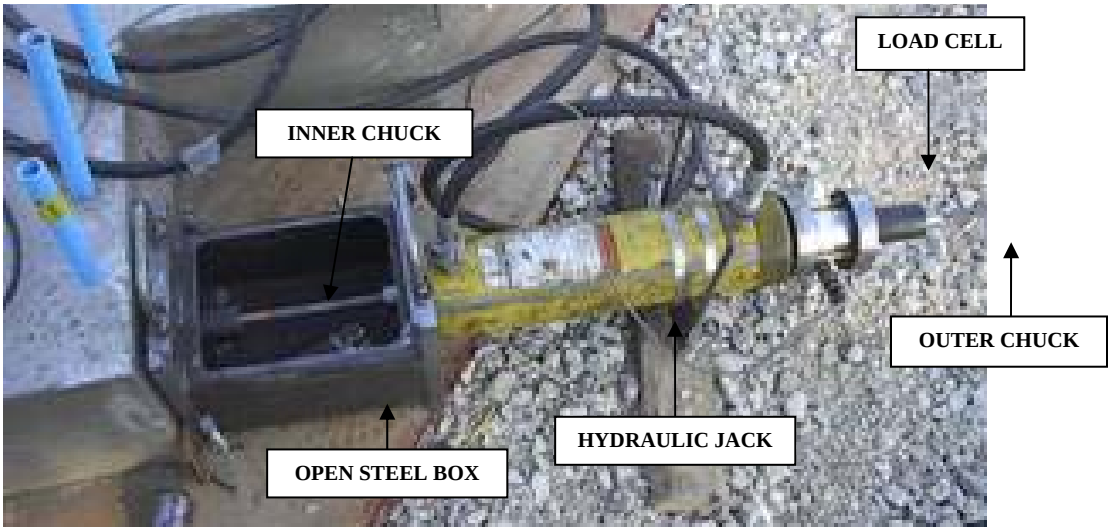

Figure 98 - New Pulling Machine Ready for Use

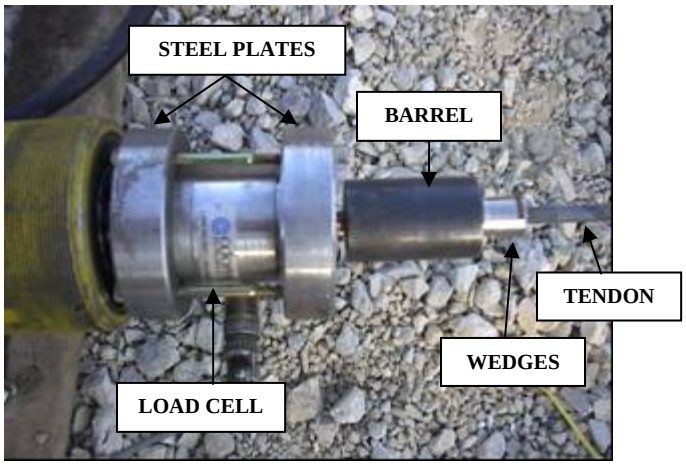

Figure 99 - Load Cell and External Chuck Detail

Before pulling the tendons, they were carefully cleaned from grout, grease, or dust. The wedges were then pushed inside the external chuck to provide a grip, using a copper sleeve (shown in the 3rd section). The tendons were pulled by means of two hydraulic jacks, connected to two pumps using load steps of 13-22 kN (3-5 kip) per side. The use of a single pump with two jacks connected in series was considered, but it was found to be harmful for the tendons as the applied load was not uniform along the tendon. A special two-part steel hammer was built to push the wedges into the barrel (see Figure 100).

The applied load was measured using a data acquisition system (Orange Box) connected to a computer monitoring the applied load in real time (see Figure 101).

Figure 100 - Hammer Detail and Use on the Site

Figure 101 - Orange Box

After reaching the desired load of 62.3 kN (14 kips), corresponding to 45 percent of the maximum allowable load to avoid the breaking of the tendons for the tight grip, the wedges were pushed inside the inner chuck, so the jacks were released, engaging in such way the inner chucks. At this point, the pulling device could be removed by cutting the FRP bar with an electric saw (see Figure 102). Figure 103 details the load vs. time diagram of the first tendon, showing how after reaching the desired load, the inner chucks let the stress be constant.

Figure 102 - Wedges Insertion and Cutting of the Tendon

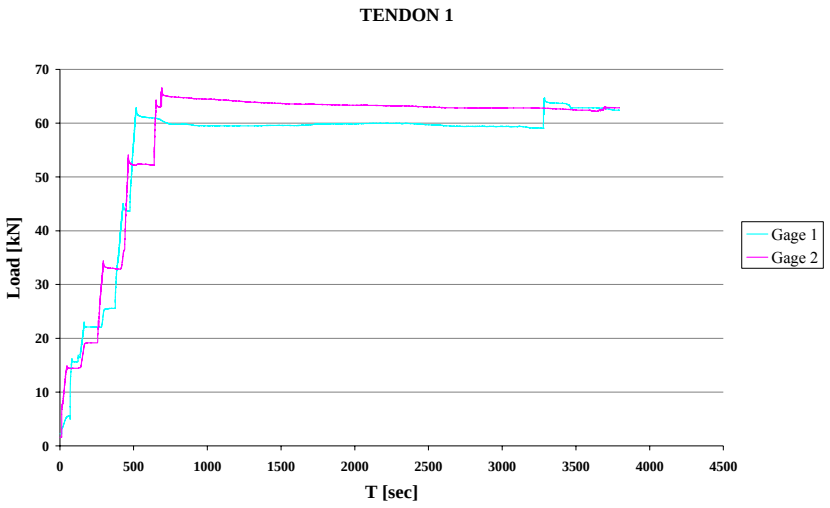

Figure 103 - Load vs. Time Diagram of Tendon 1

In two weeks, the first half of the tendons was pulled (see Figure 104). Some delays occurred due to further changes of the pulling machine to better suit the slab surface. Having a surface perfectly perpendicular to the tendon was not always possible.

Figure 104 - First Set of Pulled Tendons

The injection of grout followed the pulling of the tendons and was carried out with the use of a pump, after sealing the chucks to avoid grout leaking (see Figure 105).

Figure 105 - Grout Injection and Slots Locking

After four days of curing, the inner chucks were removed by drilling the tendons inside of those.

On October 7, 2004, the second set of tendons was pulled after a stop intermission of two weeks for a scheduled load test that the contractor had to carry out in Wisconsin. The works could then continue; thus, the grout was also injected in the safety duct.

Eventually the extra part of the slab added for the post-tension was cut using a big cutter, as shown in Figure 106. On October 15, 2004, the Southview bridge deck was completed (see Figure 107).

Figure 106 - Cutting of the Slab Edge

Figure 107 - Southview Bridge-Deck Completed

Finally, a barrier with GFRP reinforcement was built on the new "FRP side" (see Figure 108) to have a comparison over time with the steel reinforced concrete barrier on the opposite side, which was also built. This solution will contribute by showing the increased durability of a bridge deck using FRP materials as reinforcement, mainly due to the absence of corrosion. The construction of the bridge was completed in June 2005.

Figure 108 - Bridge after Completion

6 BRIDGE LOAD TESTING

Although in-situ bridge load testing is recommended by the AASHTO (2002) Specification as an "effective means of evaluating the structural performance of a bridge," no guidelines currently exist for bridge load test protocols. In each case the load test objectives, load configuration, instrumentation type and placement, and analysis techniques are to be determined by the organization conducting the test.

In order to validate the behavior of the bridge, shortly after construction of the bridge, the behavior of the bridge under load was examined. A picture of the bridge during the load test is shown in Figure 109.

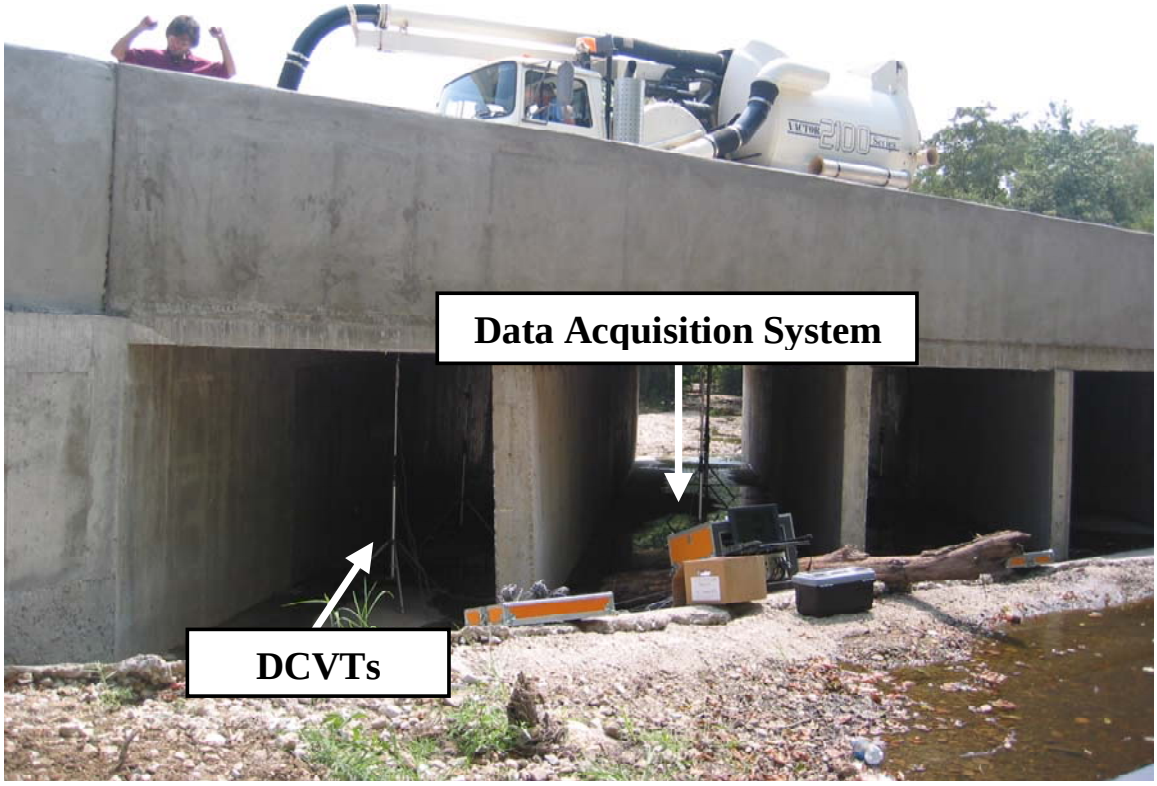

Figure 109 - In-situ Bridge Load Test

Instrumentation utilized during the testing included direct current variable transformer (DCVT) transducers installed underneath the bridge to monitor deflection and electrical strain gages bonded on the concrete surface in the direction of the traffic. The strain gages installed on the FRP bars during construction did not work at the time of the testing. The location of the sensors is illustrated in Figure 110, with the symbol denoting each individual instrument.

Eight DCVT transducers were located at mid-span between four consecutive supports. No sensors were installed on the fourth span since the cables were not long enough to reach it. The two strain gages were installed in correspondence with DCVT 1 and DCVT 3.

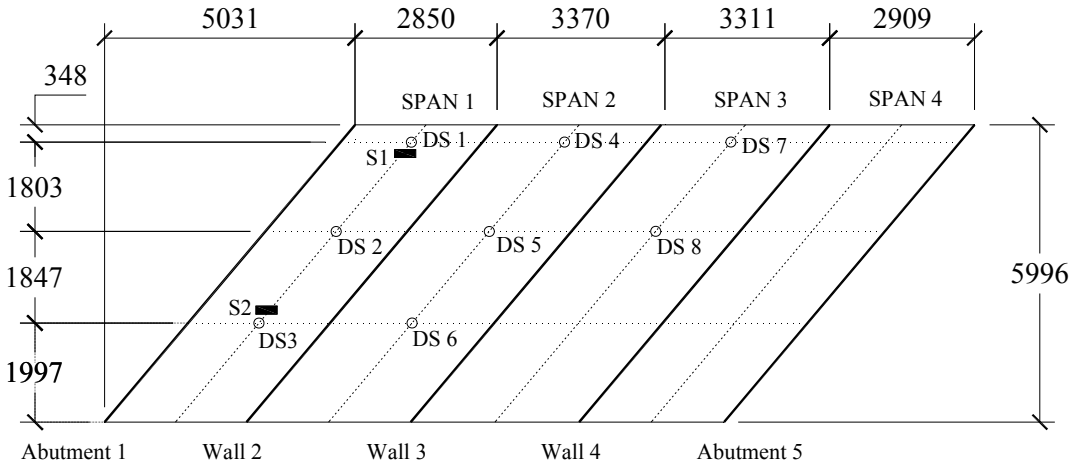

Note: DS = DCVT and S = Strain Gage

Figure 110 - Location of the Sensors

Loading of the bridge was accomplished with a loaded dump truck placed at various locations on the bridge. Figure 111 shows the truck's geometry and load per axle. The total weight of the truck was 241 kN with 148 kN and 93 kN on each of the two axles from the front to the rear of the truck, respectively. Although dump trucks and HS20 trucks differ in their geometries, the loading configuration that maximizes the stresses and deflections at mid-span could still be accomplished

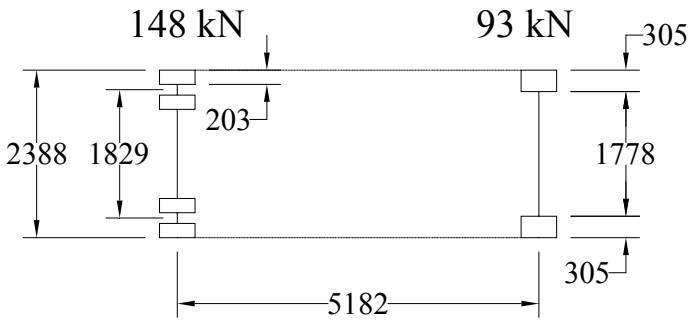

Figure 111 - Truck Used for the Load Testing

Two passes of the truck were made, each at a different transverse position on the bridge as shown in Figure 112. During each pass the truck was stopped at four longitudinal locations corresponding to the middle section of each span as shown in Figure 112. During each stop, the truck was stationary for at least two minutes before proceeding to the next location, thereby allowing stable readings.

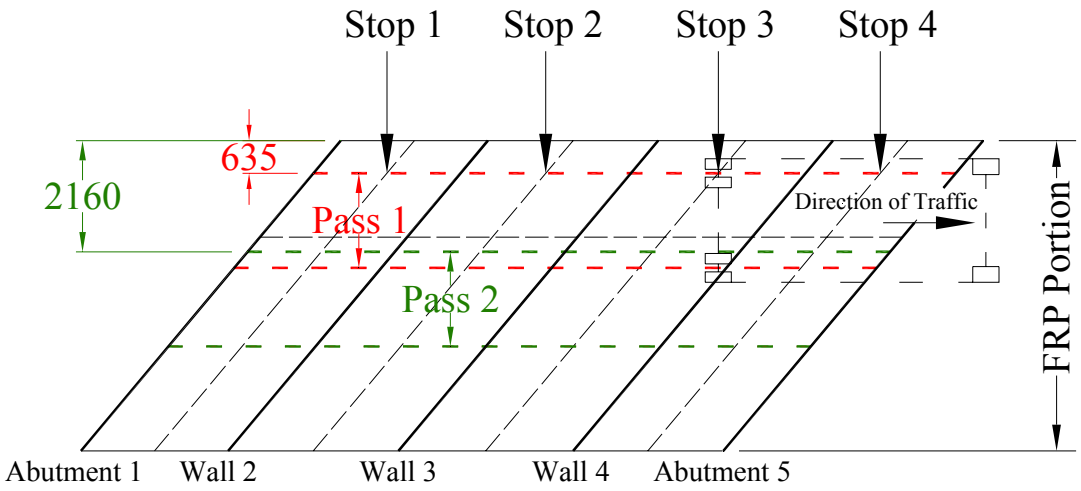

Figure 112 - Lateral Location of the Truck During the Load test

The bridge performed well in terms of overall deflection. In fact, the maximum deflection measured during the load test was 0.35 mm, which is below the allowable deflection prescribed by AASHTO, 2002, Section 8.9.3 ($\delta_{max} \leq L/800 = 3.8$ *mm)*. Such small displacements of the bridge were explained with the arching action occurring due to the short spans and considerable thickness.

To validate the data obtained from the load tests, a linear elastic FEM analysis was conducted. For this purpose a commercially available finite element program SAP2000 was used.

Solid elements were chosen to model the concrete. The solid element is a brick element defined by eight nodes having three degrees of freedom at each node.

For this project, the material properties of concrete were assumed to be isotropic and linear elastic, since the applied load was relatively low. The modulus of elasticity of the concrete was based on the measured compressive strength of the cylinders obtained at the pouring of the slab according to the standard equation ACI 318-05 Section 8.5.1:

$$E_c = 57000\sqrt{f_c'} \approx 24.8\ GPa$$

Each element was meshed to be 89 mm × 127 mm × 152 mm. The bridge was modeled as hinged in correspondence with each supporting wall. The load was applied on 8 nodes, simulating the truck wheels. A picture of the finite element model is shown in Figure 113.

The experimental and analytical results for pass 2 in the transversal direction are reported in Figure 114. The graph shows the good match in deflection between the experimental and analytical results; therefore, it can be used to asses the performance and the load rating of the bridge over time.

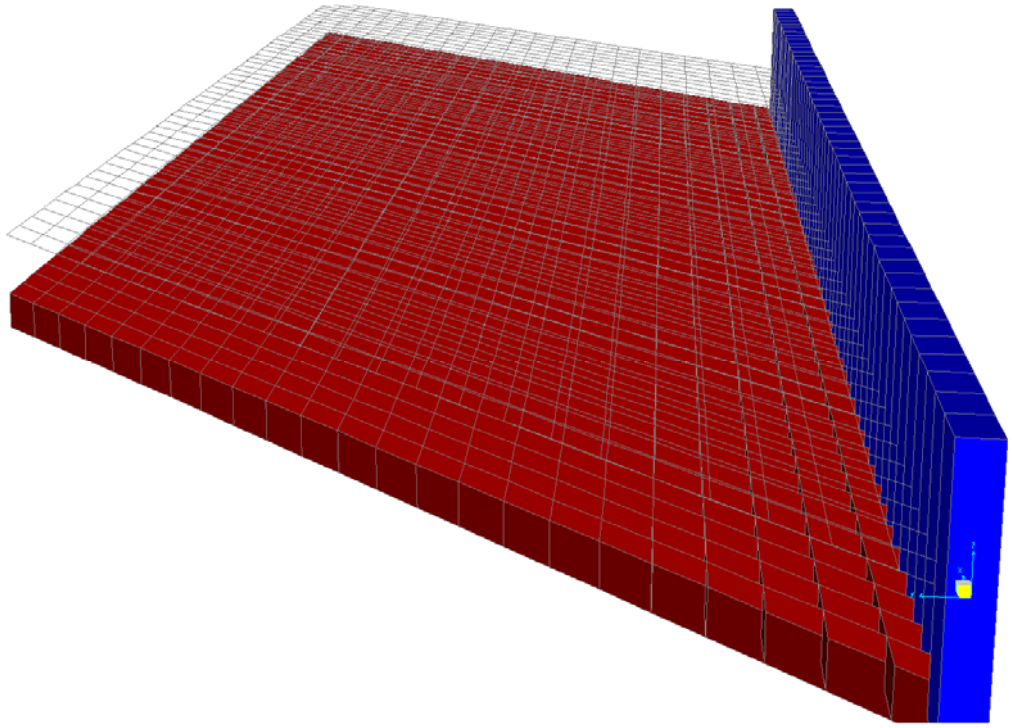

Figure 113 - FEM Model Geometry

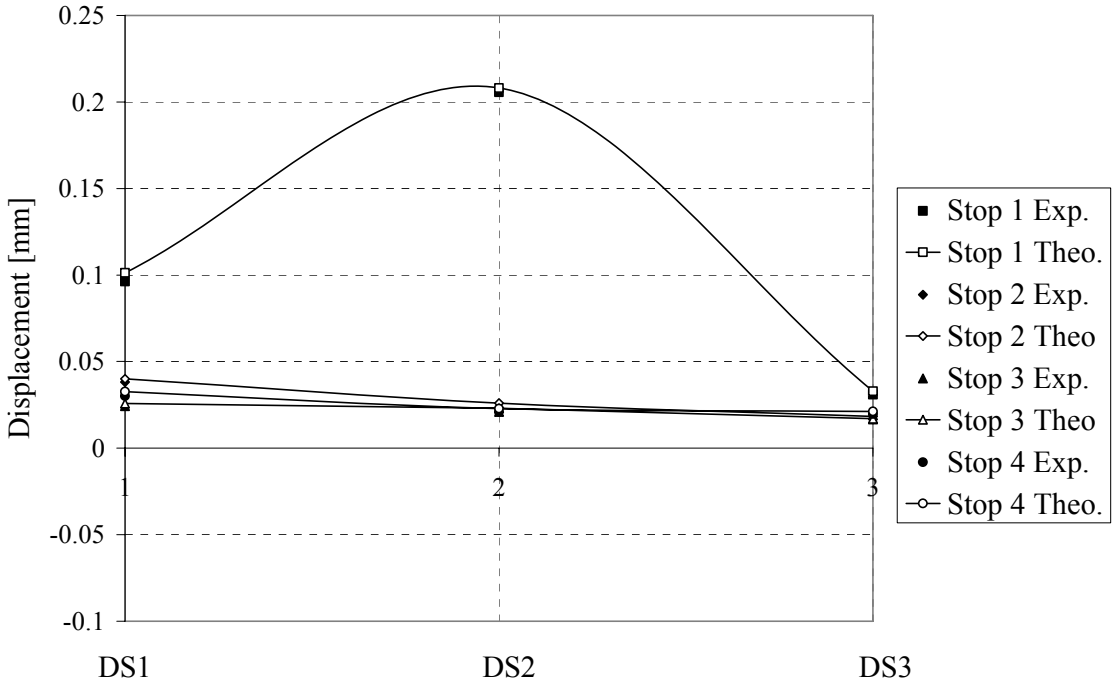

a) Span 1

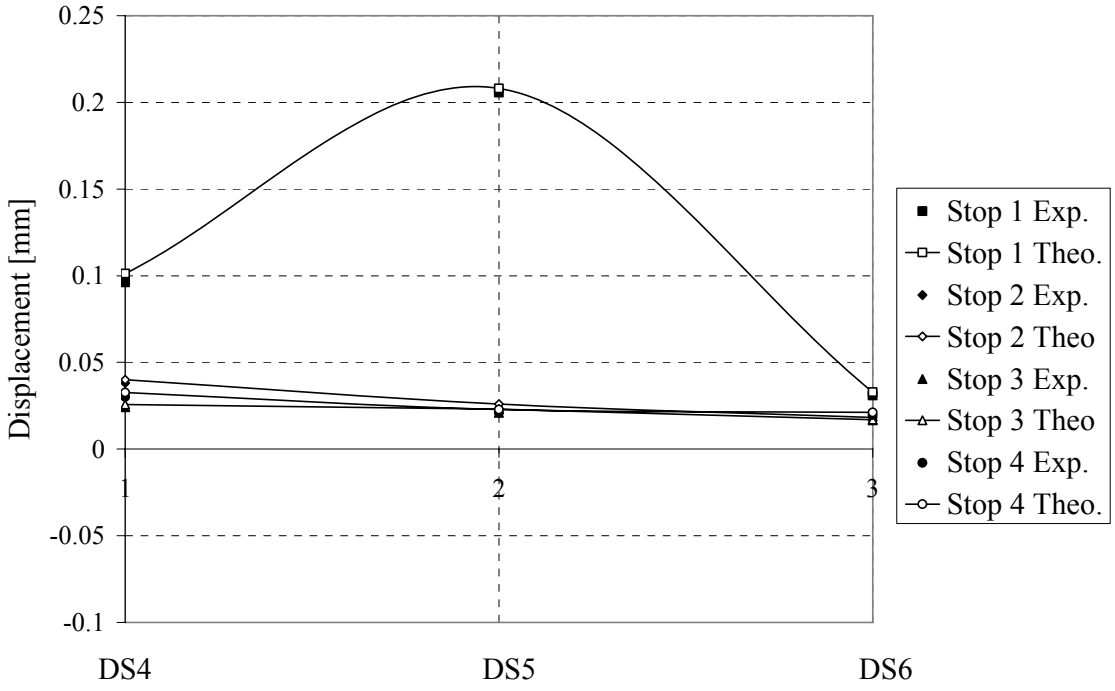

b) Span 2

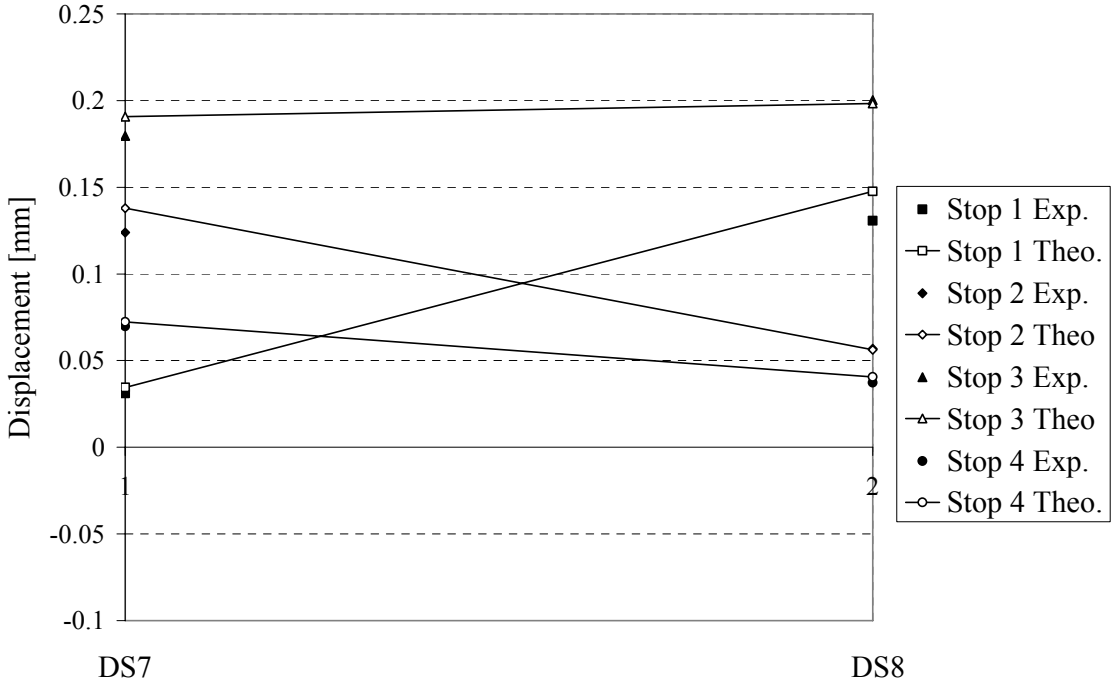

b) Span 3

Figure 114 – Comparison Between Experimental and Theoretical Results

7 CONCLUSIONS

The present thesis dealt with a new technology, explored with the literature review, validated experimentally, and verified in the field; it is part of a series of collaboration activities between the University of Naples-Federico II and the University of Missouri-Rolla (UMR).

The project developed is a further step in the study and use of FRP in civil engineering; in fact, the use of FRP both for mild reinforcement (Glass FRP) and for post-tensioned reinforcement (Carbon FRP) was required for the construction of a bridge deck in the City of Rolla, Missouri.

The objectives of the project at UMR were as follows:

1. Evaluate the feasibility, behavior, and effectiveness of the new deck system, showing how FRP, in the form of GFRP as passive and CFRP bars as active internal reinforcement, could be an excellent solution replacing the steel.

2. Provide analytical data in support of the enhanced shear capacity of the concrete slab due to the CFRP prestressing.

Information on existing prestressing and non-prestressing FRP bridge decks has been given in section two, so they can be compared with the new deck system that is the subject of this thesis. A summary of the main research works on shear behavior of prestressed FRP was also given, showing the lack of research projects on the specific topic of this thesis.

Section three dealt with pre-construction investigations that were conducted on two specimens representing a deck strip 457 mm (18 in) wide and 7 m (23 ft) long, with the same geometry and amount of reinforcement. They were built and tested, one to investigate the flexural behavior, the one to investigate the shear behavior. The two beams were constructed by the contractor peculiar for the project, which allowed him to become familiar with the use of non-conventional materials. Their testing as continuous slabs over three supports validated the design calculations in terms of flexure and shear capacities.

The specimens were reinforced using 3 ϕ19 (6/8 in) GFRP bars as top and bottom mat and 2 ϕ9 (3/8 in) CFRP bars as prestressed tendons.

The position of the prestressed tendons was varied along the slab to match the moment demand. In addition, to reproduce the actual field conditions, ϕ13 (4/8 in) GFRP bars spaced 305 mm (12 in) on center were placed in the transversal direction as temperature and shrinkage reinforcement.

The experimental results were compared with the theoretical moment and shear capacities of the slabs computed according to ACI 440.1R-03 provisions and the equation developed by Tureyen A. K. and Frosh R. J.

According to ACI 440, the shear capacity increased from 30.7 kN (6.9 kip) with mild reinforcement to 69.8 kN (15.7 kip) after adding the post-tensioned reinforcement, while the flexural capacity remained just the same, thereby showing that the prestressing material is mostly needed for shear purposes rather than for flexure.

On the basis of the experimental investigation, GFRP bars as passive and CFRP bars as active internal reinforcement can be concluded to represent a feasible solution replacing the steel reinforcement of concrete slab bridges.

The objective of section four was to provide the structural analysis of the new FRP concrete bridge deck based on the AASHTO HS20-44 design truck and provide calculations for its design using a combination of non-traditional, corrosion-resistant composites materials.

Consistent with AASHTO specifications, two load configurations were considered—the HS20-44 design truck and the design lane. The concentrated load and uniform load were considered to be applied over a *3.0 m (10ft)* width on a line normal to the center line of the lane. These loads were placed in such positions within the design lane so as to produce the maximum stress in the member.

Since the design truck analysis produced the highest stresses on the slab, only moment and shear related to this analysis were considered.

The design of the internal FRP reinforcement was carried out according to the principles of ACI 440.1R-03, using the same percentage of reinforcement already used and tested in the experimental phase.

Consistent with section 3, researchers noted that the prestressing force is most needed for shear purposes rather than for flexure. In fact, if the prestressing action was not considered, the concrete contribution to the shear capacity of the slab would have been V_c*=220.4 N/m (=15.1 kips/ft)*, and the final factored shear capacity of the bridge would have been equal to ϕV_n*=86.09 kN/m <<* V_u*=148.9 kN/m (*ϕV_n*=5.9 kips/ft <<* V_u*=10.2 kips/ft)*, that is, the shear capacity of the slab with post-tensioning. Therefore, the post-tensioning allowed the shear capacity of the slab to increase by more than 70 percent.

Section five detailed the installation of the Southview bridge deck, focusing on the post-tensioning of the slab, the most considerable and crucial part of the project.

The slab is 0.25 m (10 in) thick, 12 m long (40 ft), and 6 m (19.83 ft) wide. It is supported by three intermediate reinforced concrete vertical walls. The three spans' lengths are, from north to south, 2.89 m (9.49 ft), 3.38 m (11.10 ft), and 3.30 m (10.82 ft) on center.

The erection of the substructure started on July 21, 2004; the extension of the existing abutments and walls was performed by the City of Rolla employees prior to the slab construction.

On August 17, 2004, the installation of the deck was started, after the partial embedding of anchoring GFRP bars into the central wall to provide a fixed central section, therefore avoiding the total slipping of the superstructure during the prestressing operations. Hence, after the laying of formwork, the Neoprene pads on the two external walls and on the abutments were placed to allow the axial sliding of the middle fixed slab.

The installation of bottom and top longitudinal and transversal GFRP reinforcement was completed by August 21, 2004, after which the GFRP reinforcement for the barrier was also placed on the "FRP side."

Wooden boards were positioned to ease the post-tensioning operations, then the ductwork was placed, and the T connectors and the CFRP tendons inside the ductwork were placed by August 23, 2004.

Before pouring, some strain gages were also attached on the GFRP bars of the slab to allow for checking the behavior of the slab in service.

The bridge deck was poured by the city workers on August 25, 2004; after a week of curing, on September 1, 2004, the CFRP tendons were post-tensioned.

The pulling and releasing of the tendons were the newest and the most critical parts of the project.

The pulling of the tendons was achieved by means of the machines already used for the two test specimens, with two hydraulic jacks and special chucks to provide the grip between the machine and the tendons themselves, as detailed in the third section.

On September 15, 2004, after some delays occurred because of further changes to the pulling machine to better suit the slab surface, the first half of the tendons had been pulled, and the grout was injected inside their ductwork.

The same procedure was carried out for the second half of the tendons; thereafter, all the tendons' edges outside of the slab were cut after the curing of the grout.

On October 15, 2004, the edges of the slab were also cut. Finally, a barrier with GFRP reinforcement was built on the new "FRP side" to have a comparison over time with the steel reinforced concrete barrier on the opposite side, which was also built. This solution will contribute by showing the increased durability of a bridge deck using FRP materials as reinforcement, mainly due to the absence of corrosion. The construction of the bridge was completed in June 2005.

The main result of this project has been to show how FRP, in the form of GFRP as passive and CFRP bars as active internal reinforcement, could be a feasible solution replacing the steel reinforcement of concrete slab bridges, and specifically, enhancing the shear capacity of the slab from the CFRP prestressing. Additionally, the in situ load testing has proven to be useful and convincing and the FEM analysis has shown good match with experimental results demonstrating the effectiveness of the reinforcing technique.

Therefore, the following conclusions can be drawn:

- The real advantage in the use of FRP materials as reinforcement of a bridge deck is seen through its increased durability, mainly due to the absence of corrosion. To better show this advantage, a barrier with GFRP reinforcement was built on the new "FRP side" to have a comparison over time with the steel reinforced concrete barrier on the opposite side, which was going to be built after the FRP bridge deck installation.
- Utilizing FRP in the form of reinforcing bars allows for the use of many steel-RC concrete practices. The fabrication and installation details were nearly identical to the methods regularly utilized for steel-reinforced slabs.
- The installation of the bridge highlighted the fact that having an efficient system is as important as having the adequate components. Additionally, for a new technology to succeed, its learning curve must be overcome before its applications can be conducted proficiently.
- Further investigation must be done in this field to improve and refine the techniques related to the post-tensioning of bridge-decks using CRFP, its future development being certainly hopeful and helpful.

8 REFERENCES

Referenced standards and reports

The standards and reports listed below were the latest editions at the time this document was prepared. Because these documents are revised frequently, the reader is advised to contact the proper sponsoring group if it is desired to refer to the latest version.

AASHTO

1994 Manual for Condition Evaluation of Bridges

1996 Design Code for Highway Bridges

2002 Standard Specifications for Highway Bridges", 17th Edition

American Concrete Institute

318-99 Building Code Requirement for Structural Concrete and Commentary

440.1R-03 Guide for the Design and Construction of Concrete Reinforced with FRP Bars

These publications may be obtained from these organizations:

AASHTO
American Association of State Highway
and Transportation Officials,
Washington, D.C.

American Concrete Institute
P.O. Box 9094
Farmington Hills,
MI 48333

Cited references

Abdelrahman, A. A., Tadros, G., and Rizkalla, S. H. ''Test model for the first Canadian smart highway bridge.'' ACI Structural Journal, 92(4), 451–458 (1995).

Burgoyne C.J., "Rational Use of Advanced Composites in Concrete", Structures & Buildings 146, Issue 3, pp. 253-262.

Fico R., N. Galati, A. Prota, and A. Nanni, "Design And Construction of a Bridge Deck Using Mild and Post-Tensioned FRP Bars," ACI, Special Publication SP230-63, KC November 7-10, 1121-1138, (2005).

Galati N, G. Boschetto, A. Rizzo, R. Parretti and A. Nanni, 2004: "Pre-Construction Investigation for the Rehabilitation of a Bridge Using Internal FRP Technologies," 4th International Conference on Advanced Composite Materials in Bridges and Structures - ACMBS-IV, July 20-23, 2004, Calgary, Alberta, Canada, CD-ROM version, 12

Grace N.F., Navarre F.C., Nacey R.B., Bonus W., Collavino L., Sept.-Oct. 2002, "Design-Construction of Bridge Street Bridge-First CFRP Bridge in the United States", PCI Journal, pp.20-35.

Ibell T. and Burgoyne C.J., "Use of Fibre-Reinforced Plastics versus Steel for Shear Reinforcement of Concrete", American Concrete Institute Structural Journal, Nov-Dec 1999.

Park, S.Y. and Naaman P., "Shear Behavior of Concrete Beams Prestressed with FRP Tendons", PCI Journal, 1999, vol. 44, n.1, pp. 74-85.

Nanni, A., 2001, “Relevant Applications of FRP Composites in Concrete Structures,” Proc., CCC 2001, Composites in Construction, Porto, Portugal, Oct. 10-12, 2001, J Figueiras, L. Juvandes and R. Furia, Eds., (invited), 661-670.

Hughes Brothers Inc, October 2003 “Hughes Brothers Reinforcements” Product Guide Specification, Web site: http://www.hughesbros.com.

Sika Corporation, July 2003, “SikaGrout 300 PT” Guide Specification, Web site: http://www.sikaconstruction.com.

Tureyen A. K. and Frosh R. J., 2003: “Concrete Shear Strength: Another Perspective”, ACI Structural Journal, VOL. 100, NO.5 pp. 609-615.

Whitehead P. A. and Ibell T. J., “A Rational Approach to Shear Design In FRP-Prestressed Concrete Structures”, Submitted to ASCE Journal of Composites for Construction in Jan 2004.

Whitehead P. A. and Ibell T. J., “Novel Shear Reinforcement for FRP-Reinforced and Prestressed Concrete”, Submitted to ACI Structural Journal in Feb. 2004.

Zou P. X. W., 2003, “Long-Term Deflection and Cracking Behavior of Concrete Beams Prestressed with Carbon Fiber-Reinforced Polymer Tendons,” Journal of Composites for Construction, Vol. 7, No. 3, 187-193.

Zylstra R, Shing P. B., Xi Y., “Evaluation of FRP Prestressed Panels/Slabs for I-225/Parker Road Project”, Department of Civil, Environmental & Architectural Engineering University of Colorado Boulder, CO 80309-0428.

APPENDIX A: MORE DATA RELATED TO SECTION 2

NON-PRESTRESSED FRP REINFORCED BRIDGE DECKS

Buffalo Creek Bridge, McKinleyville, West Virginia

This is the first bridge in the world to use FRP rebar in construction of the bridge deck. The bridge is owned by the West Virginia Department of Transportation, Division of Highways.

The project to use composite rebar in the bridge deck was a joint effort between the Division of Highways (WVDOH), the Federal Highway Administration, and West Virginia University Constructed Facilities Center (CFC).

The McKinleyville bridge is a 54 m long, 3 span, continuous structure, accommodating two lanes of traffic. The design required a deck thickness of ~23 cm (9 in) and #4 FRP rebars (provided by Marshall Industries Composites, Inc.) as the main transverse reinforcement of ~15 cm (6 in) spacing. The main reinforcement was tied to ϕ9 FRP bars for distribution reinforcement, also at ~15 cm (6 in) spacing. The clean cover for top and bottom reinforcements was ~4 cm (1 ½ in) and ~2.5 cm (1 in), respectively. To support the deck and live loads, M270 grade 50 steel W33X130 rolled beams spaced at 1.5 m on center were chosen.

The bridge was opened to traffic in September 1996 (see Figure 115).

Figure 115 - Buffalo Creek Bridge Construction

Crowchild Trail Bridge, Alberta, Canada

Many of Canada's bridges require upgrading because they were not built to handle the weight of today's increased traffic loads. Calgary's Crowchild Trail Bridge is one such case. The 90 m long, 11 m wide bridge carries two lanes of traffic over its three continuous spans. While the deck slab itself is free of reinforcing, it is supported by five steel girders and external steel straps. In August 1997, GFRP C-bars were used to provide the continuity and to minimize the transverse cracks of the steel-free deck over the intermediate bridge piers. Based on the results of

a full-scale model test at the University of Manitoba, GFRP C-bars were also used to reinforce the cantilever slabs of the bridge. On a tendered basis, this option proved to be the least costly (see detail in Figure 116).

The deck has cantilevers on either side, reinforced with GFRP rods. To reduce surface cracks, the bridge deck concrete contains short random polypropylene fibers.

The bridge is also outfitted with remote monitoring technology, including 81 strain gages, 19 embedded gages, 5 thermistors, 3 smart glass rebars, and 2 fiber optic gages.

Figure 116 - Crowchild Trail Bridge Detail

Joffre Bridge, Québec, Canada

In early August of 1997, the province of Québec accepted the challenge of constructing an innovative bridge using carbon FRP. On opening day December 6, 1997, the Joffre Bridge, spanning the Saint Francois River, became another significant contribution to the ever increasing collection of polymer reinforced bridges in Canada. A portion of the Joffre Bridge concrete deck slab is reinforced with carbon FRP, as is a portion of the traffic barrier and the sidewalk (see detail in Figure 117).

The bridge is outfitted extensively with different kinds of monitoring instruments including fiber optic sensors embedded in the FRP reinforcement (smart reinforcements). Over 180 instruments (fiber optic sensors, vibrating wire strain sensors, and electrical strain gages) are installed at critical locations in the concrete deck slab and on the steel girders to monitor the behavior of the FRP reinforcement under real-time conditions. The instrumentation also provides valuable information on long-term performance of the concrete deck slab reinforced with these new materials, in that all the sensors transmit data to a telephone line for remote monitoring of the structure's behavior.

Figure 117 - Joffre Bridge in Québec

Pierce Street Bridge, Lima, Ohio

This project was originally scheduled to be completely rebuilt with steel rebar. In 1998, the Pierce Street Bridge in Lima, Ohio, was redesigned to accommodate a FRP rebar reinforced bridge deck to prevent the salt-induced corrosion and deterioration that caused the reconstruction in the first place. Using composite bars in place of steel rebar resulted in a 2 percent increase in the total cost of the bridge, but was readily accepted by the state of Ohio and the city of Lima because the inherent corrosion resistance will reduce scheduled maintenance on the bridge over its life span (see Figure 118).

Figure 118 - Pierce Street Bridge Construction

Hall's Harbour Wharf, Nova Scotia, Canada

In February 1998, the mid-section of a 94-year-old breakwater wharf in Hall's Harbour, Nova Scotia, collapsed. The consequent repair initiative resulted in Canada's first marine structure utilizing lightweight, non-corroding GFRP and a steel-free deck.

Hall's Harbour Wharf incorporates three innovative technologies: (a) the use of FRP reinforcement for concrete elements; (b) the use of short synthetic fibers to produce fiber reinforced concrete (FRC); and (c) smart reinforcements for remote monitoring.

The deck panels contain synthetic FRC and utilize an internal compressive arching technology (Figure 119). The panels also contain GFRP rods to reinforce them against the uplift force created by wave action during extreme storm events.

This innovative wharf project is the first Canadian application of both glass FRP and steel-free deck slab technology in a marine environment.

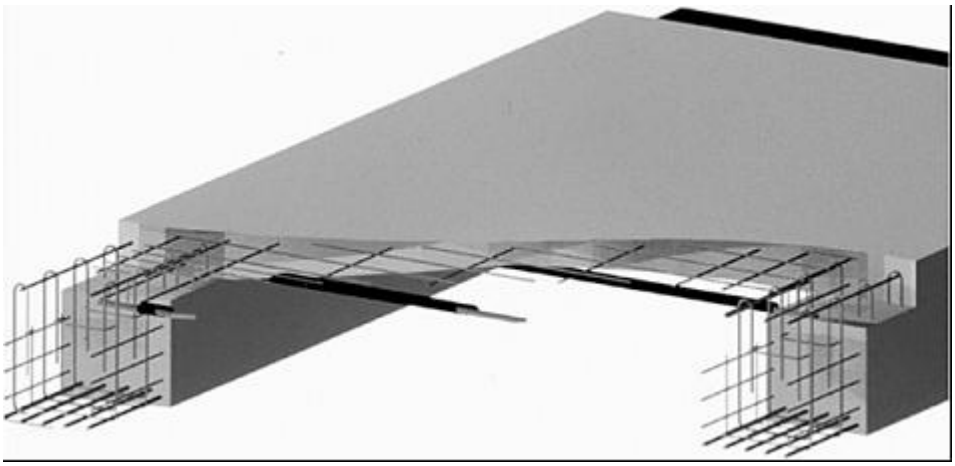

Figure 119 - Cut Away View of the Deck

Taylor Bridge, Manitoba, Canada

A significant international research breakthrough was achieved on October 8, 1998, when Manitoba's Department of Highways and Transportation opened the Taylor Bridge in Headingley. The two-lane, 165.1 m long structure has four out of 40 precast girders reinforced with CFRP stirrups. These girders are prestressed with CFRP cables and bars. GFRP reinforces portions of the barrier walls.

The deck slab was reinforced by indented leadline bars similar to the reinforcement used for prestressing. GFRP reinforcement produced by Marshall Industries Composites Inc. was used to reinforce a portion of the Jersey-type barrier wall. Double-headed stainless steel tension bars were used for the connection between the barrier wall and the deck slab (see Figure 120).

Figure 120 - Tailor Bridge in Manitoba

Salem Avenue Bridge, Dayton, Ohio

This project has a deck surface area of ~6200 m^2 (67,000 sq. ft.) and is the largest composite deck replacement project in the U.S. to date. The C-BAR composite reinforcing bars were used in conjunction with stay-in-place form panels to create the bridge deck that covered about two-thirds of the bridge (see Figure 121). The installation of the deck was completed in November 1999.

Figure 121 - Salem Avenue Bridge, Dayton, OH

Sierrita de la Cruz Creek Bridge, Amarillo, Texas

In the year 2000, the Texas Department of Transportation (TxDot) used GRFP bars as top mat reinforcement in the concrete deck of the Sierrita de la Cruz Creek Bridge constructed near Amarillo, Texas. Placed in service in January 2001, the phase-constructed bridge carries an estimated 1,650 vehicles per day (including approximately 300 trucks, many of which are fully loaded gravel trucks). The new structure replaced a functionally obsolete reinforced concrete

pan-girder structure that had exhibited significant loss of concrete cover due to corrosion-induced deterioration of the steel reinforcement. The all new 13.8 m (45.28 ft) wide bridge consists of seven 24.0 m (78.74 ft) prestressed concrete girder spans, two of which have top mat GFRP-bar reinforced concrete decks. The remaining five spans have top mat epoxy coated steel reinforced concrete decks for performance comparison with the GFRP-bar reinforced concrete decks.

The bridge is the first Texas transportation application of internal FRP reinforcement.

Figure 122 shows concrete being placed on the GFRP-bar mat (manufactured by Hughes Brothers Composites), which is chaired off the precast, prestressed concrete subdeck.

Figure 122 - Concrete Placement in the GFRP Reinforced Concrete Deck

Wotton Bridge, Québec, Canada

Through the NSERC research chair in FRP reinforcements for concrete structures, which started in 2000 at the Department of Civil Engineering, Universitè de Sherbrooke (Québec, Canada), collaboration with the Ministry of Transportation of Québec (MTQ) was established to develop and implement FRP reinforcement in concrete bridges. After the development and improvement of new carbon/glass composite bars and the satisfactory results obtained in the laboratory on concrete deck slab prototypes reinforced with these bars (Benmokrane et al. 2002; El-Salakawy et al. 2003), field applications became a requirement to move forward with this technology. The first and successful field application of these new bars was Wotton Bridge, which is located in the Municipality of Wotton on the 6th Road west, Western Bank, over the Nicolet-Center River in Québec. The bridge is made of four girders simply supported over a single span of 30.60 m. The deck is a 200 mm thick concrete slab, continuous over three spans of 2.65 m each, with an overhang of 1.15 m. The top reinforcement layer of the deck slab for half the bridge was made of GFRP composite bars. Within the same half of the bridge, a 5 m width portion of the bottom layer of the deck slab was reinforced with CFRP composite bars. The other half of the bridge was reinforced with conventional steel. More details about this bridge including the FRP reinforcement configuration and field test results can be found in Benmokrane and El-Salakawy, 2002 and El-Salakawy et al., 2003.

Magog Bridge, Québec, Canada

Located over Magog River on Highway 55 North (Québec, Canada), in the vicinity of Magog City near the US/Canadian border, this bridge has five steel girders continuously supported over three spans. The deck is a 220 mm thick concrete slab, continuous over four spans of 2.85 m each, with an overhang of 1.35 m on each side. The concrete bridge deck slab of the south end span (the first span of the bridge according to the direction of traffic - 26.2 m) was totally reinforced with FRP composite bars in the top and bottom mats. The design resulted in using GFRP (15.9 mm diameter) bars in all directions except in the transverse direction on the bottom mat, where CFRP bars (9.5 mm diameter) were used. The construction of the bridge was completed in September 2002 and opened for the traffic in October 2002 (see Figure 123).

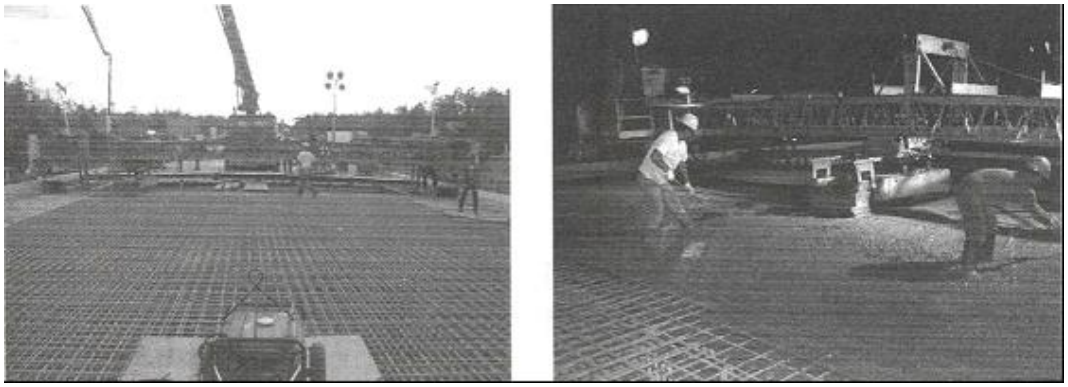

Figure 123 - Bridge Deck Construction

Chatham Bridge, Ontario, Canada

In cooperation with ISIS Canada, the Ontario Ministry of Transportation has rehabilitated the Chatham Bridge crossing Highway 401 to include the world's second steel-free concrete deck slab. (The first, the Salmon River Bridge in Nova Scotia, is also a Canadian achievement.) The two outer spans of the four-span bridge each have a 175 mm thick, steel-free deck slab that is transversely confined with steel straps welded to the top flanges of the steel girders.

The cantilever portions of the deck slab are reinforced by a NEFMAC grid of CFRP. With no steel inside the bridge deck to corrode, the concrete is immune to the damaging effects of chlorides. For engineers, this immunity revolutionizes the way bridges are designed because it means that a relatively thin concrete slab can span a long distance without embedded reinforcement. This result, in turn, means that bridge decks can be virtually maintenance free. The steel-free deck has won five national and international awards (see Figure 124).

Figure 124 - Chatham Bridge Construction

Walters Street Bridge, Missouri

As part of a larger project to investigate the use of FRP materials in bridge construction, a short span, FRP-reinforced concrete bridge was installed in central Missouri. The Walters Street Bridge consists of nine precast concrete panels, each with a depth of 0.30 m (1 ft) and a width of 0.86 m (2.83 ft). Overall, the bridge measures 7.32 m (24 ft) in span and 7.77 m (25.5 ft) in width and has a skew of approximately 12 degrees.

The longitudinal reinforcement consists of three 9.5 mm (3/8 in) CFRP bars, while for the shear stirrups, 9.5 mm (3/8 in) GFRP bars were utilized. Although their contribution to the flexural capacity of the member was not considered, 12.7 mm (1/2 in) GFRP bars were utilized in the top side of the cage. Transverse reinforcement consisting of 12.7 mm (1/2 in) GFRP bars at 1.2 m (4 ft) was also provided in the panels (see Figure 125).

Installation of the Walters Street Bridge began on June 18, 2001. The bridge was officially opened to traffic on June 28, 2001 (see Figure 126). A cast-in-place concrete box culvert would have been the alternative to this bridge technology and would have taken significantly longer to install.

Figure 125 - FRP Reinforcement Layout

Figure 126 - In Situ Load Test – Walters Street Bridge

PRESTRESSED FRP REINFORCED BRIDGE DECKS

Ulenbergstrasse Bridge, Germany

The Road, Bridge and Tunnel Department of the City of Dusseldorf decided that this bridge, which is part of a heavily frequented road, should have been built with the innovative prestressing system. Opened to traffic in 1986, the Ulenbergstrasse Bridge represents a milestone for the continuous progress in development of the glass fiber prestressing technology. Countless initial trials with the new bar material were carried out both in the laboratories of the joint venture partners and at notable German universities, so finally all the knowledge gained could be concentrated in the bridge structure.

The Ulenbergstrasse Bridge is a two span, solid slab bridge with span widths of 21.30 m and 25.60 m. The 1.44 m high and 15.0 m wide superstructure received limited longitudinal prestressing with a total of 59 HLV prestressing tendons ("HLV Elements" is a joint venture), each with a working load of 600 kN, and was subsequently grouted with a synthetic resin mortar specially developed for this purpose. Measurements taken during the work, particularly tensioning paths during prestressing and deflection after handover to traffic, conformed well to the previously calculated values (see Figure 127 and Figure 128).

Figure 127 - Overall View of the Ulenbergstrasse Road Bridge

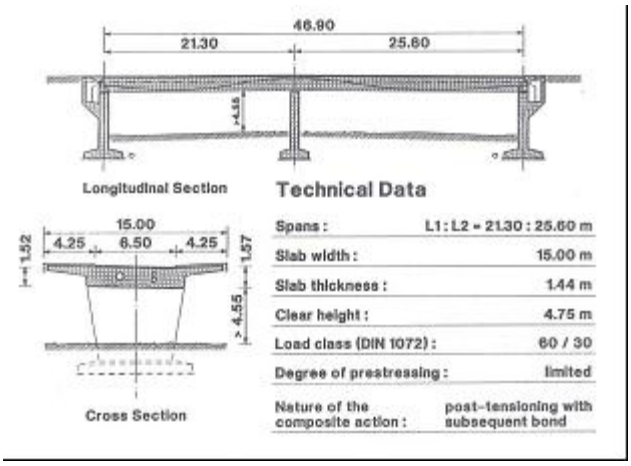

Figure 128 - Technical Data of the Ulenbergstrasse Road Bridge

Application of FRP Materials to Prestressed Concrete Bridges and Other Structures in Japan

A series of national projects to develop the necessary technology for utilizing FRP materials as tendons for prestressed concrete bridges was conducted over a four-year period in Japan, form 1989 to 1992. The project was carried out by the Public Works Research Institute of the Ministry of Construction in conjunction with 10 general contractors. Tests and studies on the properties of the various types of FRP tendons and the required anchorage systems were performed.

Here the experience of applying these materials to prestressed concrete bridges is described.

Table 13-Examples of Prestressed Concrete Bridges in Japan Using FRP Materials

Bridge name	Fiber	Structural type	Span (m)	Width (m)	Tendon	Reinforcement	Completion
Pedestrian	Glass Grid	Pretensioned slab	5.0	1.2	Grid 15 cm	Grid GFRP	1988
Shinmiya	Carbon (PAN) Strand	Pretensioned slab	5.6	7.0	Φ 12.5	Epoxy reinforcing bar	1988
Nagatsugawa	Carbon (PAN) Strand Rod	Pretensioned slab	8.0	2.5	Φ 12.5	Rod CFRP	1989
Bachigawa minami	Carbon Rod	Post-tensioned slab	17.55	12.3	8 Φ 8 Multiple	Reinforcing bar Steel	1989
Tulvas	Aramid Braided	Pretensioned slab	11.98	2.4	Φ 14	Reinforcing bar Steel	1990
Aramid PC	Aramid Deformed rod	Pretensioned slab	12.39	4.59	3 Φ 6 Multiple	Deformed rod AFRP	1990
	Aramid Deformed rod	Post-tensioned Box girder	24.88	4.59	19 Φ 6, 7 Φ 6 Multiple	Reinforcing bar Steel	1990
Birdle	Aramid Polygonal	Post-tensioned Suspended slab	46.5	2.1	8 Φ 4.86 x 19.5	Strand CFRP	1990
Hakui	Carbon (PAN) Strand	Pretensioned Hollow slab	10.5	3.5	Φ 12.5 CFRP	Strand	1991
Takahiko	Aramid Braided	Pretensioned floating	54.87	4.0	Φ 14 AFRP	Braided	1992

In 1988, CFRP strands were first used as prestressing tendons for the Shinmiya Bridge in the Ishikawa Prefecture. The bridge has a 7.0 m (22.9 ft) wide pretensioned concrete slab deck

spanning 5.76 m (18.9 ft) across the supports. It is located in the same prefecture where the oldest prestressed concrete bridge in Japan was constructed about 40 years ago.

The prestressing tendons used in Shinmiya Bridge were 12.5 mm (0.5 in) diameter CFRP strands. Six of these strands were placed in the bottom of the slab, with two strands located near the top. Epoxy-coated reinforcing bars were used as stirrups. CFRP strands were also used as prestressing tendons for the Hishinegawa Bicycle Bridge at the same prefecture in 1992 (see Figure 129).

Figure 129 - General View of Concrete Bridge Prestressed with CFRP Strands

Pre-bent CFRP rods were used as stirrups. CFRP rods were first used as prestressing tendons in a simple two-span post-tensioned concrete highway bridge in 1989 as part of the Bachigawa-Minami-Bashi Bridge in Kitakyusyu City. The two-span bridge is 12.3 m (40.5 ft) wide and 35.8 m (117.5 ft) long. The deck structure comprises an 18.25 m (59.9 ft) span with pretensioned girders and a 17.55 m (57.6 ft) span with post-tensioned girders. Details of the bridge are shown in Figure 130.

CFRP rods were used in one of the two post-tensioned girders with a solid rectangular cross section. Eight multi-cable tendons with eight 8 mm (0.3 in) diameter CFRP rods each were used in the post-tensioning.

Aramid FRP bands were used as prestressing tendons in a pedestrian bridge built on a golf course in 1990 in the Ibaraki Prefecture. The bridge has a post-tensioned suspended slab that is 54.5 m (178.8 ft) long and 2.1 m (6.9 ft) wide. Eight of these bands were combined to form a single tendon; a total of 16 tendons were used.

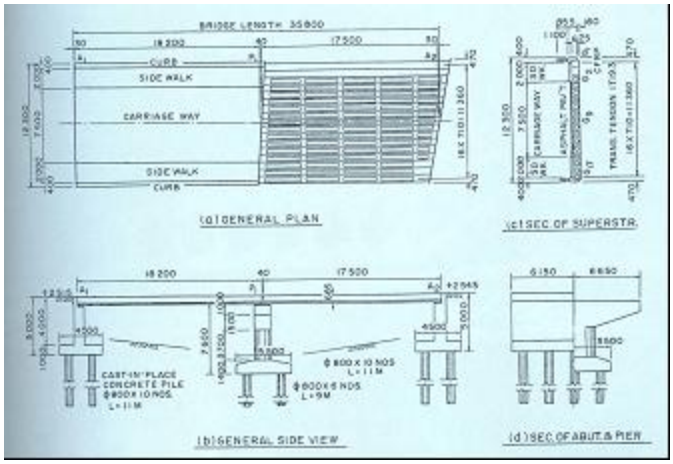

Figure 130 - General Details of Batigawa-Minami-Bashi Bridge

Schiessbergstrasse Bridge, Germany

In the course of service in connection with the Bayer multi-story car park, the Schiessbergstrasse Bridge, to the north of the Bayer plant in Leverkusen, was elevated to the second level. The three-span road bridge with span widths of 2 x 16.30 m and 1 x 20.40 m and a slab thickness of 1.10 m has limited prestressing with 27 post-bonded glass fiber prestressing tendons with a working load of 600 kN each. The handover to traffic was in November 1992 (see Figure 131 and Figure 132).

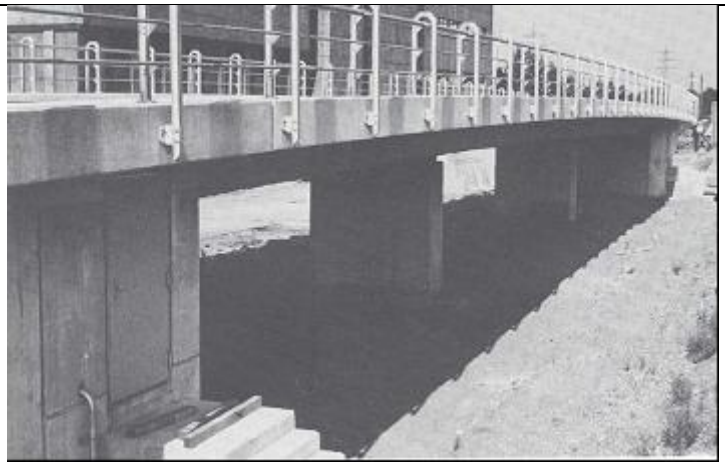

Figure 131 - Schiessbergstrasse Bridge View

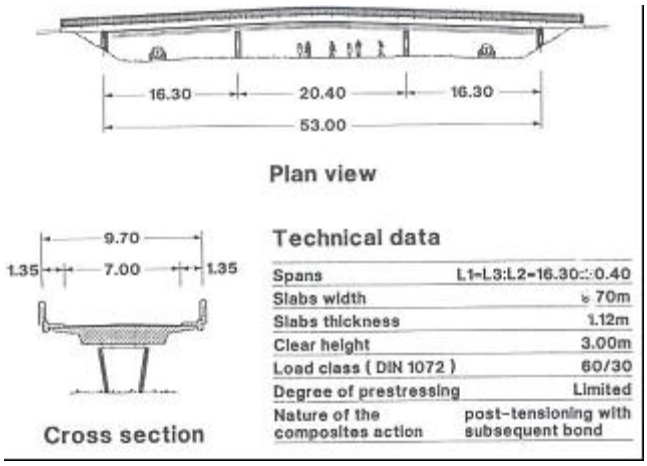

Figure 132 - Technical Data of the Schiessbergstrasse Bridge

Notsch Bridge, Austria

The Notsch Bridge is the first bridge in Austria with glass fiber prestressing tendons. The triple-span road bridge, with two span widths of 13.00 m and one of 18.00 m and a slab thickness of 0.75 m, is furnished with limited prestressing comprising 41 glass fiber prestressing tendons with post-bond and a working load of 600 kN each. The handover to traffic was in May 1992 (see Figure 133 and Figure 134).

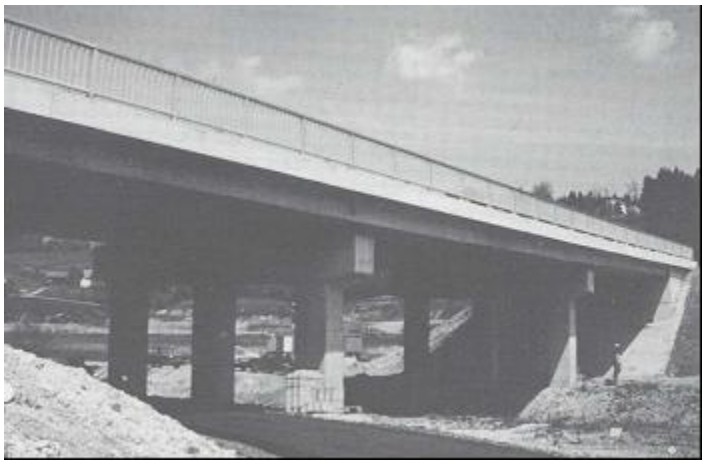

Figure 133 - Notsch Bridge View

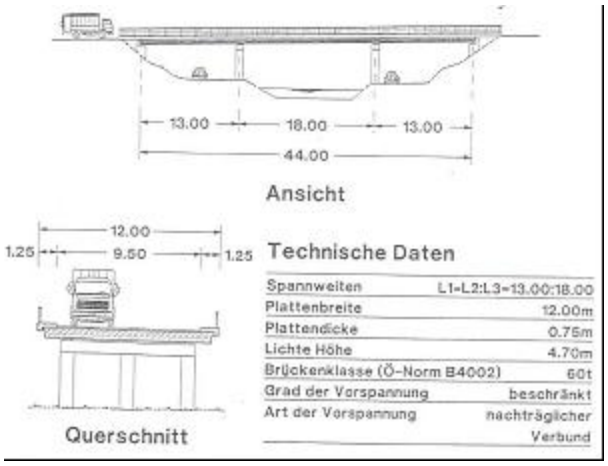

Figure 134 - Technical Data of the Notsch Bridge

APPENDIX B:

LOAD RATING DETAILED CALCULATIONS

TABLE OF CONTENTS

A. LOAD RATING 115
REFERENCES 118
APPENDIX I 119

LIST OF TABLES

Table 1 - Maximum Shear and Moment due to Live Load 116
Table 2 - Rating Factor for the New Slab (Bending Moment) 116
Table 3 - Rating Factor for the New Slab (Shear) 116

PROJECT 206-IBRC

SOUTHVIEW BRIDGE REHABILITATION
Federal Aid Project No. IBRC 5200 (910)

Supplement N.1
ADITIONAL LOAD RATING

Missouri Department of Transportation
- City of Rolla -

By

Center for Infrastructure Engineering Studies
University of Missouri-Rolla (UMR)
in collaboration with
Co-Force America, Rolla, MO

October 26, 2003

A. LOAD RATING

Bridge load rating calculations provide a basis for determining the safe load carrying capacity of a bridge. According to the Missouri Department of Transportation (MoDOT), anytime a bridge is built, rehabilitated, or reevaluated for any reason, inventory and operating ratings are required using the Load Factor rating. All bridges should be rated at two load levels, the maximum load level called the Operating Rating and a lower load level called the Inventory Rating. The Operating Rating is the maximum permissible load that should be allowed on the bridge. Exceeding this level could damage the bridge. The Inventory Rating is the load level the bridge can carry on a daily basis without damaging the bridge.

In Missouri, for the Load Factor Method the Operating Rating is based on the appropriate ultimate capacity using current AASHTO specifications (AASHTO, 1996). The Inventory Rating is taken as 60% of the Operating Rating.

The vehicle used for the live load calculations in the Load Factor Method is the HS20 truck. If the stress levels produced by this vehicle configuration are exceeded, load posting may be required.

The tables below show the Rating Factor and Load Rating for this bridge. The method for determining the rating factor is that outlined by AASHTO in the Manual for Condition Evaluation of Bridges (AASHTO, 1994). Equation (1) was used:

$$RF = \frac{C - A_1 D}{A_2 L (1 + I)} \tag{1}$$

where: RF is the Rating Factor, C is the capacity of the member, D is the dead load effect on the member, L is the live load effect on the member, I is the impact factor to be used with the live load effect, A_1 is the factor for dead loads, and A_2 is the factor for live loads. Since the load factor method is being used, A_1 is taken as 1.3 and A_2 varies depending on the desired rating level. For Inventory rating, A_2 = 2.17, and for Operating Rating, A_2 = 1.3.

To determine the rating (RT) of the bridge Equation (2) was used:

$$RT = (RF)W \tag{2}$$

In the above equation, W is the weight of the nominal truck used to determine the live load effect.

For the Southview Bridge, the Load Rating was calculated for a number of different trucks, HS20, H20, 3S2, and MO5. The different ratings are used for different purposes

by the bridge owner. For each of the different loading conditions, the maximum shear and maximum moment were calculated. Impact factors are also taken into account for Load Ratings. This value is 30% for the Southview Bridge. The shear and moment values for the deck are shown in below in Table 1.

Table 1 - Maximum Shear and Moment due to Live Load

Truck	Maximum Shear (kip)	Maximum Moment (k-ft)	Maximum Shear with Impact (kip)	Maximum Moment with Impact (k-ft)
HS20	3.40	6.55	4.42	8.52
MO5	3.30	4.68	4.29	6.08
H20	2.86	4.29	3.72	5.57
3S2	2.93	4.26	3.81	5.54

Table 2 gives the results of the Load Rating pertaining to moment and Table 3 shows the results for shear. All calculations for the load rating are located in APPENDIX I.

Table 2 - Rating Factor for the New Slab (Bending Moment)

Truck	Rating Factor (RF)	Rating (RT) (Tons)	Rating Type
HS20	1.793	64.5	Operating
HS20	1.074	38.7	Inventory
MO5	2.482	89.4	Operating
H20	2.330	46.6	Posting
3S2	2.345	85.9	Posting

* All Units Expressed in English System

Table 3 - Rating Factor for the New Slab (Shear)

Truck	Rating Factor (RF)	Rating (RT) (Tons)	Rating Type
HS20	2.152	77.5	Operating
HS20	1.289	46.4	Inventory
MO5	2.217	81.2	Operating
H20	2.202	44.0	Posting
3S2	2.148	78.7	Posting

* All Units Expressed in English System

Since the factors RF are greater than 1 than the bridge does not need to be load posted. In addition, from Table 2 and Table 3 the maximum operating and inventory load can be found as 64.5 T and 38.7 T respectively.

REFERENCES

AASHTO, 2002: "Standard Specifications for Highway Bridges," 17th Edition, Published by the American Association of State Highway and Transportation Officials, Washington D.C.

AASHTO, 1996 "LRFD Design Code for Highway Bridges"", Published by the American Association of State Highway and Transportation Officials, Washington, D.C.

AASHTO, 1994"Manual for Condition Evaluation of Bridges", Published by the American Association of State Highway and Transportation Officials, Washington, D.C.

APPENDIX I

Load Rating Detailed Calculations

TRUCK HS-20

Geometric-Mechanic Data Input

$j := 4$ number of spans

$i := 1, 2 .. j + 2$ number of spans and cantilever beams

Length of the spans:

$l_1 := 0 \cdot ft$ left cantilever beam length (the j+1 is th rigth cantilever beam length)

$l_2 := 9.49 \cdot ft$

$l_3 := 11.10 \cdot ft$

$l_4 := 10.82 \cdot ft$

$l_5 := 9.35 \cdot ft$

$l_6 := 0 \cdot ft$

Geometric-Mechanic Data Input

Geometric-Mechanic Utilities

$ii := 1, 2 .. 6$

Total length until the ii span included:

$$l_{t_{ii}} := \begin{cases} \left(\sum_{ii=1}^{ii} l_{ii} \right) & \text{if } ii \le j + 2 \\ (0\,ft) & \text{otherwise} \end{cases}$$

Partial length until the ii span excluding the first cantilever beam:

$$l_{p_{ii}} := \begin{cases} \sum_{i1=2}^{ii} l_{i1} & \text{if } ii > 1 \wedge ii \le j + 2 \\ (0\,ft) & \text{otherwise} \end{cases}$$

Stiffness Calculation:

$$C_i := \begin{cases} 1 \cdot ksi^{-1} \cdot in^{-4} & \text{if } mode_{01} = 1 \\ \frac{1}{E_i \cdot I_i} & \text{otherwise} \end{cases}$$

Geometric-Mechanic Utilities

Moving Load Case

Load Data Input

Concentrated load:

$n_P := 3$ number of concentrated load

$P_1 := 16kip$

$P_2 := 16kip$

$P_3 := 4kip$

$P_4 := 0kip$

$P_5 := 0kip$

Distance between consecutive loads:

$dP_1 := 14ft$

$dP_2 := 14ft$

$dP_3 := 0ft$

$dP_4 := 0 \cdot ft$

$dP_5 := 0 \cdot ft$

Distance between the first load and the other:

$$iP := \begin{cases} (1, 2 .. nP - 1) & \text{if } nP > 1 \\ 1 & \text{otherwise} \end{cases}$$

$$dPt_{iP} := \sum_{iP=1}^{iP} dP_{iP}$$

$dPt_{iP} =$

168
336

in

Load Data Input

Matrix View

This procedure is valid only if the stiffness is the same for all the spans!

$$C := \frac{1}{ksi \cdot ft^4}$$

$$Ac_{LL}(i1, i2) := C \cdot \left[-\left[\frac{\left(lp_{j+1} - lp_{i1+2}\right) \cdot \left(lp_{i2+2}\right)^3}{6 \cdot lp_{j+1}} \right] + \left[\frac{lp_{i1+2} \cdot \left(lp_{j+1} - lp_{i1+2}\right) \cdot \left(lp_{j+1} \cdot 2 - lp_{i1+2}\right) \cdot lp_{i2+2}}{6 \cdot lp_{j+1}} \right] \ldots \right] \cdot kip$$
$$+ \left[\begin{cases} \frac{\left(lp_{i2+2} - lp_{i1+2}\right)^3}{6} & \text{if } i2 > i1 \\ 0\,ft^3 & \text{otherwise} \end{cases} \right]$$

$$A_{LL} := \text{matrix}\left(j - 1, j - 1, Ac_{LL}\right)$$

$$A_{LL} = \begin{pmatrix} 1.5244 & 1.9292 & 1.1396 \\ 1.9292 & 2.9855 & 1.9162 \\ 1.1396 & 1.9162 & 1.493 \end{pmatrix}$$

Matrix View

Movement of the Loads:

Choose $mode_{kP}$ the range to find the load factor:

1 = total with less than the maximum number of the forces
2 = rational with all the load inside the width
3 = Renato (to check!)...

$$n_{loop} := \frac{lt_{j+2}}{3 \cdot in}$$

$$n_{loop} := \text{round}\left(n_{loop}\right)$$

$$n_{loop} = 163$$

$w_{curb} := 0in$ width of the curb or guardrail

$wp := 0\left(w_{curb} + 12in\right) \quad wp = 0\,ft$ max distance from the side of the deck (AASHTO Figure 3.7.6A)

$$l_{max} := lt_{j+2} - 0wp \qquad l_{min} := 0wp - dPt_{nP-1}$$

$$iPP := 1, 2 .. nP$$

$$x := l_{min}, \left[l_{min} + \frac{\left(l_{max} - l_{min}\right)}{n_{loop}} \right] .. l_{max} \qquad l_{max} = 40.76\,ft \qquad l_{min} = -28\,ft$$

Moment on the Cantilever Beams

Moment due to the load on the cantilever beams:

$$M_{Plc}(x, ipp) := \begin{cases} \begin{cases} -P_{ipp} \cdot \begin{cases} \left[l_1 - \left(x + dPt_{ipp-1}\right)\right] & \text{if } ipp > 1 \\ \left(l_1 - x\right) & \text{if } ipp = 1 \end{cases} \end{cases} & \text{if } 0in \le \begin{cases} \left(x + dPt_{ipp-1}\right) & \text{if } ipp > 1 \\ x & \text{if } ipp = 1 \end{cases} \le l_1 \\ 0kip \cdot ft & \text{otherwise} \end{cases}$$

$$M_{Pl}(x) := \sum_{iP1=1}^{nP} M_{Plc}(x, iP1)$$

$$M_{Prc}(x, ipp) := \begin{cases} \begin{cases} -P_{ipp} \cdot \begin{cases} \left[\left(x + dPt_{ipp-1}\right) - l_{t_{j+1}}\right] & \text{if } ipp > 1 \\ \left(x - l_{t_{j+1}}\right) & \text{if } ipp = 1 \end{cases} \end{cases} & \text{if } l_{t_{j+1}} \le \begin{cases} \left(x + dPt_{ipp-1}\right) & \text{if } ipp > 1 \\ x & \text{if } ipp = 1 \end{cases} \le l_{t_{j+2}} \\ 0kip \cdot ft & \text{otherwise} \end{cases}$$

$$M_{Pr}(x) := \sum_{iP1=1}^{nP} M_{Plc}(x, iP1)$$

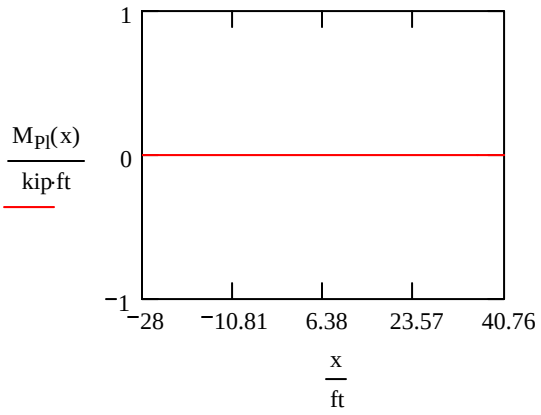

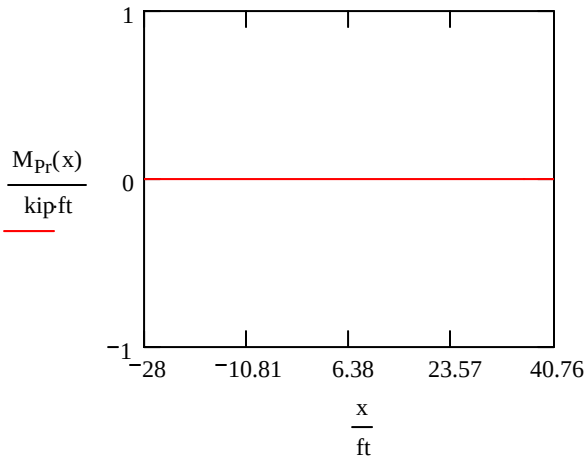

Moment on the Cantilever Beams

Supports Reactions for IN-Loads

Left support reaction due to the load between the 2 external supports (to solve the unknown):

$$R_{Pl}(x) := \sum_{iP1=1}^{nP} \begin{cases} \begin{cases} \begin{cases} P_{iP1} \cdot \begin{cases} \dfrac{l_{p_{j+1}} - \left[\left(x - l_1\right) + dPt_{iP1-1}\right]}{l_{p_{j+1}}} & \text{if } iP1 > 1 \\ \dfrac{\left[l_{p_{j+1}} - \left(x - l_1\right)\right]}{l_{p_{j+1}}} & \text{if } iP1 = 1 \end{cases} \end{cases} & \text{if } l_{t_1} \le \begin{cases} \left(x + dPt_{iP1-1}\right) & \text{if } iP1 > 1 \\ x & \text{if } iP1 = 1 \end{cases} \le l_{t_{j+1}} \\ 0kip & \text{otherwise} \end{cases} \end{cases}$$

$$R_{Pr}(x) := \sum_{i_{P1}=1}^{n_P} \left[P_{i_{P1}} \cdot \left| \left[\begin{array}{l} \dfrac{(x - l_1) + d_{Pt_{i_{P1}-1}}}{l_{p_{j+1}}} \quad \text{if } i_{P1} > 1 \\ \dfrac{(x - l_1)}{l_{p_{j+1}}} \quad \text{if } i_{P1} = 1 \end{array} \right] \right| \text{if } l_{t_1} \le \left[\left| \begin{array}{l} \left(x + d_{Pt_{i_{P1}-1}}\right) \quad \text{if } i_{P1} > 1 \\ x \quad \text{if } i_{P1} = 1 \end{array} \right| \right] \le l_{t_{j+1}} \right]$$

$$0 \quad \text{otherwise}$$

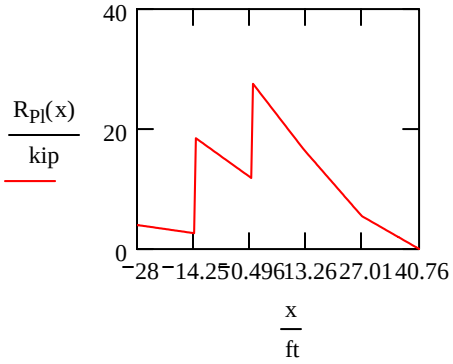

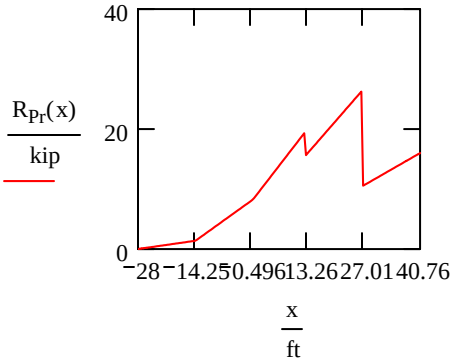

Supports Reactions for IN-Loads

System Solution

$k := 1, 2 .. j - 1$

$b(x, k) := \Delta pp\left(x, l_{p_{k+1}}\right)$

Solution of this linear system: (A)(M_2, M_3, M_i) = (b_1, b_2, b_i)

WARNING
Add rows, matrix and "solutions" if j > 4.

WARNING
The dimension of the A_{LLi} is [m].

$$A_{LL2}(x) := \begin{pmatrix} b(x,1) & \left| \begin{array}{l} Ac_{LL}(0,1) \quad \text{if } j \ge 3 \\ 0 \quad \text{otherwise} \end{array} \right. & \left| \begin{array}{l} Ac_{LL}(0,2) \quad \text{if } j \ge 4 \\ 0 \quad \text{otherwise} \end{array} \right. \\ \left| \begin{array}{l} b(x,2) \quad \text{if } j \ge 3 \\ 0 \quad \text{otherwise} \end{array} \right. & \left| \begin{array}{l} Ac_{LL}(1,1) \quad \text{if } j \ge 3 \\ 1m \quad \text{otherwise} \end{array} \right. & \left| \begin{array}{l} Ac_{LL}(1,2) \quad \text{if } j \ge 4 \\ 0 \quad \text{otherwise} \end{array} \right. \\ \left| \begin{array}{l} b(x,3) \quad \text{if } j \ge 4 \\ 0 \quad \text{otherwise} \end{array} \right. & \left| \begin{array}{l} Ac_{LL}(2,1) \quad \text{if } j \ge 4 \\ 0 \quad \text{otherwise} \end{array} \right. & \left| \begin{array}{l} Ac_{LL}(2,2) \quad \text{if } j \ge 4 \\ 1m \quad \text{otherwise} \end{array} \right. \end{pmatrix}$$

$$A_{LL3}(x) := \begin{cases} \begin{pmatrix} Ac_{LL}(0,0) & \begin{cases} b(x,1) & \text{if } j \geq 3 \\ 0 & \text{otherwise} \end{cases} & \begin{cases} Ac_{LL}(0,2) & \text{if } j \geq 4 \\ 0 & \text{otherwise} \end{cases} \\ \begin{cases} Ac_{LL}(1,0) & \text{if } j \geq 3 \\ 0 & \text{otherwise} \end{cases} & \begin{cases} b(x,2) & \text{if } j \geq 3 \\ 1m & \text{otherwise} \end{cases} & \begin{cases} Ac_{LL}(1,2) & \text{if } j \geq 4 \\ 0ft & \text{otherwise} \end{cases} \\ \begin{cases} Ac_{LL}(2,0) & \text{if } j \geq 4 \\ 0 & \text{otherwise} \end{cases} & \begin{cases} b(x,3) & \text{if } j \geq 4 \\ 0 & \text{otherwise} \end{cases} & \begin{cases} Ac_{LL}(2,2) & \text{if } j \geq 4 \\ 1m & \text{otherwise} \end{cases} \end{pmatrix} & \text{if } j \geq 3 \\ 0m^3 & \text{otherwise} \end{cases}$$

$$A_{LL4}(x) := \begin{cases} \begin{pmatrix} Ac_{LL}(0,0) & \begin{cases} Ac_{LL}(0,1) & \text{if } j \geq 3 \\ 0 & \text{otherwise} \end{cases} & \begin{cases} b(x,1) & \text{if } j \geq 4 \\ 0 & \text{otherwise} \end{cases} \\ \begin{cases} Ac_{LL}(1,0) & \text{if } j \geq 3 \\ 0 & \text{otherwise} \end{cases} & \begin{cases} Ac_{LL}(1,1) & \text{if } j \geq 3 \\ 1m & \text{otherwise} \end{cases} & \begin{cases} b(x,2) & \text{if } j \geq 4 \\ 0 & \text{otherwise} \end{cases} \\ \begin{cases} Ac_{LL}(2,0) & \text{if } j \geq 4 \\ 0 & \text{otherwise} \end{cases} & \begin{cases} Ac_{LL}(2,1) & \text{if } j \geq 4 \\ 0 & \text{otherwise} \end{cases} & \begin{cases} b(x,3) & \text{if } j \geq 4 \\ 1m & \text{otherwise} \end{cases} \end{pmatrix} & \text{if } j \geq 4 \\ 0m^3 & \text{otherwise} \end{cases}$$

System Solution

$$R_{LL2}(x) := \left(\frac{|A_{LL2}(x)|}{|A_{LL}|} \right) \cdot \frac{kip}{m^3}$$

WARNING
The dimension of the !A_{cLL}! is [m³] while A_{LL} is dimensionless and the results have to be in kip.
The power in the denominator has to be j_{max} available.

$$R_{LL3}(x) := \left(\frac{|A_{LL3}(x)|}{|A_{LL}|} \right) \cdot \frac{kip}{m^3}$$

$$R_{LL4}(x) := \left(\frac{|A_{LL4}(x)|}{|A_{LL}|} \right) \cdot \frac{kip}{m^3}$$

$$R_{LLl}(x) := \frac{\sum_{i_{P1}=1}^{n_P} \left[\begin{cases} P_{i_{P1}} \cdot \left[l_{t_{j+1}} - \left[\begin{cases} \left(x + dp_{t_{i_{P1}-1}} \right) & \text{if } i_{P1} > 1 \\ x & \text{if } i_{P1} = 1 \end{cases} \right] \right] & \text{if } 0 \cdot in \leq \left[\begin{cases} \left(x + dp_{t_{i_{P1}-1}} \right) & \text{if } i_{P1} > 1 \\ x & \text{if } i_{P1} = 1 \end{cases} \right] \leq l_{t_{j+2}} \\ 0 \cdot kip \cdot ft & \text{otherwise} \end{cases} \right] \ldots}{l_{p_{j+1}}}$$
$$+ (-1) \cdot \left[R_{LL2}(x) \cdot \left(l_{p_{j+1}} - l_{p_2} \right) + \begin{cases} R_{LL3}(x) \cdot \left(l_{p_{j+1}} - l_{p_3} \right) & \text{if } j \geq 3 \\ 0kip \cdot ft & \text{otherwise} \end{cases} + \begin{cases} R_{LL4}(x) \cdot \left(l_{p_{j+1}} - l_{p_4} \right) & \text{if } j \geq 4 \\ 0kip \cdot ft & \text{otherwise} \end{cases} \right]$$

$$R_{LLr}(x) := \frac{\sum_{i_{P1}=1}^{n_P} \left[\begin{cases} P_{i_{P1}} \cdot \left[\begin{cases} \left(x + dPt_{i_{P1}-1}\right) & \text{if } i_{P1} > 1 \\ x & \text{if } i_{P1} = 1 \end{cases} - l_{p_1} \right] & \text{if } 0in \le \left[\begin{cases} \left(x + dPt_{i_{P1}-1}\right) & \text{if } i_{P1} > 1 \\ x & \text{if } i_{P1} = 1 \end{cases} \right] \le l_{t_{j+2}} \\ 0kip \cdot ft & \text{otherwise} \end{cases} \right] \ldots}{l_{p_{j+1}}}$$

$$+ (-1) \cdot \left[R_{LL2}(x) \cdot \left(l_{p_2} - l_{p_1}\right) + \begin{cases} R_{LL3}(x) \cdot \left(l_{p_3} - l_{p_1}\right) & \text{if } j \ge 3 \\ 0kip \cdot ft & \text{otherwise} \end{cases} + \begin{cases} R_{LL4}(x) \cdot \left(l_{p_4} - l_{p_1}\right) & \text{if } j \ge 4 \\ 0kip \cdot ft & \text{otherwise} \end{cases} \right]$$

$x_{prova} := 20ft$

$R_{LLl}(x_{prova}) = -0.2408\,kip$

$R_{LL2}(x_{prova}) = 1.2127\,kip$

$R_{LL3}(x_{prova}) = 14.032\,kip$

$R_{LL4}(x_{prova}) = 13.8168\,kip$

$R_{LLr}(x_{prova}) = 3.1793\,kip$

$b(x_{prova}, 1) = 146.5368\,ft$

$b(x_{prova}, 2) = 231.9813\,ft$

$b(x_{prova}, 3) = 160.4267\,ft$

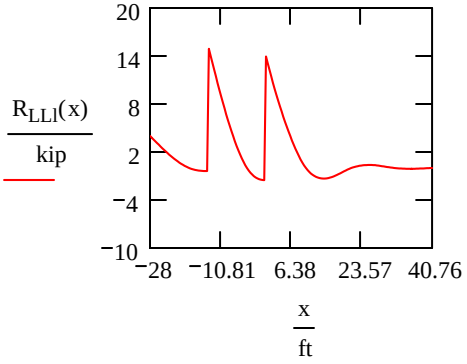

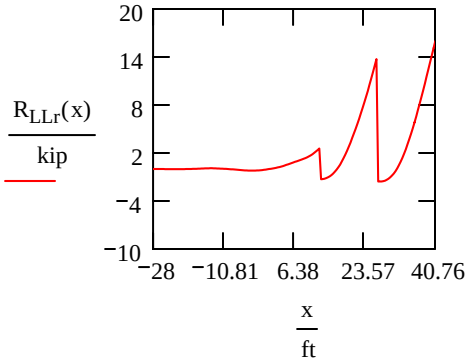

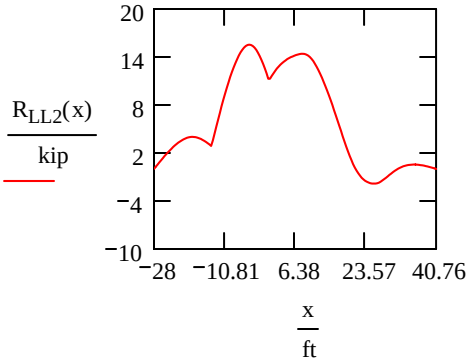

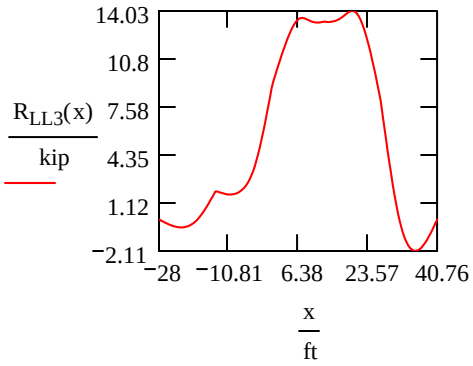

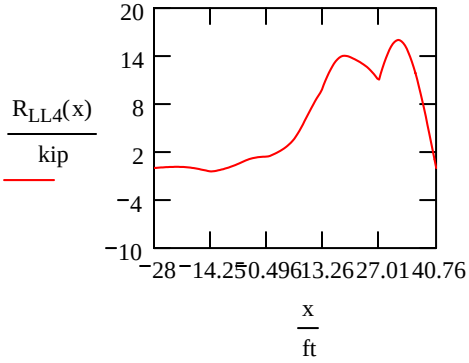

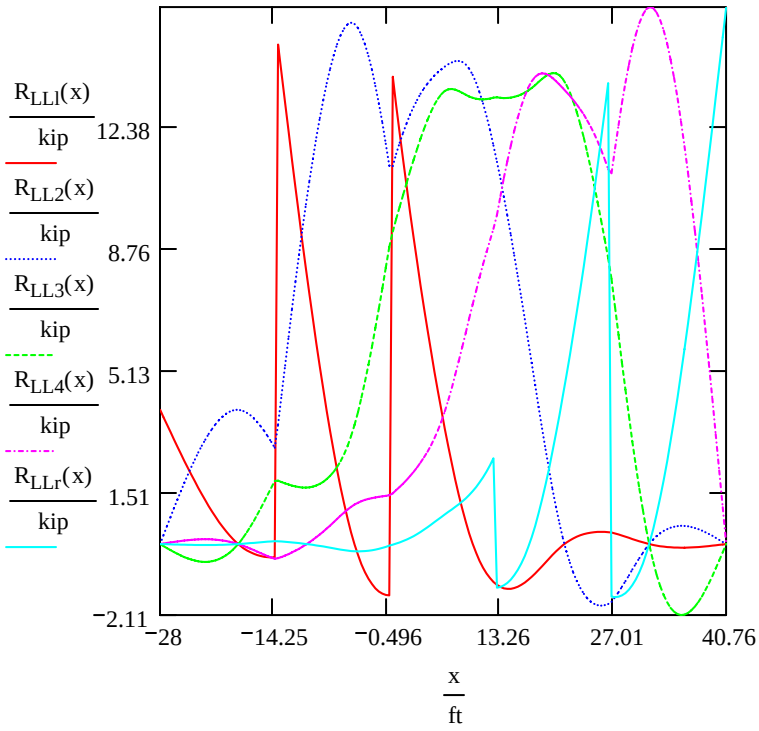

$$R(x) := R_{LLl}(x) + R_{LL2}(x) + R_{LL3}(x) + R_{LL4}(x) + R_{LLr}(x) - \left[\sum_{i_{P1}=1}^{n_P} \left[\begin{array}{ll} P_{i_{P1}} & \text{if } 0\text{in} \le \left[\begin{array}{ll} \left(x + d_{Pt_{i_{P1}-1}}\right) & \text{if } i_{P1} > 1 \\ x & \text{if } i_{P1} = 1 \end{array} \right] \le l_{t_{j+2}} \\ 0\text{kip} & \text{otherwise} \end{array} \right] \right]$$

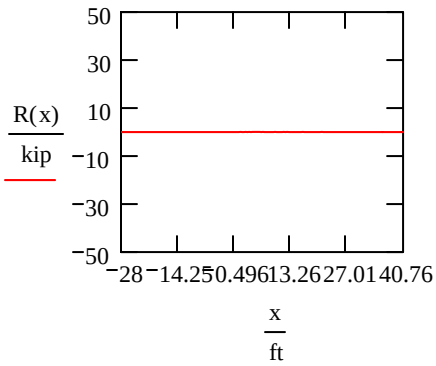

$$\Delta y := \frac{l_{t_{j+2}}}{n_{loop}}$$

$$jj := 0, 1 .. n_{loop}$$

$$jjj := 0, 1 .. n_{loop}$$

$$y := -\Delta y, 0\text{in} .. l_{t_{j+2}} + \Delta y$$

$$yy_{jj} := \frac{l_{t_{j+2}} \cdot jj}{n_{loop}}$$

$$xx_{jjj} := l_{min} + \frac{(l_{max} - l_{min}) \cdot jjj}{n_{loop}}$$

$$x_1 := 0.000005 \cdot l_{p_1}$$

$$x_2 := x_1 + 0.5 \cdot l_3$$

$x_3 := x_2 + 0.5 \cdot l_4$

$x_4 := x_3 + 0.5 \cdot l_5$

Shear Analysis

Shear expressions:

$$T_{LL}(x,y) := \sum_{i_{P1}=1}^{n_P} \left[\begin{cases} -P_{i_{P1}} & \text{if } y \geq x + d_{Pt_{i_{P1}-1}} \geq 0ft \wedge 0ft \leq y \leq l_{t_{j+2}} \\ (0kip) & \text{otherwise} \end{cases} \right] + \left[\begin{cases} R_{LLl}(x) & \text{if } l_{t_1} \leq y \leq l_{t_{j+2}} \\ (0kip) & \text{otherwise} \end{cases} \right] \ldots$$
$$+ \left[\begin{cases} R_{LL2}(x) & \text{if } l_{t_2} \leq y \leq l_{t_{j+2}} \\ (0 \cdot kip) & \text{otherwise} \end{cases} \right] + \left[\begin{cases} R_{LL3}(x) & \text{if } l_{t_3} \leq y \leq l_{t_{j+2}} \\ (0 \cdot kip) & \text{otherwise} \end{cases} \right] + \left[\begin{cases} R_{LL4}(x) & \text{if } l_{t_4} \leq y \leq l_{t_{j+2}} \\ (0kip) & \text{otherwise} \end{cases} \right] \ldots$$
$$+ \begin{cases} R_{LLr}(x) & \text{if } l_{t_{j+1}} \leq y \leq l_{t_{j+2}} \\ (0kip) & \text{otherwise} \end{cases}$$

Shear Analysis

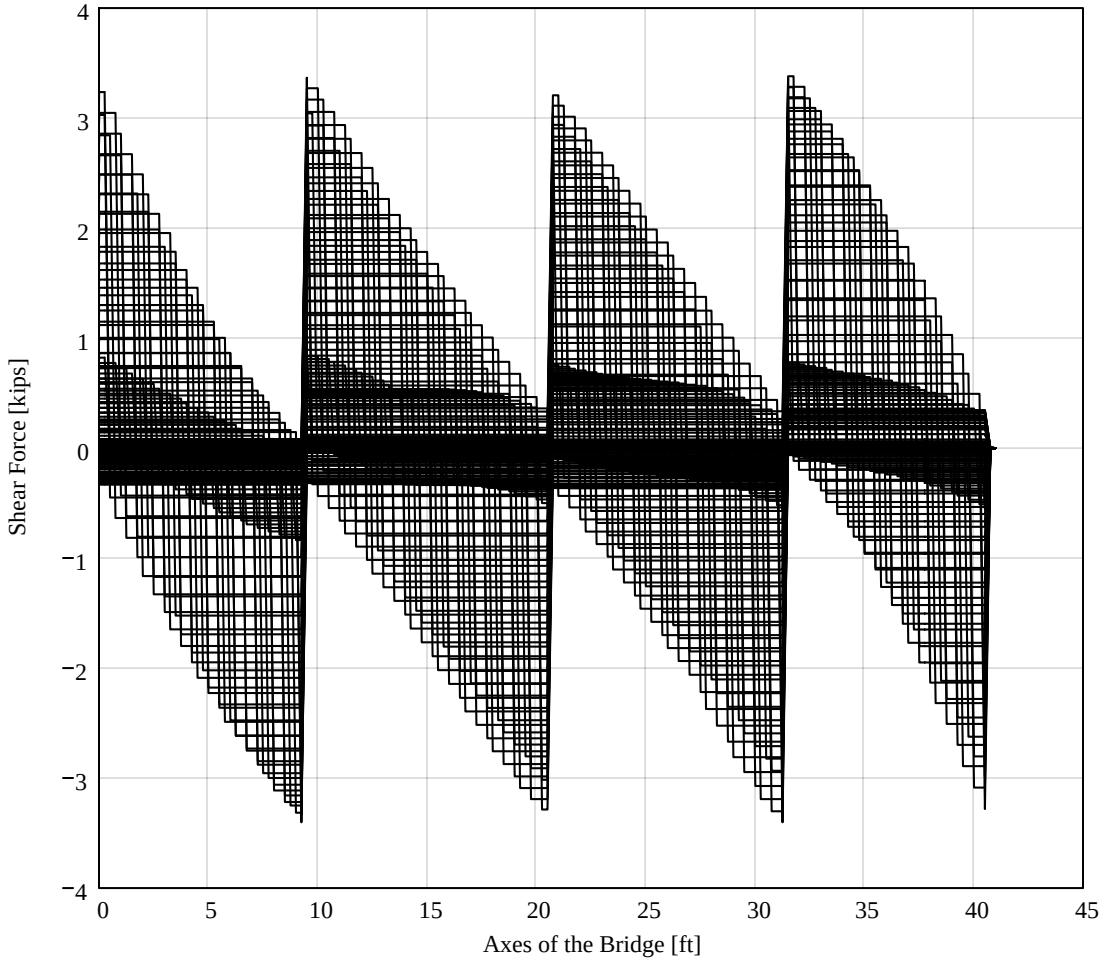

Moment expressions

Moment Analysis

$$M_{LL}(x,y) := \sum_{i_{P1}=1}^{n_P} \left[\begin{cases} -P_{i_{P1}} \cdot \left[y - \left(x + d_{Pt_{i_{P1}-1}} \right) \right] & \text{if } y \geq x + d_{Pt_{i_{P1}-1}} \geq 0ft \wedge 0ft \leq y \leq l_{t_{j+2}} \\ (0 \cdot kip \cdot ft) & \text{otherwise} \end{cases} \right] \ldots$$
$$+ \left[\begin{cases} R_{LLl}(x) \cdot \left(y - l_{t_1} \right) & \text{if } l_{t_1} \leq y \leq l_{t_{j+2}} \\ (0 \cdot kip \cdot ft) & \text{otherwise} \end{cases} \right] + \left[\begin{cases} R_{LLr}(x) \cdot \left(y - l_{t_{j+1}} \right) & \text{if } l_{t_{j+1}} \leq y \leq l_{t_{j+2}} \\ (0 \cdot kip \cdot ft) & \text{otherwise} \end{cases} \right] \ldots$$
$$+ \left[\begin{cases} R_{LL2}(x) \cdot \left(y - l_{t_2} \right) & \text{if } l_{t_2} \leq y \leq l_{t_{j+2}} \\ (0 \cdot kip \cdot ft) & \text{otherwise} \end{cases} \right] + \left[\begin{cases} R_{LL3}(x) \cdot \left(y - l_{t_3} \right) & \text{if } l_{t_3} \leq y \leq l_{t_{j+2}} \\ (0 \cdot kip \cdot ft) & \text{otherwise} \end{cases} \right] \ldots$$
$$+ \left[\begin{cases} R_{LL4}(x) \cdot \left(y - l_{t_4} \right) & \text{if } l_{t_4} \leq y \leq l_{t_{j+2}} \\ (0 \cdot kip \cdot ft) & \text{otherwise} \end{cases} \right]$$

Moment Analysis

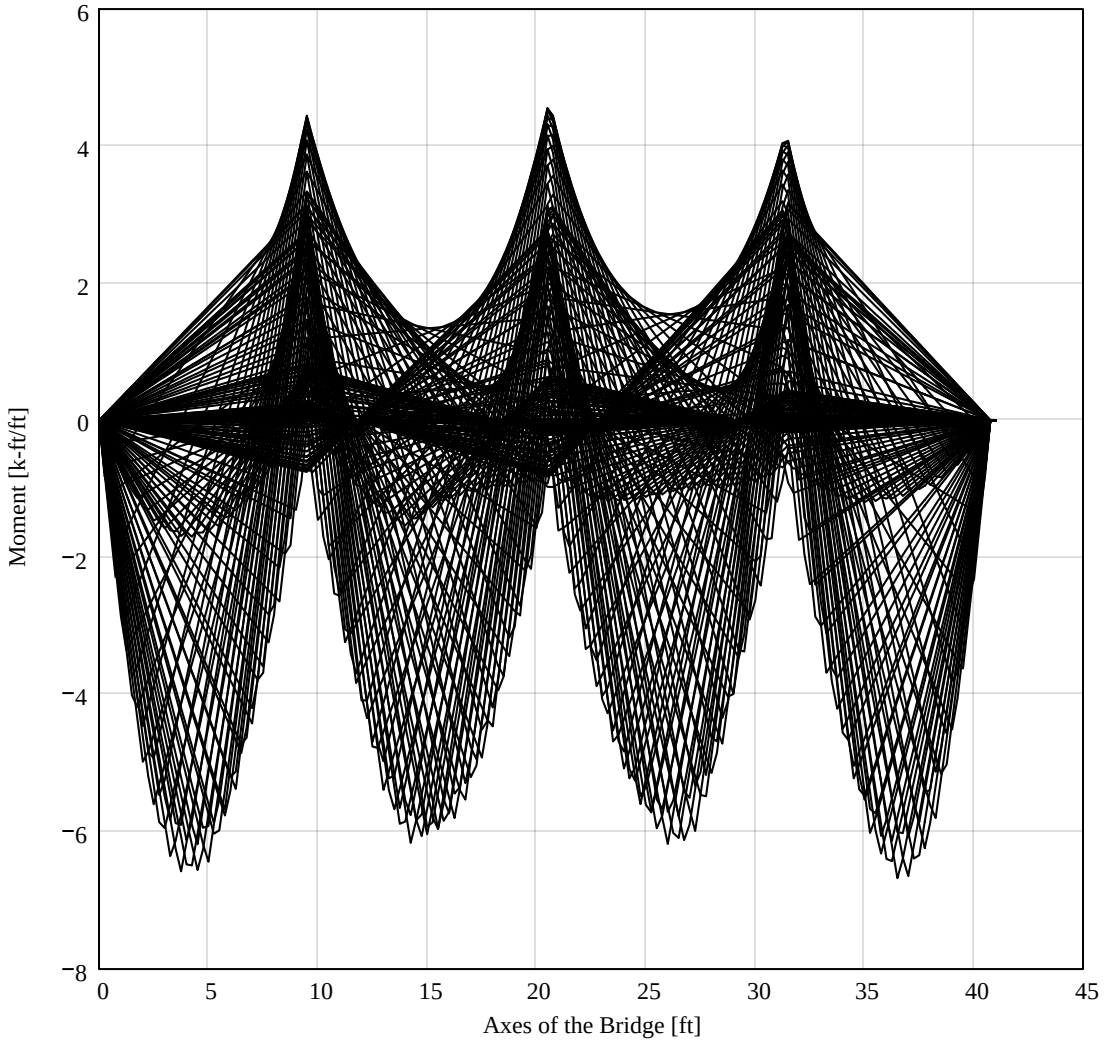

TRUCK MO5

Geometric-Mechanic Data Input

$j := 4$ number of spans

$i := 1, 2 .. j + 2$ number of spans and cantilever beams

Length of the spans:

$l_1 := 0 \cdot ft$ left cantilever beam length (the j+1 is th rigth cantilever beam length)

$l_2 := 9.49 \cdot ft$

$l_3 := 11.10 \cdot ft$

$l_4 := 10.82 \cdot ft$

$l_5 := 9.35 \cdot ft$

$l_6 := 0 \cdot ft$

Geometric-Mechanic Data Input

Geometric-Mechanic Utilities

$ii := 1, 2 .. 6$

Total length until the ii span included:

$$l_{t_{ii}} := \begin{cases} \left(\sum_{ii=1}^{ii} l_{ii} \right) & \text{if } ii \le j + 2 \\ (0\,ft) & \text{otherwise} \end{cases}$$

Partial length until the ii span excluding the first cantilever beam:

$$l_{p_{ii}} := \begin{cases} \sum_{i1=2}^{ii} l_{i1} & \text{if } ii > 1 \wedge ii \le j + 2 \\ (0\,ft) & \text{otherwise} \end{cases}$$

Stiffness Calculation:

$$C_i := \begin{cases} 1 \cdot ksi^{-1} \cdot in^{-4} & \text{if } mode_{01} = 1 \\ \dfrac{1}{E_i \cdot I_i} & \text{otherwise} \end{cases}$$

Geometric-Mechanic Utilities

Moving Load Case

Load Data Input

Concentrated load:

$n_P := 5$ number of concentrated load

$P_1 := 8kip$

$P_2 := 8kip$

$P_3 := 8kip$

$P_4 := 8kip$

$P_5 := 4.64kip$

Distance between consecutive loads:

$dP_1 := 3.7917ft$

$dP_2 := 3.7917ft$

$dP_3 := 23.4167ft$

$dP_4 := 12.1042ft$

Distance between the first load and the other:

$$i_P := \begin{cases} (1, 2 .. n_P - 1) & \text{if } n_P > 1 \\ 1 & \text{otherwise} \end{cases}$$

$$dPt_{i_P} := \sum_{i_P = 1}^{i_P} dP_{i_P}$$

$dPt_{i_P} =$

45.5004	in
91.0008	
372.0012	
517.2516	

Load Data Input

Matrix View

This procedure is valid only if the stiffness is the same for all the spans!

$$C := \frac{1}{ksi \cdot ft^4}$$

$$Ac_{LL}(i1, i2) := C \cdot \left[-\left[\frac{\left(lp_{j+1} - lp_{i1+2}\right) \cdot \left(lp_{i2+2}\right)^3}{6 \cdot lp_{j+1}} \right] + \left[\frac{lp_{i1+2} \cdot \left(lp_{j+1} - lp_{i1+2}\right) \cdot \left(lp_{j+1} \cdot 2 - lp_{i1+2}\right) \cdot lp_{i2+2}}{6 \cdot lp_{j+1}} \right] \ldots \right] \cdot kip$$
$$+ \left[\begin{cases} \frac{\left(lp_{i2+2} - lp_{i1+2}\right)^3}{6} & \text{if } i2 > i1 \\ 0\,ft^3 & \text{otherwise} \end{cases} \right]$$

$$A_{LL} := \text{matrix}\left(j - 1, j - 1, Ac_{LL}\right)$$

$$A_{LL} = \begin{pmatrix} 1.5244 & 1.9292 & 1.1396 \\ 1.9292 & 2.9855 & 1.9162 \\ 1.1396 & 1.9162 & 1.493 \end{pmatrix}$$

Matrix View

Movement of the Loads:

Choose $mode_{kP}$ the range to find the load factor:
1 = total with less than the maximum number of the forces
2 = rational with all the load inside the width
3 = Renato (to check!)...

$$n_{loop} := \frac{lt_{j+2}}{3 \cdot in}$$

$$n_{loop} := \text{round}\left(n_{loop}\right)$$

$$n_{loop} = 163$$

$w_{curb} := 0in$ width of the curb or guardrail

$wp := 0\left(w_{curb} + 12in\right)$ $wp = 0\ ft$ max distance from the side of the deck (AASHTO Figure 3.7.6A)

$$l_{max} := lt_{j+2} - 0wp \qquad l_{min} := 0wp - dPt_{nP-1}$$

$$ipp := 1, 2 .. nP$$

$$x := l_{min}, \left[l_{min} + \frac{\left(l_{max} - l_{min}\right)}{n_{loop}} \right] .. l_{max}$$ $l_{max} = 40.76\ ft$ $l_{min} = -43.1043\ ft$

Moment on the Cantilever Beams

Moment due to the load on the cantilever beams:

$$M_{Plc}(x, ipp) := \begin{cases} \begin{cases} -P_{ipp} \cdot \begin{cases} \left[l_1 - \left(x + dPt_{ipp-1}\right)\right] & \text{if } ipp > 1 \\ \left(l_1 - x\right) & \text{if } ipp = 1 \end{cases} \end{cases} & \text{if } 0in \le \begin{cases} \left(x + dPt_{ipp-1}\right) & \text{if } ipp > 1 \\ x & \text{if } ipp = 1 \end{cases} \le l_1 \\ 0kip \cdot ft & \text{otherwise} \end{cases}$$

$$M_{Pl}(x) := \sum_{ip1=1}^{np} M_{Plc}(x, ip1)$$

$$M_{Prc}(x, ipp) := \begin{cases} \begin{cases} -P_{ipp} \cdot \begin{cases} \left[\left(x + dPt_{ipp-1}\right) - lt_{j+1}\right] & \text{if } ipp > 1 \\ \left(x - lt_{j+1}\right) & \text{if } ipp = 1 \end{cases} \end{cases} & \text{if } lt_{j+1} \le \begin{cases} \left(x + dPt_{ipp-1}\right) & \text{if } ipp > 1 \\ x & \text{if } ipp = 1 \end{cases} \le lt_{j+2} \\ 0kip \cdot ft & \text{otherwise} \end{cases}$$

$$M_{Pr}(x) := \sum_{ip1=1}^{np} M_{Plc}(x, ip1)$$

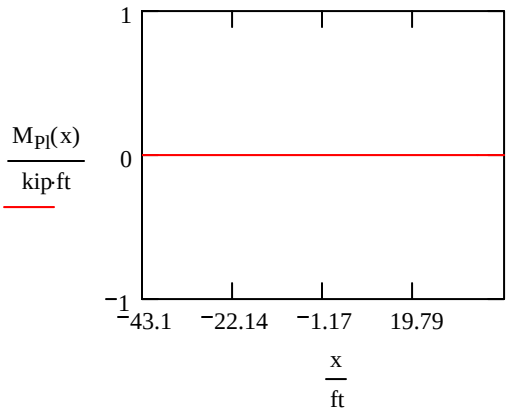

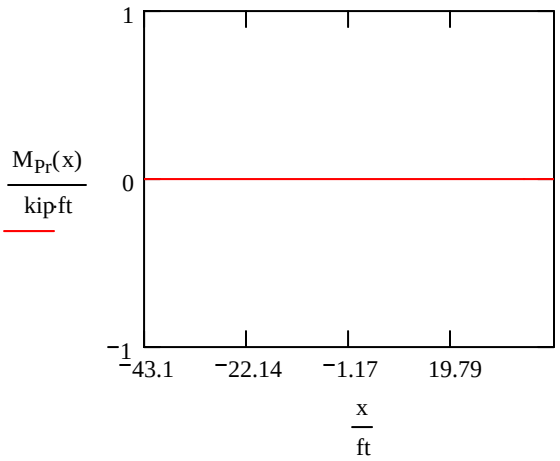

Moment on the Cantilever Beams

Supports Reactions for IN-Loads

Left support reaction due to the load between the 2 external supports (to solve the unknown):

$$R_{Pl}(x) := \sum_{ip1=1}^{np} \begin{cases} \begin{cases} P_{ip1} \cdot \begin{cases} \dfrac{lp_{j+1} - \left[\left(x - l_1\right) + dPt_{ip1-1}\right]}{lp_{j+1}} & \text{if } ip1 > 1 \\ \dfrac{\left[lp_{j+1} - \left(x - l_1\right)\right]}{lp_{j+1}} & \text{if } ip1 = 1 \end{cases} \end{cases} & \text{if } lt_1 \le \begin{cases} \left(x + dPt_{ip1-1}\right) & \text{if } ip1 > 1 \\ x & \text{if } ip1 = 1 \end{cases} \le lt_{j+1} \\ 0kip & \text{otherwise} \end{cases}$$

$$R_{Pr}(x) := \sum_{i_{P1}=1}^{n_P} \left[P_{i_{P1}} \cdot \left[\begin{cases} \left[\begin{cases} \dfrac{(x - l_1) + dPt_{i_{P1}-1}}{lp_{j+1}} & \text{if } i_{P1} > 1 \\ \dfrac{(x - l_1)}{lp_{j+1}} & \text{if } i_{P1} = 1 \end{cases} \right] & \text{if } l_{t_1} \le \left[\begin{cases} (x + dPt_{i_{P1}-1}) & \text{if } i_{P1} > 1 \\ x & \text{if } i_{P1} = 1 \end{cases} \right] \le l_{t_{j+1}} \\ 0 \quad \text{otherwise} \end{cases} \right] \right]$$

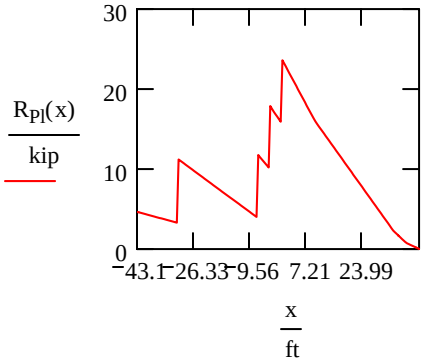

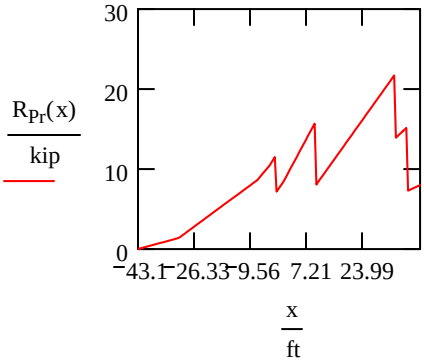

Supports Reactions for IN-Loads

System Solution

$k := 1, 2 .. j - 1$

$b(x, k) := \Delta pp\left(x, lp_{k+1}\right)$

Solution of this linear system: (A)(M_2, M_3, M_i) = (b_1, b_2, b_i)

WARNING
Add rows, matrix and "solutions" if j > 4.

WARNING
The dimension of the A_{LLi} is [m].

$$A_{LL2}(x) := \begin{pmatrix} b(x,1) & \begin{cases} Ac_{LL}(0,1) & \text{if } j \ge 3 \\ 0 & \text{otherwise} \end{cases} & \begin{cases} Ac_{LL}(0,2) & \text{if } j \ge 4 \\ 0 & \text{otherwise} \end{cases} \\ \begin{cases} b(x,2) & \text{if } j \ge 3 \\ 0 & \text{otherwise} \end{cases} & \begin{cases} Ac_{LL}(1,1) & \text{if } j \ge 3 \\ 1m & \text{otherwise} \end{cases} & \begin{cases} Ac_{LL}(1,2) & \text{if } j \ge 4 \\ 0 & \text{otherwise} \end{cases} \\ \begin{cases} b(x,3) & \text{if } j \ge 4 \\ 0 & \text{otherwise} \end{cases} & \begin{cases} Ac_{LL}(2,1) & \text{if } j \ge 4 \\ 0 & \text{otherwise} \end{cases} & \begin{cases} Ac_{LL}(2,2) & \text{if } j \ge 4 \\ 1m & \text{otherwise} \end{cases} \end{pmatrix}$$

$$A_{LL3}(x) := \begin{cases} \begin{pmatrix} Ac_{LL}(0,0) & \begin{cases} b(x,1) & \text{if } j \geq 3 \\ 0 & \text{otherwise} \end{cases} & \begin{cases} Ac_{LL}(0,2) & \text{if } j \geq 4 \\ 0 & \text{otherwise} \end{cases} \\ \begin{cases} Ac_{LL}(1,0) & \text{if } j \geq 3 \\ 0 & \text{otherwise} \end{cases} & \begin{cases} b(x,2) & \text{if } j \geq 3 \\ 1m & \text{otherwise} \end{cases} & \begin{cases} Ac_{LL}(1,2) & \text{if } j \geq 4 \\ 0ft & \text{otherwise} \end{cases} \\ \begin{cases} Ac_{LL}(2,0) & \text{if } j \geq 4 \\ 0 & \text{otherwise} \end{cases} & \begin{cases} b(x,3) & \text{if } j \geq 4 \\ 0 & \text{otherwise} \end{cases} & \begin{cases} Ac_{LL}(2,2) & \text{if } j \geq 4 \\ 1m & \text{otherwise} \end{cases} \end{pmatrix} & \text{if } j \geq 3 \\ 0m^3 & \text{otherwise} \end{cases}$$

$$A_{LL4}(x) := \begin{cases} \begin{pmatrix} Ac_{LL}(0,0) & \begin{cases} Ac_{LL}(0,1) & \text{if } j \geq 3 \\ 0 & \text{otherwise} \end{cases} & \begin{cases} b(x,1) & \text{if } j \geq 4 \\ 0 & \text{otherwise} \end{cases} \\ \begin{cases} Ac_{LL}(1,0) & \text{if } j \geq 3 \\ 0 & \text{otherwise} \end{cases} & \begin{cases} Ac_{LL}(1,1) & \text{if } j \geq 3 \\ 1m & \text{otherwise} \end{cases} & \begin{cases} b(x,2) & \text{if } j \geq 4 \\ 0 & \text{otherwise} \end{cases} \\ \begin{cases} Ac_{LL}(2,0) & \text{if } j \geq 4 \\ 0 & \text{otherwise} \end{cases} & \begin{cases} Ac_{LL}(2,1) & \text{if } j \geq 4 \\ 0 & \text{otherwise} \end{cases} & \begin{cases} b(x,3) & \text{if } j \geq 4 \\ 1m & \text{otherwise} \end{cases} \end{pmatrix} & \text{if } j \geq 4 \\ 0m^3 & \text{otherwise} \end{cases}$$

System Solution

$$R_{LL2}(x) := \left(\frac{|A_{LL2}(x)|}{|A_{LL}|} \right) \cdot \frac{kip}{m^3}$$

WARNING
The dimension of the !A_{cLL}! is [m³] while A_{LL} is dimensionless and the results have to be in kip.
The power in the denominator has to be j_{max} available.

$$R_{LL3}(x) := \left(\frac{|A_{LL3}(x)|}{|A_{LL}|} \right) \cdot \frac{kip}{m^3}$$

$$R_{LL4}(x) := \left(\frac{|A_{LL4}(x)|}{|A_{LL}|} \right) \cdot \frac{kip}{m^3}$$

$$R_{LLl}(x) := \frac{\sum_{i_{P1}=1}^{n_P} \left[\begin{cases} P_{i_{P1}} \cdot \left[l_{t_{j+1}} - \left[\begin{cases} \left(x + dP_{t_{i_{P1}-1}} \right) & \text{if } i_{P1} > 1 \\ x & \text{if } i_{P1} = 1 \end{cases} \right] \right] & \text{if } 0 \cdot in \leq \left[\begin{cases} \left(x + dP_{t_{i_{P1}-1}} \right) & \text{if } i_{P1} > 1 \\ x & \text{if } i_{P1} = 1 \end{cases} \right] \leq l_{t_{j+2}} \\ 0 \cdot kip \cdot ft & \text{otherwise} \end{cases} \right] \ldots}{l_{p_{j+1}}}$$
$$+ (-1) \cdot \left[R_{LL2}(x) \cdot \left(l_{p_{j+1}} - l_{p_2} \right) + \begin{cases} R_{LL3}(x) \cdot \left(l_{p_{j+1}} - l_{p_3} \right) & \text{if } j \geq 3 \\ 0kip \cdot ft & \text{otherwise} \end{cases} + \begin{cases} R_{LL4}(x) \cdot \left(l_{p_{j+1}} - l_{p_4} \right) & \text{if } j \geq 4 \\ 0kip \cdot ft & \text{otherwise} \end{cases} \right]$$

$$R_{LLr}(x) := \frac{\sum_{i_{P1}=1}^{n_P} \left[\begin{array}{l} P_{i_{P1}} \cdot \left[\begin{array}{l} \left(x + d_{Pt_{i_{P1}-1}}\right) \text{ if } i_{P1} > 1 \quad - l_{p_1} \\ x \text{ if } i_{P1} = 1 \end{array} \right] \text{ if } 0\text{in} \le \left[\begin{array}{l} \left(x + d_{Pt_{i_{P1}-1}}\right) \text{ if } i_{P1} > 1 \\ x \text{ if } i_{P1} = 1 \end{array} \right] \le l_{t_{j+2}} \\ 0\text{kip} \cdot \text{ft} \quad \text{otherwise} \end{array} \right] \ldots}{l_{p_{j+1}}}$$
$$+ (-1) \cdot \left[\begin{array}{l} R_{LL2}(x) \cdot \left(l_{p_2} - l_{p_1}\right) + \left[\begin{array}{l} R_{LL3}(x) \cdot \left(l_{p_3} - l_{p_1}\right) \text{ if } j \ge 3 \\ 0\text{kip} \cdot \text{ft} \quad \text{otherwise} \end{array} \right] + \left[\begin{array}{l} R_{LL4}(x) \cdot \left(l_{p_4} - l_{p_1}\right) \text{ if } j \ge 4 \\ 0\text{kip} \cdot \text{ft} \quad \text{otherwise} \end{array} \right] \end{array} \right]$$

$x_{prova} := 20\text{ft}$

$R_{LLl}(x_{prova}) = 0.2724\,\text{kip}$

$R_{LL2}(x_{prova}) = -1.3679\,\text{kip}$

$R_{LL3}(x_{prova}) = 17.8463\,\text{kip}$

$R_{LL4}(x_{prova}) = 8.444\,\text{kip}$

$R_{LLr}(x_{prova}) = -1.1948\,\text{kip}$

$b(x_{prova}, 1) = 137.6852\,\text{ft}$

$b(x_{prova}, 2) = 219.2323\,\text{ft}$

$b(x_{prova}, 3) = 148.4405\,\text{ft}$

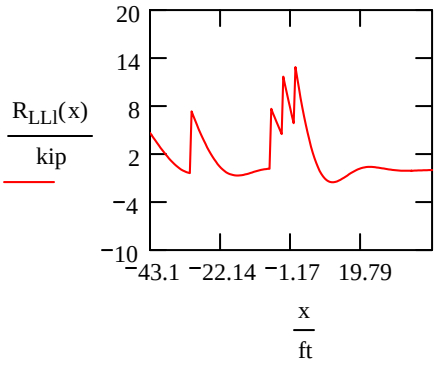

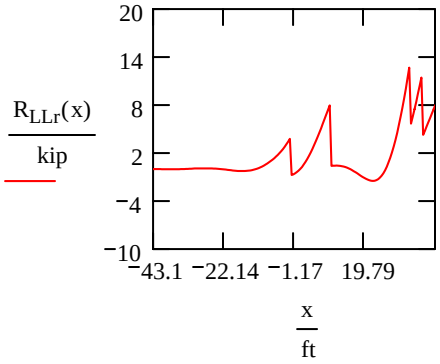

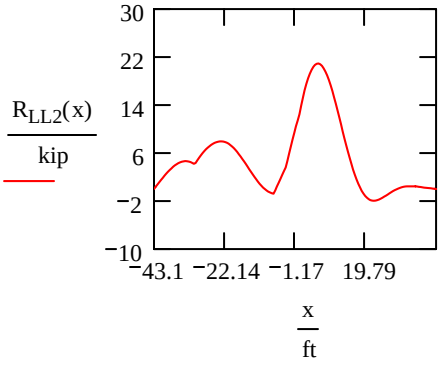

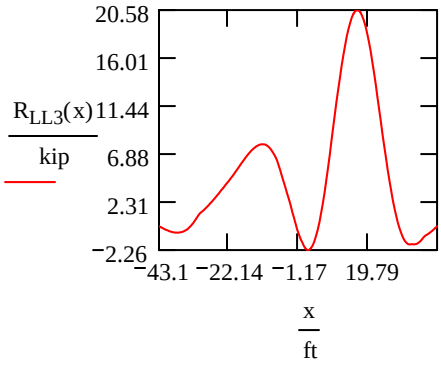

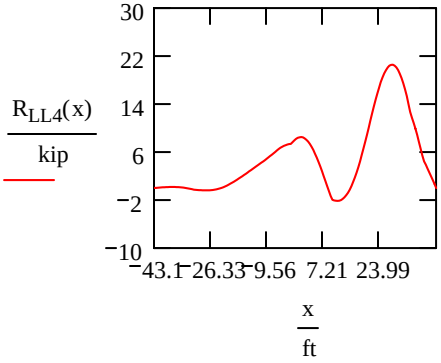

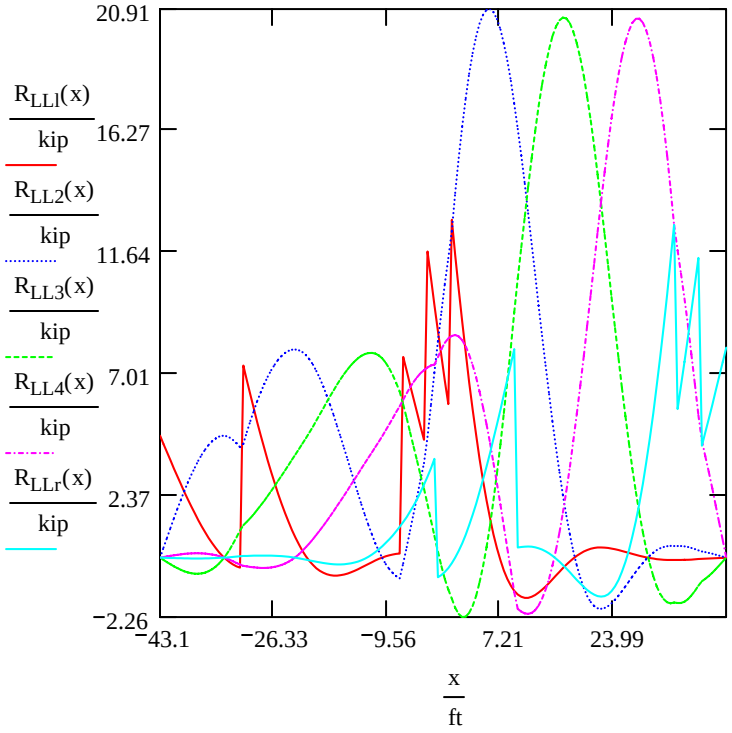

$$R(x) := R_{LLl}(x) + R_{LL2}(x) + R_{LL3}(x) + R_{LL4}(x) + R_{LLr}(x) - \left[\sum_{i_{P1}=1}^{n_P} \left[\begin{array}{ll} P_{i_{P1}} & \text{if } 0\text{in} \le \left[\begin{array}{ll} \left(x + d_{Pt_{i_{P1}-1}}\right) & \text{if } i_{P1} > 1 \\ x & \text{if } i_{P1} = 1 \end{array} \right] \le l_{t_{j+2}} \\ 0\text{kip} & \text{otherwise} \end{array} \right] \right]$$

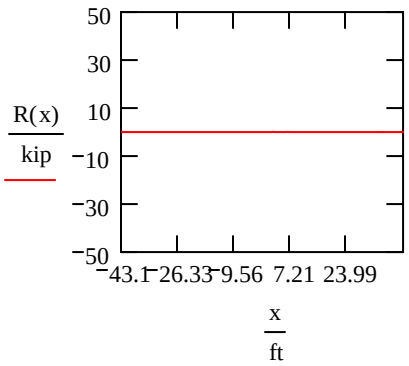

$$\Delta y := \frac{l_{t_{j+2}}}{n_{loop}}$$

$jj := 0, 1 .. n_{loop}$

$jjj := 0, 1 .. n_{loop}$

$y := -\Delta y, 0\text{in} .. l_{t_{j+2}} + \Delta y$

$$yy_{jj} := \frac{l_{t_{j+2}} \cdot jj}{n_{loop}}$$

$$xx_{jjj} := l_{min} + \frac{(l_{max} - l_{min}) \cdot jjj}{n_{loop}}$$

$x_1 := 0.000005 \cdot l_{p_1}$

$x_2 := x_1 + 0.5 \cdot l_3$

$x_3 := x_2 + 0.5 \cdot l_4$

$x_4 := x_3 + 0.5 \cdot l_5$

Shear Analysis

Shear expressions:

$$T_{LL}(x,y) := \sum_{i_{P1}=1}^{n_P} \left[\begin{cases} -P_{i_{P1}} & \text{if } y \geq x + d_{Pt_{i_{P1}-1}} \geq 0ft \wedge 0ft \leq y \leq l_{t_{j+2}} \\ (0kip) & \text{otherwise} \end{cases} \right] + \left[\begin{cases} R_{LLl}(x) & \text{if } l_{t_1} \leq y \leq l_{t_{j+2}} \\ (0kip) & \text{otherwise} \end{cases} \right] \ldots$$
$$+ \left[\begin{cases} R_{LL2}(x) & \text{if } l_{t_2} \leq y \leq l_{t_{j+2}} \\ (0 \cdot kip) & \text{otherwise} \end{cases} \right] + \left[\begin{cases} R_{LL3}(x) & \text{if } l_{t_3} \leq y \leq l_{t_{j+2}} \\ (0 \cdot kip) & \text{otherwise} \end{cases} \right] + \left[\begin{cases} R_{LL4}(x) & \text{if } l_{t_4} \leq y \leq l_{t_{j+2}} \\ (0kip) & \text{otherwise} \end{cases} \right] \ldots$$
$$+ \begin{cases} R_{LLr}(x) & \text{if } l_{t_{j+1}} \leq y \leq l_{t_{j+2}} \\ (0kip) & \text{otherwise} \end{cases}$$

Shear Analysis

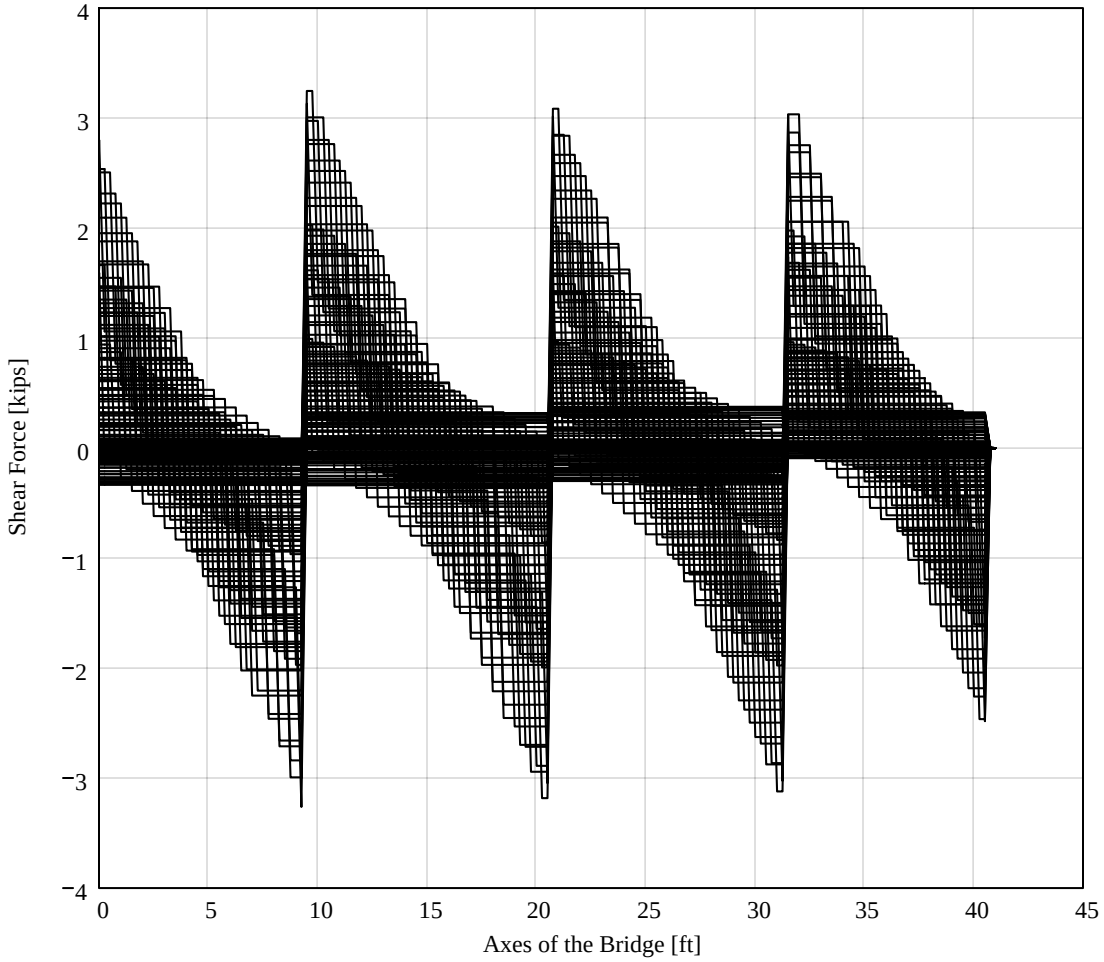

Moment expressions

Moment Analysis

$$M_{LL}(x,y) := \sum_{i_{P1}=1}^{n_P} \left[\begin{cases} -P_{i_{P1}} \cdot \left[y - \left(x + d_{Pt_{i_{P1}-1}} \right) \right] & \text{if } y \geq x + d_{Pt_{i_{P1}-1}} \geq 0\text{ft} \wedge 0\text{ft} \leq y \leq l_{t_{j+2}} \\ (0 \cdot \text{kip} \cdot \text{ft}) & \text{otherwise} \end{cases} \right] \ldots$$
$$+ \left[\begin{cases} R_{LLl}(x) \cdot \left(y - l_{t_1} \right) & \text{if } l_{t_1} \leq y \leq l_{t_{j+2}} \\ (0 \cdot \text{kip} \cdot \text{ft}) & \text{otherwise} \end{cases} \right] + \left[\begin{cases} R_{LLr}(x) \cdot \left(y - l_{t_{j+1}} \right) & \text{if } l_{t_{j+1}} \leq y \leq l_{t_{j+2}} \\ (0 \cdot \text{kip} \cdot \text{ft}) & \text{otherwise} \end{cases} \right] \ldots$$
$$+ \left[\begin{cases} R_{LL2}(x) \cdot \left(y - l_{t_2} \right) & \text{if } l_{t_2} \leq y \leq l_{t_{j+2}} \\ (0 \cdot \text{kip} \cdot \text{ft}) & \text{otherwise} \end{cases} \right] + \left[\begin{cases} R_{LL3}(x) \cdot \left(y - l_{t_3} \right) & \text{if } l_{t_3} \leq y \leq l_{t_{j+2}} \\ (0 \cdot \text{kip} \cdot \text{ft}) & \text{otherwise} \end{cases} \right] \ldots$$
$$+ \left[\begin{cases} R_{LL4}(x) \cdot \left(y - l_{t_4} \right) & \text{if } l_{t_4} \leq y \leq l_{t_{j+2}} \\ (0 \cdot \text{kip} \cdot \text{ft}) & \text{otherwise} \end{cases} \right]$$

Moment Analysis

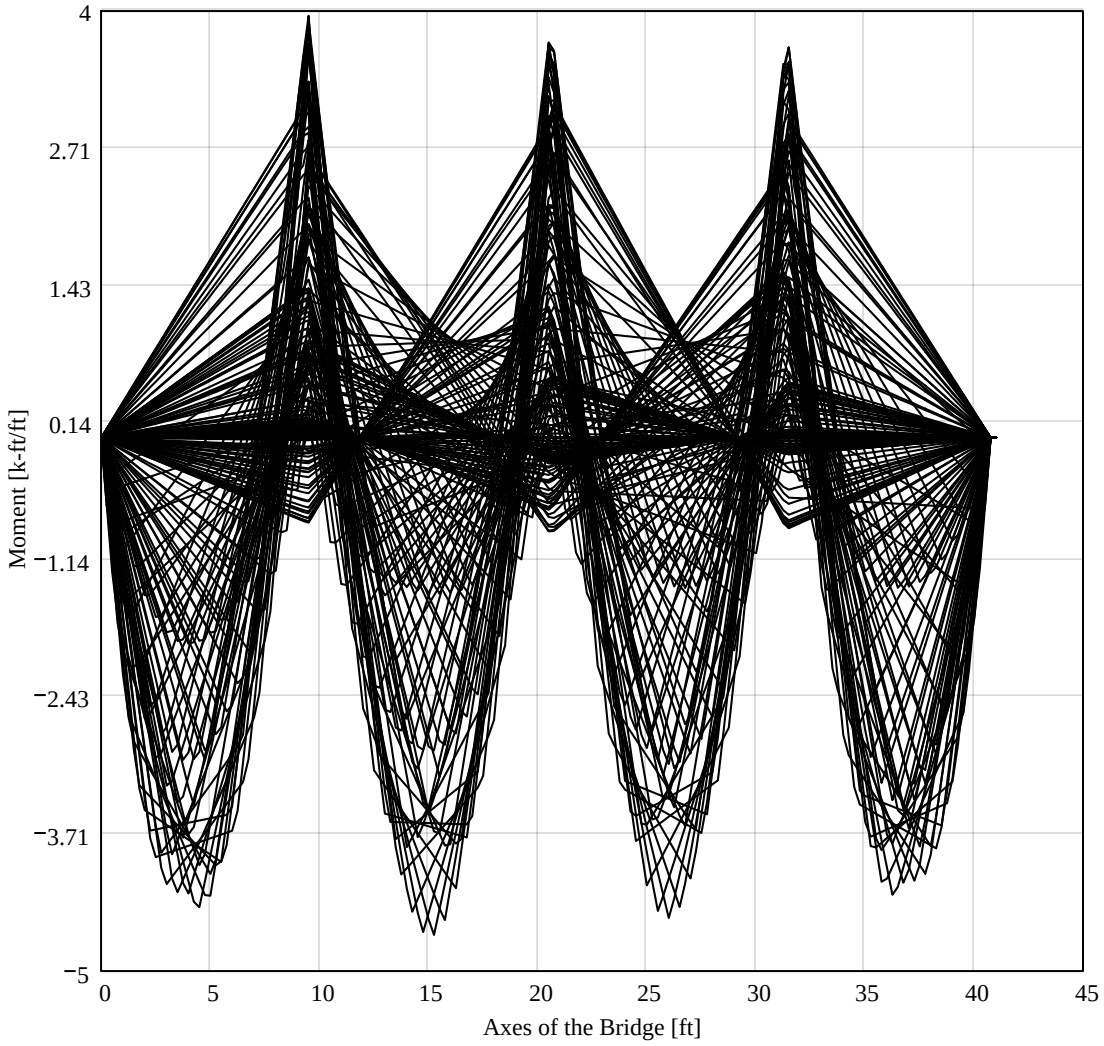

TRUCK H20

Geometric-Mechanic Data Input

$j := 4$ number of spans

$i := 1, 2 .. j + 2$ number of spans and cantilever beams

Length of the spans:

$l_1 := 0 \cdot ft$ left cantilever beam length (the j+1 is th rigth cantilever beam length)

$l_2 := 9.49 \cdot ft$

$l_3 := 11.10 \cdot ft$

$l_4 := 10.82 \cdot ft$

$l_5 := 9.35 \cdot ft$

$l_6 := 0 \cdot ft$

Geometric-Mechanic Data Input

Geometric-Mechanic Utilities

$ii := 1, 2 .. 6$

Total length until the ii span included:

$$l_{t_{ii}} := \begin{cases} \left(\sum_{ii=1}^{ii} l_{ii} \right) & \text{if } ii \le j + 2 \\ (0\,ft) & \text{otherwise} \end{cases}$$

Partial length until the ii span excluding the first cantilever beam:

$$l_{p_{ii}} := \begin{cases} \sum_{i1=2}^{ii} l_{i1} & \text{if } ii > 1 \wedge ii \le j + 2 \\ (0\,ft) & \text{otherwise} \end{cases}$$

Stiffness Calculation:

$$C_i := \begin{cases} 1 \cdot ksi^{-1} \cdot in^{-4} & \text{if } mode_{01} = 1 \\ \frac{1}{E_i \cdot I_i} & \text{otherwise} \end{cases}$$

Geometric-Mechanic Utilities

Moving Load Case

Load Data Input

Concentrated load:

$n_P := 3$ number of concentrated load

$P_1 := 8kip$

$P_2 := 8kip$

$P_3 := 4kip$

$P_4 := 0kip$

$P_5 := 0kip$

Distance between consecutive loads:

$dP_1 := 3.7917ft$

$dP_2 := 12.1042ft$

$dP_3 := 0ft$

$dP_4 := 0 \cdot ft$

$dP_5 := 0 \cdot ft$

Distance between the first load and the other:

$$i_P := \begin{cases} (1, 2 .. n_P - 1) & \text{if } n_P > 1 \\ 1 & \text{otherwise} \end{cases}$$

$$dPt_{i_P} := \sum_{i_P = 1}^{i_P} dP_{i_P}$$

$dPt_{i_P} =$

45.5004
190.7508

in

Load Data Input

Matrix View

This procedure is valid only if the stiffness is the same for all the spans!

$$C := \frac{1}{ksi \cdot ft^4}$$

$$Ac_{LL}(i1, i2) := C \cdot \left[-\left[\frac{\left(lp_{j+1} - lp_{i1+2}\right) \cdot \left(lp_{i2+2}\right)^3}{6 \cdot lp_{j+1}} \right] + \left[\frac{lp_{i1+2} \cdot \left(lp_{j+1} - lp_{i1+2}\right) \cdot \left(lp_{j+1} \cdot 2 - lp_{i1+2}\right) \cdot lp_{i2+2}}{6 \cdot lp_{j+1}} \right] \ldots \right] \cdot kip$$
$$+ \left[\begin{cases} \frac{\left(lp_{i2+2} - lp_{i1+2}\right)^3}{6} & \text{if } i2 > i1 \\ 0\,ft^3 & \text{otherwise} \end{cases} \right]$$

$$A_{LL} := \text{matrix}\left(j - 1, j - 1, Ac_{LL}\right)$$

$$A_{LL} = \begin{pmatrix} 1.5244 & 1.9292 & 1.1396 \\ 1.9292 & 2.9855 & 1.9162 \\ 1.1396 & 1.9162 & 1.493 \end{pmatrix}$$

Matrix View

Movement of the Loads:

Choose $mode_{kP}$ the range to find the load factor:
1 = total with less than the maximum number of the forces
2 = rational with all the load inside the width
3 = Renato (to check!)...

$$n_{loop} := \frac{lt_{j+2}}{3 \cdot in}$$

$$n_{loop} := \text{round}\left(n_{loop}\right)$$

$$n_{loop} = 163$$

$w_{curb} := 0in$ width of the curb or guardrail

$wp := 0\left(w_{curb} + 12in\right)$ $wp = 0\,ft$ max distance from the side of the deck (AASHTO Figure 3.7.6A)

$$l_{max} := lt_{j+2} - 0wp \qquad l_{min} := 0wp - dPt_{nP-1}$$

$$ipp := 1, 2 .. nP$$

$$x := l_{min}, \left[l_{min} + \frac{\left(l_{max} - l_{min}\right)}{n_{loop}} \right] .. l_{max}$$

$l_{max} = 40.76\,ft$ $l_{min} = -15.8959\,ft$

Moment on the Cantilever Beams

Moment due to the load on the cantilever beams:

$$M_{Plc}(x, ipp) := \begin{cases} \begin{cases} -P_{ipp} \cdot \left[l_1 - \left(x + dPt_{ipp-1} \right) \right] & \text{if } ipp > 1 \\ -P_{ipp} \cdot \left(l_1 - x \right) & \text{if } ipp = 1 \end{cases} & \text{if } 0in \le \begin{cases} x + dPt_{ipp-1} & \text{if } ipp > 1 \\ x & \text{if } ipp = 1 \end{cases} \le l_1 \\ 0kip \cdot ft & \text{otherwise} \end{cases}$$

$$M_{Pl}(x) := \sum_{ip1=1}^{np} M_{Plc}(x, ip1)$$

$$M_{Prc}(x, ipp) := \begin{cases} \begin{cases} -P_{ipp} \cdot \left[\left(x + dPt_{ipp-1} \right) - lt_{j+1} \right] & \text{if } ipp > 1 \\ -P_{ipp} \cdot \left(x - lt_{j+1} \right) & \text{if } ipp = 1 \end{cases} & \text{if } lt_{j+1} \le \begin{cases} x + dPt_{ipp-1} & \text{if } ipp > 1 \\ x & \text{if } ipp = 1 \end{cases} \le lt_{j+2} \\ 0kip \cdot ft & \text{otherwise} \end{cases}$$

$$M_{Pr}(x) := \sum_{ip1=1}^{np} M_{Plc}(x, ip1)$$

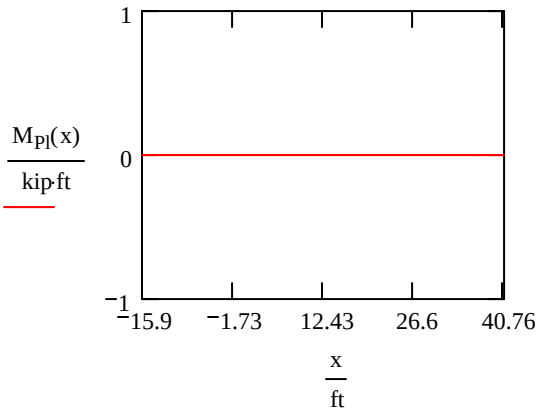

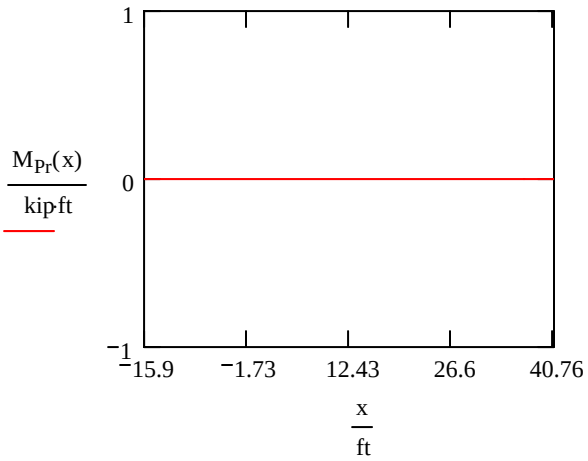

Moment on the Cantilever Beams

Supports Reactions for IN-Loads

Left support reaction due to the load between the 2 external supports (to solve the unknown):

$$R_{Pl}(x) := \sum_{ip1=1}^{np} \begin{cases} \begin{cases} P_{ip1} \cdot \begin{cases} \dfrac{lp_{j+1} - \left[\left(x - l_1 \right) + dPt_{ip1-1} \right]}{lp_{j+1}} & \text{if } ip1 > 1 \\ \dfrac{\left[lp_{j+1} - \left(x - l_1 \right) \right]}{lp_{j+1}} & \text{if } ip1 = 1 \end{cases} & \text{if } lt_1 \le \begin{cases} x + dPt_{ip1-1} & \text{if } ip1 > 1 \\ x & \text{if } ip1 = 1 \end{cases} \le lt_{j+1} \\ 0kip & \text{otherwise} \end{cases} \end{cases}$$

$$R_{Pr}(x) := \sum_{i_{P1}=1}^{n_P} \left[P_{i_{P1}} \cdot \left[\begin{cases} \left[\begin{cases} \dfrac{(x - l_1) + dPt_{i_{P1}-1}}{lp_{j+1}} & \text{if } i_{P1} > 1 \\ \dfrac{(x - l_1)}{lp_{j+1}} & \text{if } i_{P1} = 1 \end{cases} \right] & \text{if } l_{t_1} \le \left[\begin{cases} (x + dPt_{i_{P1}-1}) & \text{if } i_{P1} > 1 \\ x & \text{if } i_{P1} = 1 \end{cases} \right] \le l_{t_{j+1}} \\ 0 \quad \text{otherwise} \end{cases} \right] \right]$$

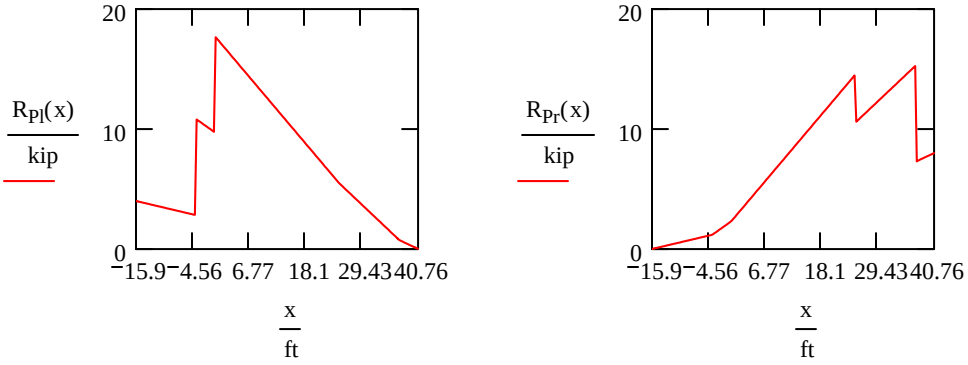

Supports Reactions for IN-Loads

System Solution

$k := 1, 2 .. j - 1$

$b(x, k) := \Delta pp\left(x, lp_{k+1}\right)$

Solution of this linear system: (A)(M_2, M_3, M_i) = (b_1, b_2, b_i)

WARNING
Add rows, matrix and "solutions" if j > 4.

WARNING
The dimension of the A_{LLi} is [m].

$$A_{LL2}(x) := \begin{pmatrix} b(x,1) & \begin{cases} Ac_{LL}(0,1) & \text{if } j \ge 3 \\ 0 & \text{otherwise} \end{cases} & \begin{cases} Ac_{LL}(0,2) & \text{if } j \ge 4 \\ 0 & \text{otherwise} \end{cases} \\ \begin{cases} b(x,2) & \text{if } j \ge 3 \\ 0 & \text{otherwise} \end{cases} & \begin{cases} Ac_{LL}(1,1) & \text{if } j \ge 3 \\ 1m & \text{otherwise} \end{cases} & \begin{cases} Ac_{LL}(1,2) & \text{if } j \ge 4 \\ 0 & \text{otherwise} \end{cases} \\ \begin{cases} b(x,3) & \text{if } j \ge 4 \\ 0 & \text{otherwise} \end{cases} & \begin{cases} Ac_{LL}(2,1) & \text{if } j \ge 4 \\ 0 & \text{otherwise} \end{cases} & \begin{cases} Ac_{LL}(2,2) & \text{if } j \ge 4 \\ 1m & \text{otherwise} \end{cases} \end{pmatrix}$$

$$A_{LL3}(x) := \begin{cases} \begin{pmatrix} Ac_{LL}(0,0) & \begin{cases} b(x,1) & \text{if } j \geq 3 \\ 0 & \text{otherwise} \end{cases} & \begin{cases} Ac_{LL}(0,2) & \text{if } j \geq 4 \\ 0 & \text{otherwise} \end{cases} \\ \begin{cases} Ac_{LL}(1,0) & \text{if } j \geq 3 \\ 0 & \text{otherwise} \end{cases} & \begin{cases} b(x,2) & \text{if } j \geq 3 \\ 1m & \text{otherwise} \end{cases} & \begin{cases} Ac_{LL}(1,2) & \text{if } j \geq 4 \\ 0ft & \text{otherwise} \end{cases} \\ \begin{cases} Ac_{LL}(2,0) & \text{if } j \geq 4 \\ 0 & \text{otherwise} \end{cases} & \begin{cases} b(x,3) & \text{if } j \geq 4 \\ 0 & \text{otherwise} \end{cases} & \begin{cases} Ac_{LL}(2,2) & \text{if } j \geq 4 \\ 1m & \text{otherwise} \end{cases} \end{pmatrix} & \text{if } j \geq 3 \\ 0m^3 & \text{otherwise} \end{cases}$$

$$A_{LL4}(x) := \begin{cases} \begin{pmatrix} Ac_{LL}(0,0) & \begin{cases} Ac_{LL}(0,1) & \text{if } j \geq 3 \\ 0 & \text{otherwise} \end{cases} & \begin{cases} b(x,1) & \text{if } j \geq 4 \\ 0 & \text{otherwise} \end{cases} \\ \begin{cases} Ac_{LL}(1,0) & \text{if } j \geq 3 \\ 0 & \text{otherwise} \end{cases} & \begin{cases} Ac_{LL}(1,1) & \text{if } j \geq 3 \\ 1m & \text{otherwise} \end{cases} & \begin{cases} b(x,2) & \text{if } j \geq 4 \\ 0 & \text{otherwise} \end{cases} \\ \begin{cases} Ac_{LL}(2,0) & \text{if } j \geq 4 \\ 0 & \text{otherwise} \end{cases} & \begin{cases} Ac_{LL}(2,1) & \text{if } j \geq 4 \\ 0 & \text{otherwise} \end{cases} & \begin{cases} b(x,3) & \text{if } j \geq 4 \\ 1m & \text{otherwise} \end{cases} \end{pmatrix} & \text{if } j \geq 4 \\ 0m^3 & \text{otherwise} \end{cases}$$

System Solution

$$R_{LL2}(x) := \left(\frac{|A_{LL2}(x)|}{|A_{LL}|} \right) \cdot \frac{kip}{m^3}$$

WARNING
The dimension of the !A_{cLL}! is [m³] while A_{LL} is dimensionless and the results have to be in kip.
The power in the denominator has to be j_{max} available.

$$R_{LL3}(x) := \left(\frac{|A_{LL3}(x)|}{|A_{LL}|} \right) \cdot \frac{kip}{m^3}$$

$$R_{LL4}(x) := \left(\frac{|A_{LL4}(x)|}{|A_{LL}|} \right) \cdot \frac{kip}{m^3}$$

$$R_{LLl}(x) := \frac{\sum_{iP1=1}^{nP} \left[\begin{cases} P_{iP1} \cdot \left[l_{t_{j+1}} - \left[\begin{cases} \left(x + dP_{t_{iP1-1}} \right) & \text{if } iP1 > 1 \\ x & \text{if } iP1 = 1 \end{cases} \right] \right] & \text{if } 0 \cdot in \leq \left[\begin{cases} \left(x + dP_{t_{iP1-1}} \right) & \text{if } iP1 > 1 \\ x & \text{if } iP1 = 1 \end{cases} \right] \leq l_{t_{j+2}} \\ 0 \cdot kip \cdot ft & \text{otherwise} \end{cases} \right] ... + (-1) \cdot \left[R_{LL2}(x) \cdot \left(l_{p_{j+1}} - l_{p_2} \right) + \begin{cases} R_{LL3}(x) \cdot \left(l_{p_{j+1}} - l_{p_3} \right) & \text{if } j \geq 3 \\ 0kip \cdot ft & \text{otherwise} \end{cases} + \begin{cases} R_{LL4}(x) \cdot \left(l_{p_{j+1}} - l_{p_4} \right) & \text{if } j \geq 4 \\ 0kip \cdot ft & \text{otherwise} \end{cases} \right]}{l_{p_{j+1}}}$$

$$R_{LLr}(x) := \frac{\sum_{i_{P1}=1}^{n_P} \left[\begin{array}{l} P_{i_{P1}} \cdot \left[\begin{array}{l} \left(x + d_{Pt_{i_{P1}-1}}\right) \text{ if } i_{P1} > 1 \quad - l_{p_1} \\ x \text{ if } i_{P1} = 1 \end{array} \right] \text{ if } 0in \le \left[\begin{array}{l} \left(x + d_{Pt_{i_{P1}-1}}\right) \text{ if } i_{P1} > 1 \\ x \text{ if } i_{P1} = 1 \end{array} \right] \le l_{t_{j+2}} \\ 0kip \cdot ft \quad \text{otherwise} \end{array} \right] \ldots}{l_{p_{j+1}}}$$
$$+ (-1) \cdot \left[\begin{array}{l} R_{LL2}(x) \cdot \left(l_{p_2} - l_{p_1}\right) + \left[\begin{array}{l} R_{LL3}(x) \cdot \left(l_{p_3} - l_{p_1}\right) \text{ if } j \ge 3 \quad + \left[\begin{array}{l} R_{LL4}(x) \cdot \left(l_{p_4} - l_{p_1}\right) \text{ if } j \ge 4 \\ 0kip \cdot ft \quad \text{otherwise} \end{array} \right. \\ 0kip \cdot ft \quad \text{otherwise} \end{array} \right. \end{array} \right]$$

$x_{prova} := 20ft$

$R_{LLl}(x_{prova}) = 0.0996\,kip$

$R_{LL2}(x_{prova}) = -0.4993\,kip$

$R_{LL3}(x_{prova}) = 14.1116\,kip$

$R_{LL4}(x_{prova}) = 5.1556\,kip$

$R_{LLr}(x_{prova}) = 1.1325\,kip$

$b(x_{prova}, 1) = 106.0965\,ft$

$b(x_{prova}, 2) = 167.4757\,ft$

$b(x_{prova}, 3) = 112.102\,ft$

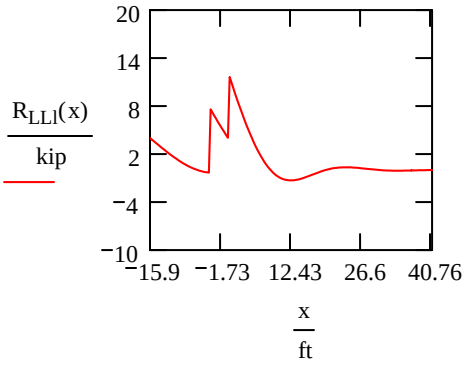

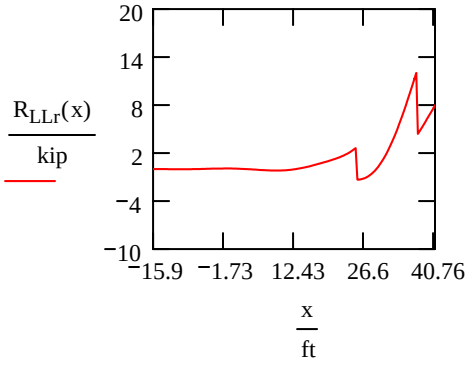

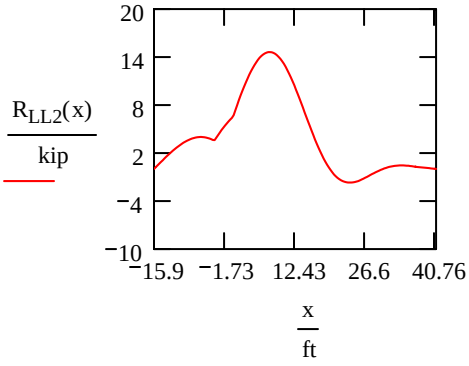

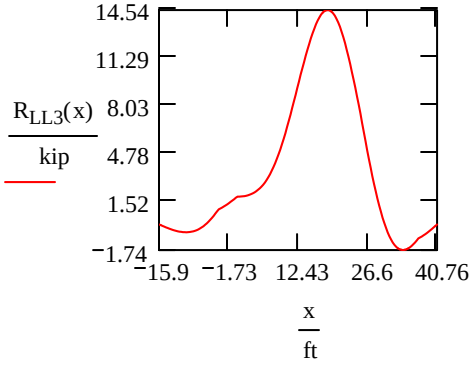

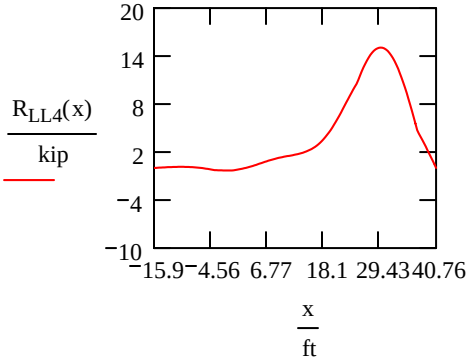

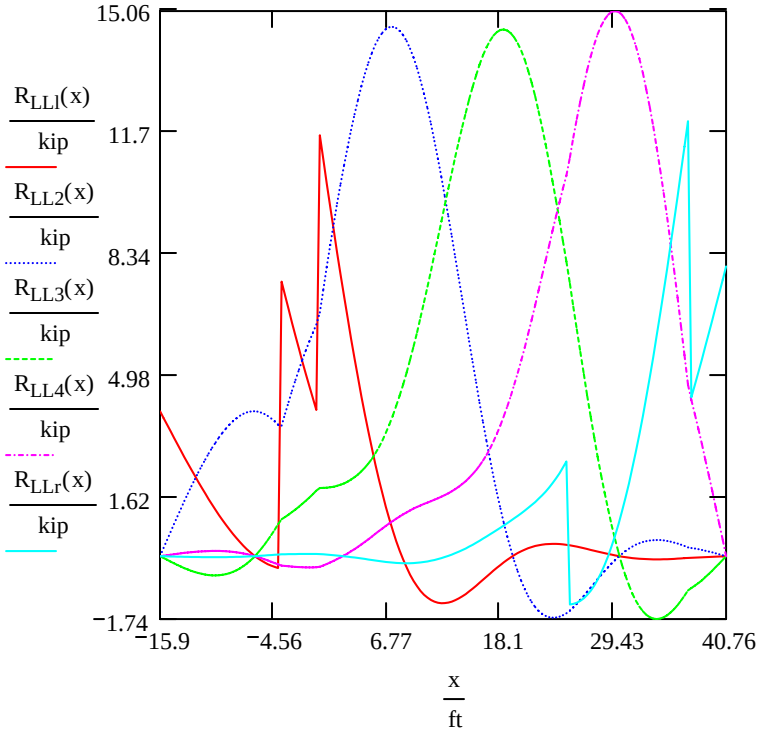

$$R(x) := R_{LLl}(x) + R_{LL2}(x) + R_{LL3}(x) + R_{LL4}(x) + R_{LLr}(x) - \left[\sum_{i_{P1}=1}^{n_P} \left[\begin{array}{l} P_{i_{P1}} \text{ if } 0in \le \left[\begin{array}{l} \left(x + d_{Pt_{i_{P1}-1}}\right) \text{ if } i_{P1} > 1 \\ x \text{ if } i_{P1} = 1 \end{array} \right] \le l_{t_{j+2}} \\ 0kip \text{ otherwise} \end{array} \right] \right]$$

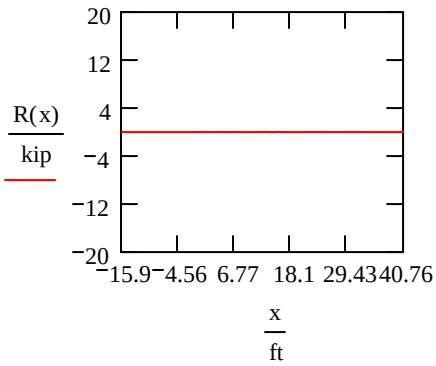

$$\Delta y := \frac{l_{t_{j+2}}}{n_{loop}}$$

$jj := 0, 1 .. n_{loop}$

$jjj := 0, 1 .. n_{loop}$

$y := -\Delta y, 0in .. l_{t_{j+2}} + \Delta y$

$$yy_{jj} := \frac{l_{t_{j+2}} \cdot jj}{n_{loop}}$$

$$xx_{jjj} := l_{min} + \frac{(l_{max} - l_{min}) \cdot jjj}{n_{loop}}$$

$x_1 := 0.000005 \cdot l_{p_1}$

$x_2 := x_1 + 0.5 \cdot l_3$

$x_3 := x_2 + 0.5 \cdot l_4$

$x_4 := x_3 + 0.5 \cdot l_5$

Shear Analysis

Shear expressions:

$$T_{LL}(x,y) := \sum_{i_{P1}=1}^{n_P} \left[\begin{cases} -P_{i_{P1}} & \text{if } y \geq x + d_{Pt_{i_{P1}-1}} \geq 0ft \wedge 0ft \leq y \leq l_{t_{j+2}} \\ (0kip) & \text{otherwise} \end{cases} \right] + \left[\begin{cases} R_{LLl}(x) & \text{if } l_{t_1} \leq y \leq l_{t_{j+2}} \\ (0kip) & \text{otherwise} \end{cases} \right] \ldots$$
$$+ \left[\begin{cases} R_{LL2}(x) & \text{if } l_{t_2} \leq y \leq l_{t_{j+2}} \\ (0 \cdot kip) & \text{otherwise} \end{cases} \right] + \left[\begin{cases} R_{LL3}(x) & \text{if } l_{t_3} \leq y \leq l_{t_{j+2}} \\ (0 \cdot kip) & \text{otherwise} \end{cases} \right] + \left[\begin{cases} R_{LL4}(x) & \text{if } l_{t_4} \leq y \leq l_{t_{j+2}} \\ (0kip) & \text{otherwise} \end{cases} \right] \ldots$$
$$+ \begin{cases} R_{LLr}(x) & \text{if } l_{t_{j+1}} \leq y \leq l_{t_{j+2}} \\ (0kip) & \text{otherwise} \end{cases}$$

Shear Analysis

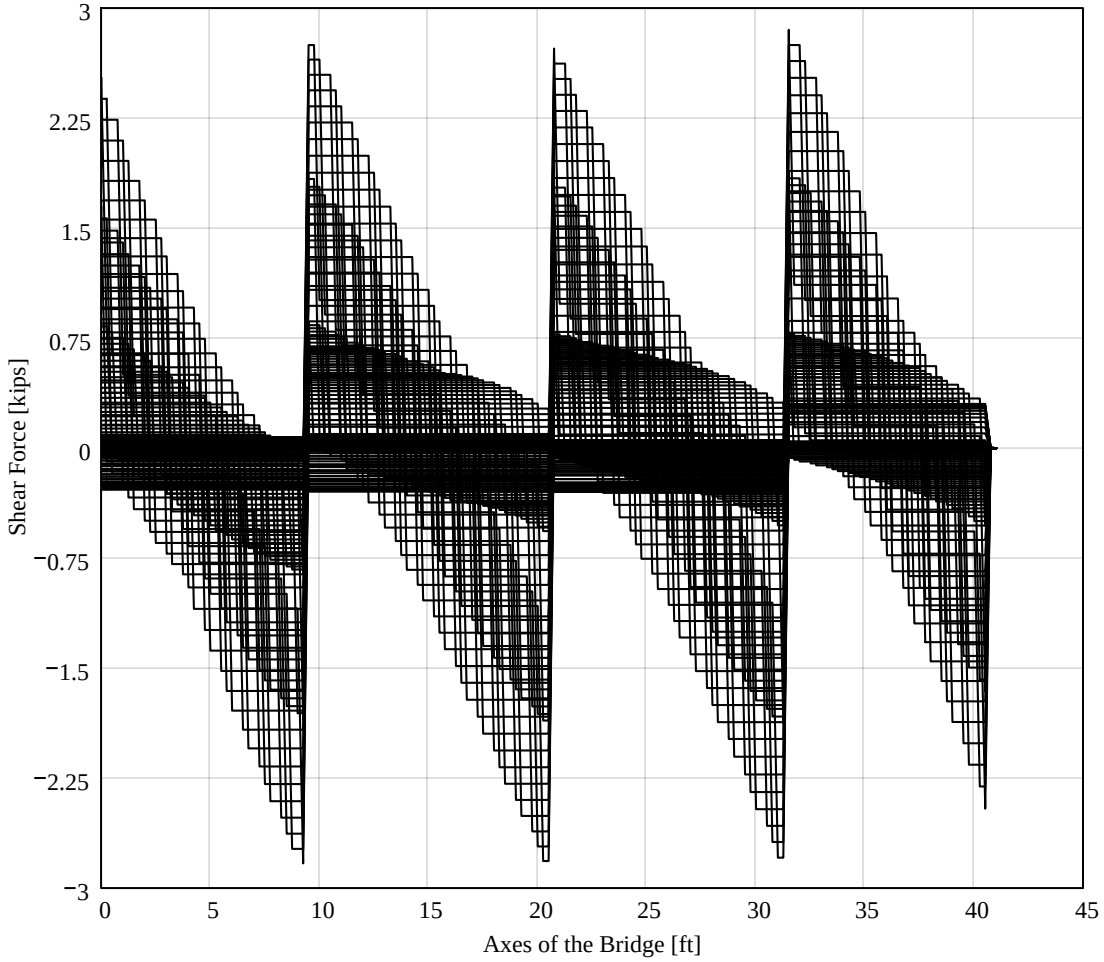

Moment expressions

Moment Analysis

$$M_{LL}(x,y) := \sum_{i_{P1}=1}^{n_P} \left[\begin{cases} -P_{i_{P1}} \cdot \left[y - \left(x + d_{Pt_{i_{P1}-1}} \right) \right] & \text{if } y \geq x + d_{Pt_{i_{P1}-1}} \geq 0\text{ft} \wedge 0\text{ft} \leq y \leq l_{t_{j+2}} \\ (0 \cdot \text{kip} \cdot \text{ft}) & \text{otherwise} \end{cases} \right] \ldots$$
$$+ \left[\begin{cases} R_{LLl}(x) \cdot \left(y - l_{t_1} \right) & \text{if } l_{t_1} \leq y \leq l_{t_{j+2}} \\ (0 \cdot \text{kip} \cdot \text{ft}) & \text{otherwise} \end{cases} \right] + \left[\begin{cases} R_{LLr}(x) \cdot \left(y - l_{t_{j+1}} \right) & \text{if } l_{t_{j+1}} \leq y \leq l_{t_{j+2}} \\ (0 \cdot \text{kip} \cdot \text{ft}) & \text{otherwise} \end{cases} \right] \ldots$$
$$+ \left[\begin{cases} R_{LL2}(x) \cdot \left(y - l_{t_2} \right) & \text{if } l_{t_2} \leq y \leq l_{t_{j+2}} \\ (0 \cdot \text{kip} \cdot \text{ft}) & \text{otherwise} \end{cases} \right] + \left[\begin{cases} R_{LL3}(x) \cdot \left(y - l_{t_3} \right) & \text{if } l_{t_3} \leq y \leq l_{t_{j+2}} \\ (0 \cdot \text{kip} \cdot \text{ft}) & \text{otherwise} \end{cases} \right] \ldots$$
$$+ \left[\begin{cases} R_{LL4}(x) \cdot \left(y - l_{t_4} \right) & \text{if } l_{t_4} \leq y \leq l_{t_{j+2}} \\ (0 \cdot \text{kip} \cdot \text{ft}) & \text{otherwise} \end{cases} \right]$$

Moment Analysis

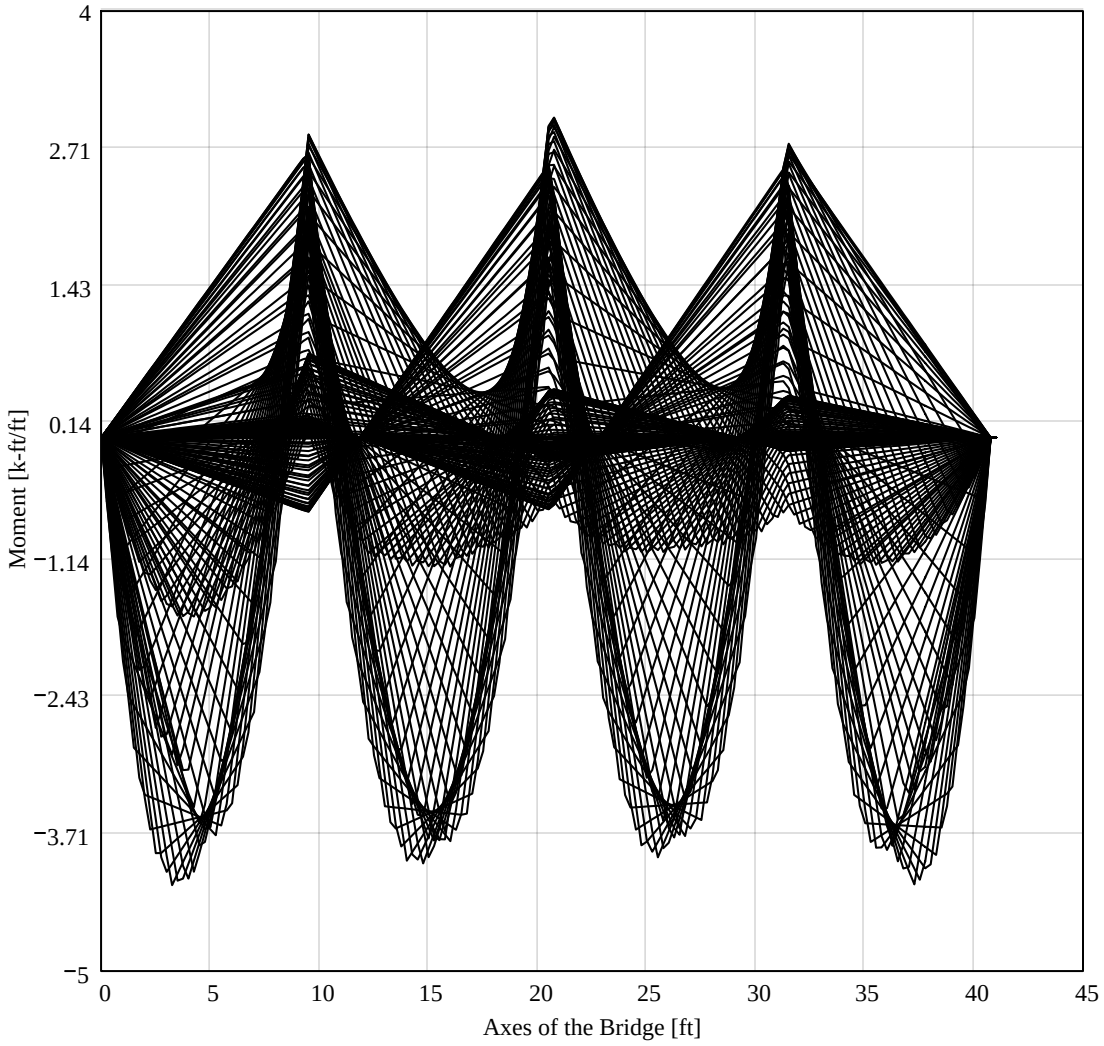

TRUCK 3S2

Geometric-Mechanic Data Input

$j := 4$ number of spans

$i := 1, 2 .. j + 2$ number of spans and cantilever beams

Length of the spans:

$l_1 := 0 \cdot ft$ left cantilever beam length (the j+1 is th rigth cantilever beam length)

$l_2 := 9.49 \cdot ft$

$l_3 := 11.10 \cdot ft$

$l_4 := 10.82 \cdot ft$

$l_5 := 9.35 \cdot ft$

$l_6 := 0 \cdot ft$

Geometric-Mechanic Data Input

Geometric-Mechanic Utilities

$ii := 1, 2 .. 6$

Total length until the ii span included:

$$l_{t_{ii}} := \begin{cases} \left(\sum_{ii=1}^{ii} l_{ii} \right) & \text{if } ii \le j + 2 \\ (0\,ft) & \text{otherwise} \end{cases}$$

Partial length until the ii span excluding the first cantilever beam:

$$l_{p_{ii}} := \begin{cases} \sum_{i1=2}^{ii} l_{i1} & \text{if } ii > 1 \wedge ii \le j + 2 \\ (0\,ft) & \text{otherwise} \end{cases}$$

Stiffness Calculation:

$$C_i := \begin{cases} 1 \cdot ksi^{-1} \cdot in^{-4} & \text{if } mode_{01} = 1 \\ \frac{1}{E_i \cdot I_i} & \text{otherwise} \end{cases}$$

Geometric-Mechanic Utilities

Moving Load Case

Load Data Input

Concentrated load:

$n_P := 5$ number of concentrated load

$P_1 := 8kip$

$P_2 := 8kip$

$P_3 := 8kip$

$P_4 := 8kip$

$P_5 := 4.64kip$

Distance between consecutive loads:

$dp_1 := 3.7917ft$

$dp_2 := 23.4167ft$

$dp_3 := 3.7917ft$

$dp_4 := 12.1042ft$

Distance between the first load and the other:

$$i_P := \begin{cases} (1, 2 .. n_P - 1) & \text{if } n_P > 1 \\ 1 & \text{otherwise} \end{cases}$$

$$dpt_{i_P} := \sum_{i_P = 1}^{i_P} dp_{i_P}$$

$dpt_{i_P} =$

45.5004	in
326.5008	
372.0012	
517.2516	

Load Data Input

Fundamental matrix of UNIT LOAD in the internal girders positions:

Matrix View

This procedure is valid only if the stiffness is the same for all the spans!

$$C := \frac{1}{ksi \cdot ft^4}$$

$$Ac_{LL}(i1, i2) := C \cdot \left[-\left[\frac{\left(lp_{j+1} - lp_{i1+2}\right) \cdot \left(lp_{i2+2}\right)^3}{6 \cdot lp_{j+1}} \right] + \left[\frac{lp_{i1+2} \cdot \left(lp_{j+1} - lp_{i1+2}\right) \cdot \left(lp_{j+1} \cdot 2 - lp_{i1+2}\right) \cdot lp_{i2+2}}{6 \cdot lp_{j+1}} \right] \ldots \right] \cdot kip$$
$$+ \left[\begin{cases} \frac{\left(lp_{i2+2} - lp_{i1+2}\right)^3}{6} & \text{if } i2 > i1 \\ 0\,ft^3 & \text{otherwise} \end{cases} \right]$$

$$A_{LL} := \text{matrix}\left(j - 1, j - 1, Ac_{LL}\right)$$

$$A_{LL} = \begin{pmatrix} 1.5244 & 1.9292 & 1.1396 \\ 1.9292 & 2.9855 & 1.9162 \\ 1.1396 & 1.9162 & 1.493 \end{pmatrix}$$

Matrix View

Movement of the Loads:

Choose $mode_{kP}$ the range to find the load factor:
1 = total with less than the maximum number of the forces
2 = rational with all the load inside the width
3 = Renato (to check!)...

$$n_{loop} := \frac{lt_{j+2}}{3 \cdot in}$$

$$n_{loop} := \text{round}\left(n_{loop}\right)$$

$$n_{loop} = 163$$

$w_{curb} := 0in$ width of the curb or guardrail

$wp := 0\left(w_{curb} + 12in\right) \quad wp = 0\ ft$ max distance from the side of the deck (AASHTO Figure 3.7.6A)

$$l_{max} := lt_{j+2} - 0wp \qquad l_{min} := 0wp - dPt_{nP-1}$$

$$ipp := 1, 2 .. nP$$

$$x := l_{min}, \left[l_{min} + \frac{\left(l_{max} - l_{min}\right)}{n_{loop}} \right] .. l_{max} \qquad l_{max} = 40.76\ ft \qquad l_{min} = -43.1043\ ft$$

Moment on the Cantilever Beams

Moment due to the load on the cantilever beams:

$$M_{Plc}(x, ipp) := \begin{cases} \begin{cases} -P_{ipp} \cdot \begin{cases} \left[l_1 - \left(x + dPt_{ipp-1}\right)\right] & \text{if } ipp > 1 \\ \left(l_1 - x\right) & \text{if } ipp = 1 \end{cases} \end{cases} & \text{if } 0in \le \begin{cases} \left(x + dPt_{ipp-1}\right) & \text{if } ipp > 1 \\ x & \text{if } ipp = 1 \end{cases} \le l_1 \\ 0kip \cdot ft & \text{otherwise} \end{cases}$$

$$M_{Pl}(x) := \sum_{ip1=1}^{np} M_{Plc}(x, ip1)$$

$$M_{Prc}(x, ipp) := \begin{cases} \begin{cases} -P_{ipp} \cdot \begin{cases} \left[\left(x + dPt_{ipp-1}\right) - lt_{j+1}\right] & \text{if } ipp > 1 \\ \left(x - lt_{j+1}\right) & \text{if } ipp = 1 \end{cases} \end{cases} & \text{if } lt_{j+1} \le \begin{cases} \left(x + dPt_{ipp-1}\right) & \text{if } ipp > 1 \\ x & \text{if } ipp = 1 \end{cases} \le lt_{j+2} \\ 0kip \cdot ft & \text{otherwise} \end{cases}$$

$$M_{Pr}(x) := \sum_{ip1=1}^{np} M_{Plc}(x, ip1)$$

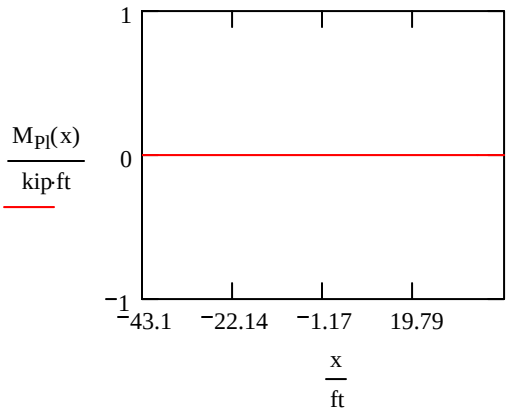

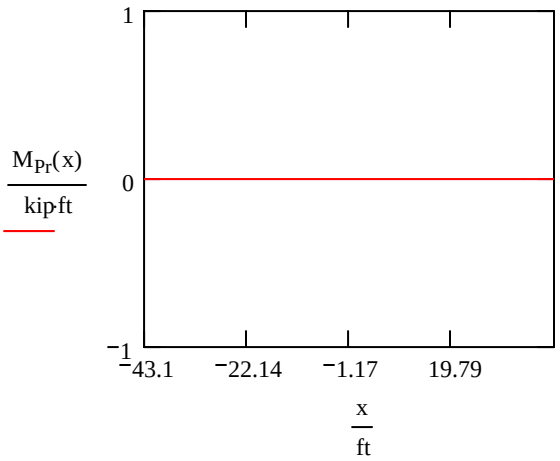

Moment on the Cantilever Beams

Supports Reactions for IN-Loads

Left support reaction due to the load between the 2 external supports (to solve the unknown):

$$R_{Pl}(x) := \sum_{ip1=1}^{np} \begin{cases} \begin{cases} P_{ip1} \cdot \begin{cases} \dfrac{lp_{j+1} - \left[\left(x - l_1\right) + dPt_{ip1-1}\right]}{lp_{j+1}} & \text{if } ip1 > 1 \\ \dfrac{\left[lp_{j+1} - \left(x - l_1\right)\right]}{lp_{j+1}} & \text{if } ip1 = 1 \end{cases} \end{cases} & \text{if } lt_1 \le \begin{cases} \left(x + dPt_{ip1-1}\right) & \text{if } ip1 > 1 \\ x & \text{if } ip1 = 1 \end{cases} \le lt_{j+1} \\ 0kip & \text{otherwise} \end{cases}$$

$$R_{Pr}(x) := \sum_{i_{P1}=1}^{n_P} \left[P_{i_{P1}} \cdot \left[\begin{cases} \left[\begin{cases} \dfrac{(x - l_1) + dPt_{i_{P1}-1}}{lp_{j+1}} & \text{if } i_{P1} > 1 \\ \dfrac{(x - l_1)}{lp_{j+1}} & \text{if } i_{P1} = 1 \end{cases} \right] & \text{if } l_{t_1} \le \left[\begin{cases} (x + dPt_{i_{P1}-1}) & \text{if } i_{P1} > 1 \\ x & \text{if } i_{P1} = 1 \end{cases} \right] \le l_{t_{j+1}} \\ 0 \quad \text{otherwise} \end{cases} \right] \right]$$

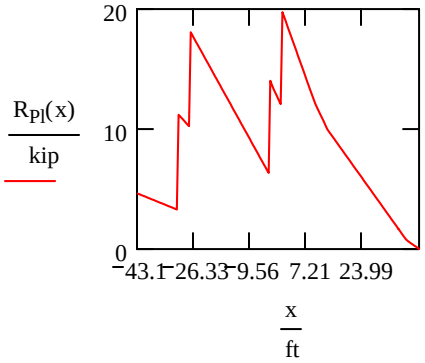

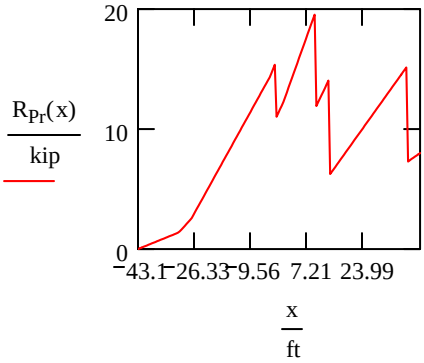

Supports Reactions for IN-Loads

System Solution

$k := 1, 2 .. j - 1$

$b(x, k) := \Delta pp\left(x, lp_{k+1}\right)$

Solution of this linear system: (A)(M_2, M_3, M_i) = (b_1, b_2, b_i)

WARNING
Add rows, matrix and "solutions" if j > 4.

WARNING
The dimension of the A_{LLi} is [m].

$$A_{LL2}(x) := \begin{pmatrix} b(x,1) & \begin{cases} Ac_{LL}(0,1) & \text{if } j \ge 3 \\ 0 & \text{otherwise} \end{cases} & \begin{cases} Ac_{LL}(0,2) & \text{if } j \ge 4 \\ 0 & \text{otherwise} \end{cases} \\ \begin{cases} b(x,2) & \text{if } j \ge 3 \\ 0 & \text{otherwise} \end{cases} & \begin{cases} Ac_{LL}(1,1) & \text{if } j \ge 3 \\ 1m & \text{otherwise} \end{cases} & \begin{cases} Ac_{LL}(1,2) & \text{if } j \ge 4 \\ 0 & \text{otherwise} \end{cases} \\ \begin{cases} b(x,3) & \text{if } j \ge 4 \\ 0 & \text{otherwise} \end{cases} & \begin{cases} Ac_{LL}(2,1) & \text{if } j \ge 4 \\ 0 & \text{otherwise} \end{cases} & \begin{cases} Ac_{LL}(2,2) & \text{if } j \ge 4 \\ 1m & \text{otherwise} \end{cases} \end{pmatrix}$$

$$A_{LL3}(x) := \begin{cases} \begin{pmatrix} Ac_{LL}(0,0) & \begin{cases} b(x,1) & \text{if } j \geq 3 \\ 0 & \text{otherwise} \end{cases} & \begin{cases} Ac_{LL}(0,2) & \text{if } j \geq 4 \\ 0 & \text{otherwise} \end{cases} \\ \begin{cases} Ac_{LL}(1,0) & \text{if } j \geq 3 \\ 0 & \text{otherwise} \end{cases} & \begin{cases} b(x,2) & \text{if } j \geq 3 \\ 1m & \text{otherwise} \end{cases} & \begin{cases} Ac_{LL}(1,2) & \text{if } j \geq 4 \\ 0ft & \text{otherwise} \end{cases} \\ \begin{cases} Ac_{LL}(2,0) & \text{if } j \geq 4 \\ 0 & \text{otherwise} \end{cases} & \begin{cases} b(x,3) & \text{if } j \geq 4 \\ 0 & \text{otherwise} \end{cases} & \begin{cases} Ac_{LL}(2,2) & \text{if } j \geq 4 \\ 1m & \text{otherwise} \end{cases} \end{pmatrix} & \text{if } j \geq 3 \\ 0m^3 & \text{otherwise} \end{cases}$$

$$A_{LL4}(x) := \begin{cases} \begin{pmatrix} Ac_{LL}(0,0) & \begin{cases} Ac_{LL}(0,1) & \text{if } j \geq 3 \\ 0 & \text{otherwise} \end{cases} & \begin{cases} b(x,1) & \text{if } j \geq 4 \\ 0 & \text{otherwise} \end{cases} \\ \begin{cases} Ac_{LL}(1,0) & \text{if } j \geq 3 \\ 0 & \text{otherwise} \end{cases} & \begin{cases} Ac_{LL}(1,1) & \text{if } j \geq 3 \\ 1m & \text{otherwise} \end{cases} & \begin{cases} b(x,2) & \text{if } j \geq 4 \\ 0 & \text{otherwise} \end{cases} \\ \begin{cases} Ac_{LL}(2,0) & \text{if } j \geq 4 \\ 0 & \text{otherwise} \end{cases} & \begin{cases} Ac_{LL}(2,1) & \text{if } j \geq 4 \\ 0 & \text{otherwise} \end{cases} & \begin{cases} b(x,3) & \text{if } j \geq 4 \\ 1m & \text{otherwise} \end{cases} \end{pmatrix} & \text{if } j \geq 4 \\ 0m^3 & \text{otherwise} \end{cases}$$

System Solution

$$R_{LL2}(x) := \left(\frac{|A_{LL2}(x)|}{|A_{LL}|} \right) \cdot \frac{kip}{m^3}$$

WARNING
The dimension of the !A_{cLL}! is [m³] while A_{LL} is dimensionless and the results have to be in kip.
The power in the denominator has to be j_{max} available.

$$R_{LL3}(x) := \left(\frac{|A_{LL3}(x)|}{|A_{LL}|} \right) \cdot \frac{kip}{m^3}$$

$$R_{LL4}(x) := \left(\frac{|A_{LL4}(x)|}{|A_{LL}|} \right) \cdot \frac{kip}{m^3}$$

$$R_{LLl}(x) := \frac{\sum_{i_{P1}=1}^{n_P} \left[\begin{cases} P_{i_{P1}} \cdot \left[l_{t_{j+1}} - \left[\begin{cases} \left(x + dP_{t_{i_{P1}-1}} \right) & \text{if } i_{P1} > 1 \\ x & \text{if } i_{P1} = 1 \end{cases} \right] \right] & \text{if } 0 \cdot in \leq \left[\begin{cases} \left(x + dP_{t_{i_{P1}-1}} \right) & \text{if } i_{P1} > 1 \\ x & \text{if } i_{P1} = 1 \end{cases} \right] \leq l_{t_{j+2}} \\ 0 \cdot kip \cdot ft & \text{otherwise} \end{cases} \right] \ldots}{l_{p_{j+1}}}$$
$$+ (-1) \cdot \left[R_{LL2}(x) \cdot \left(l_{p_{j+1}} - l_{p_2} \right) + \begin{cases} R_{LL3}(x) \cdot \left(l_{p_{j+1}} - l_{p_3} \right) & \text{if } j \geq 3 \\ 0kip \cdot ft & \text{otherwise} \end{cases} + \begin{cases} R_{LL4}(x) \cdot \left(l_{p_{j+1}} - l_{p_4} \right) & \text{if } j \geq 4 \\ 0kip \cdot ft & \text{otherwise} \end{cases} \right]$$

$$R_{LLr}(x) := \frac{\sum_{i_{P1}=1}^{n_P} \left[\begin{cases} P_{i_{P1}} \cdot \left[\begin{cases} \left(x + d_{Pt_{i_{P1}-1}}\right) & \text{if } i_{P1} > 1 \\ x & \text{if } i_{P1} = 1 \end{cases} - l_{p_1} \right] & \text{if } 0\text{in} \le \left[\begin{cases} \left(x + d_{Pt_{i_{P1}-1}}\right) & \text{if } i_{P1} > 1 \\ x & \text{if } i_{P1} = 1 \end{cases} \right] \le l_{t_{j+2}} \\ 0\text{kip} \cdot \text{ft} & \text{otherwise} \end{cases} \right] \ldots}{l_{p_{j+1}}}$$
$$+ (-1) \cdot \left[R_{LL2}(x) \cdot \left(l_{p_2} - l_{p_1}\right) + \begin{cases} R_{LL3}(x) \cdot \left(l_{p_3} - l_{p_1}\right) & \text{if } j \ge 3 \\ 0\text{kip} \cdot \text{ft} & \text{otherwise} \end{cases} + \begin{cases} R_{LL4}(x) \cdot \left(l_{p_4} - l_{p_1}\right) & \text{if } j \ge 4 \\ 0\text{kip} \cdot \text{ft} & \text{otherwise} \end{cases} \right]$$

$x_{prova} := 20\text{ft}$

$R_{LLl}(x_{prova}) = 0.1262\,\text{kip}$

$R_{LL2}(x_{prova}) = -0.6332\,\text{kip}$

$R_{LL3}(x_{prova}) = 14.6328\,\text{kip}$

$R_{LL4}(x_{prova}) = 2.2821\,\text{kip}$

$R_{LLr}(x_{prova}) = -0.408\,\text{kip}$

$b(x_{prova}, 1) = 97.9821\,\text{ft}$

$b(x_{prova}, 2) = 153.6685\,\text{ft}$

$b(x_{prova}, 3) = 100.8027\,\text{ft}$

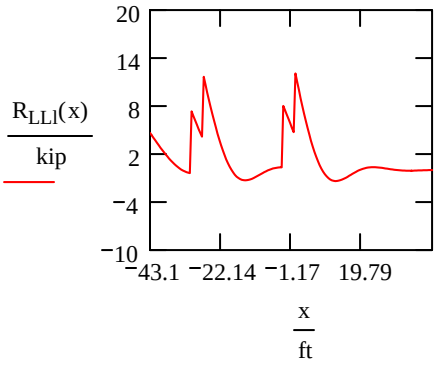

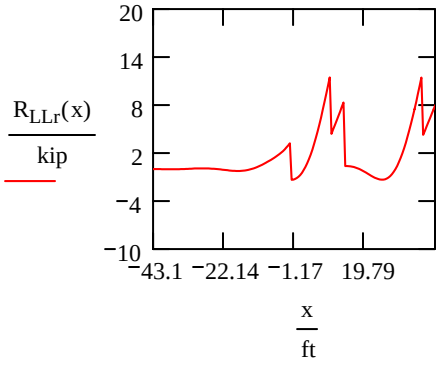

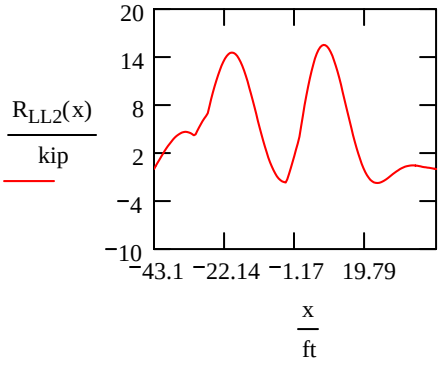

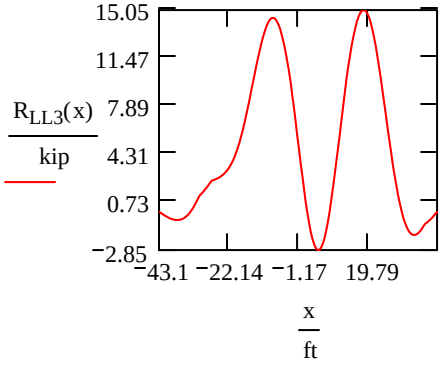

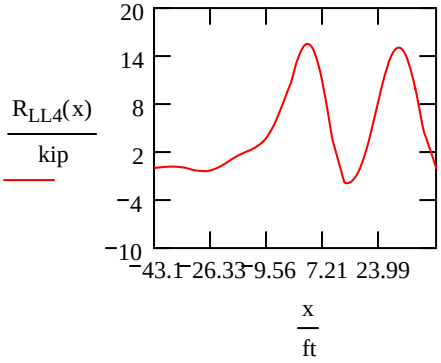

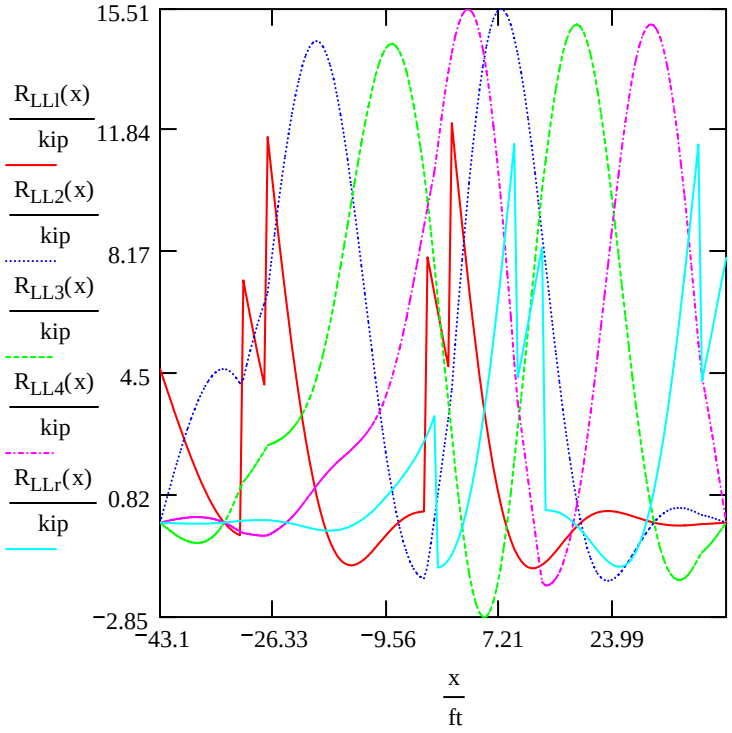

$$R(x) := R_{LLl}(x) + R_{LL2}(x) + R_{LL3}(x) + R_{LL4}(x) + R_{LLr}(x) - \left[\sum_{i_{P1}=1}^{n_P} \left[\begin{array}{ll} P_{i_{P1}} & \text{if } 0in \le \left[\begin{array}{ll} \left(x + d_{Pt_{i_{P1}-1}}\right) & \text{if } i_{P1} > 1 \\ x & \text{if } i_{P1} = 1 \end{array} \right] \le l_{t_{j+2}} \\ 0kip & \text{otherwise} \end{array} \right] \right]$$

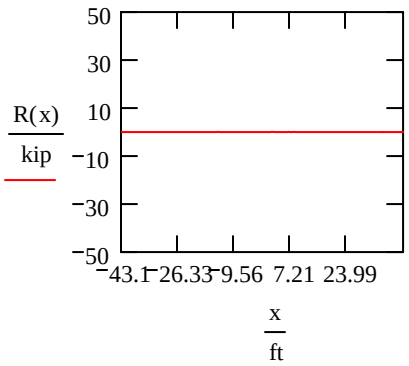

$$\Delta y := \frac{l_{t_{j+2}}}{n_{loop}}$$

$jj := 0, 1 .. n_{loop}$

$jjj := 0, 1 .. n_{loop}$

$y := -\Delta y, 0in .. l_{t_{j+2}} + \Delta y$

$$yy_{jj} := \frac{l_{t_{j+2}} \cdot jj}{n_{loop}}$$

$$xx_{jjj} := l_{min} + \frac{(l_{max} - l_{min}) \cdot jjj}{n_{loop}}$$

$x_1 := 0.000005 \cdot l_{p_1}$

$x_2 := x_1 + 0.5 \cdot l_3$

$x_3 := x_2 + 0.5 \cdot l_4$

$x_4 := x_3 + 0.5 \cdot l_5$

Shear Analysis

Shear expressions:

$$T_{LL}(x,y) := \sum_{i_{P1}=1}^{n_P} \left[\begin{cases} -P_{i_{P1}} & \text{if } y \geq x + d_{Pt_{i_{P1}-1}} \geq 0ft \wedge 0ft \leq y \leq l_{t_{j+2}} \\ (0kip) & \text{otherwise} \end{cases} \right] + \left[\begin{cases} R_{LLl}(x) & \text{if } l_{t_1} \leq y \leq l_{t_{j+2}} \\ (0kip) & \text{otherwise} \end{cases} \right] \ldots$$
$$+ \left[\begin{cases} R_{LL2}(x) & \text{if } l_{t_2} \leq y \leq l_{t_{j+2}} \\ (0 \cdot kip) & \text{otherwise} \end{cases} \right] + \left[\begin{cases} R_{LL3}(x) & \text{if } l_{t_3} \leq y \leq l_{t_{j+2}} \\ (0 \cdot kip) & \text{otherwise} \end{cases} \right] + \left[\begin{cases} R_{LL4}(x) & \text{if } l_{t_4} \leq y \leq l_{t_{j+2}} \\ (0kip) & \text{otherwise} \end{cases} \right] \ldots$$
$$+ \begin{cases} R_{LLr}(x) & \text{if } l_{t_{j+1}} \leq y \leq l_{t_{j+2}} \\ (0kip) & \text{otherwise} \end{cases}$$

Shear Analysis

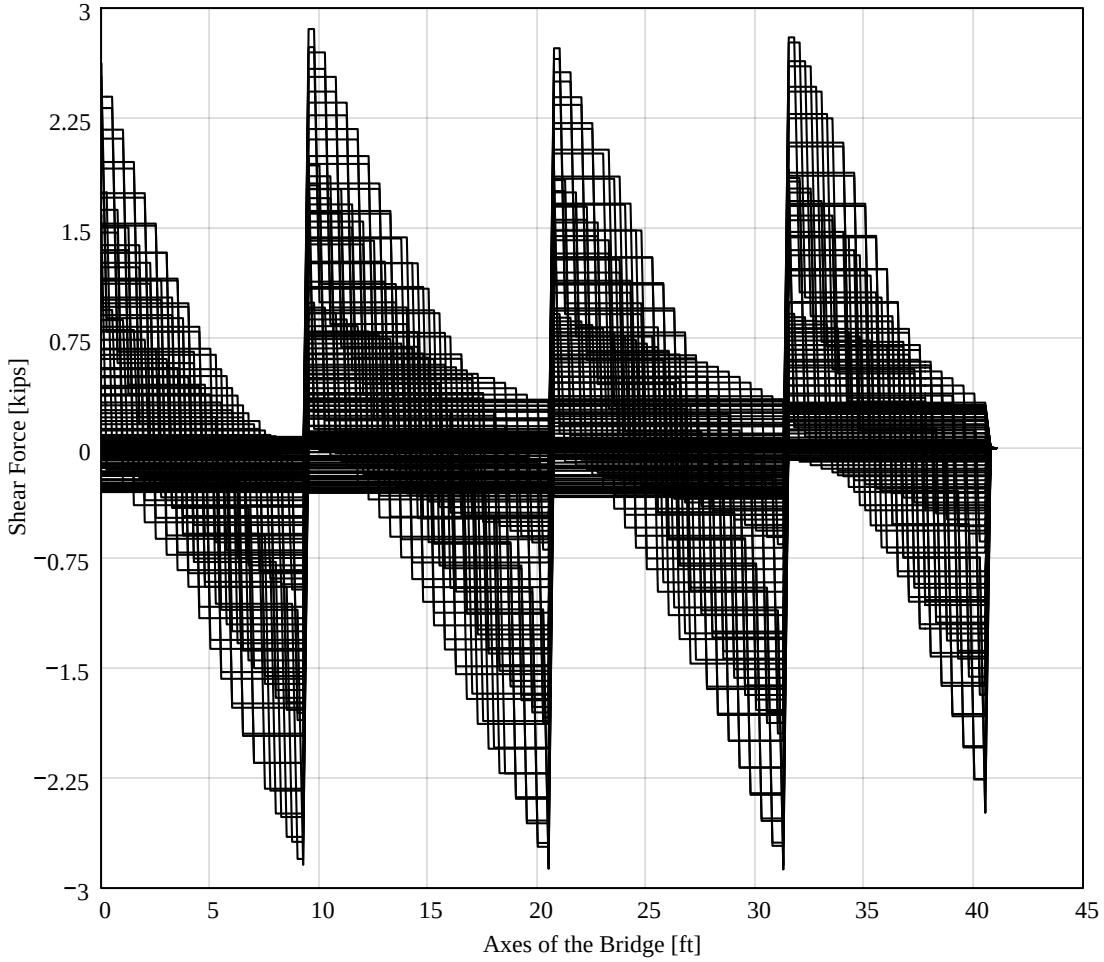

Moment expressions

Moment Analysis

$$M_{LL}(x,y) := \sum_{i_{P1}=1}^{n_P} \left[\begin{cases} -P_{i_{P1}} \cdot \left[y - \left(x + d_{Pt_{i_{P1}-1}} \right) \right] & \text{if } y \geq x + d_{Pt_{i_{P1}-1}} \geq 0\text{ft} \wedge 0\text{ft} \leq y \leq l_{t_{j+2}} \\ (0 \cdot \text{kip} \cdot \text{ft}) & \text{otherwise} \end{cases} \right] \ldots$$
$$+ \left[\begin{cases} R_{LLl}(x) \cdot \left(y - l_{t_1} \right) & \text{if } l_{t_1} \leq y \leq l_{t_{j+2}} \\ (0 \cdot \text{kip} \cdot \text{ft}) & \text{otherwise} \end{cases} \right] + \left[\begin{cases} R_{LLr}(x) \cdot \left(y - l_{t_{j+1}} \right) & \text{if } l_{t_{j+1}} \leq y \leq l_{t_{j+2}} \\ (0 \cdot \text{kip} \cdot \text{ft}) & \text{otherwise} \end{cases} \right] \ldots$$
$$+ \left[\begin{cases} R_{LL2}(x) \cdot \left(y - l_{t_2} \right) & \text{if } l_{t_2} \leq y \leq l_{t_{j+2}} \\ (0 \cdot \text{kip} \cdot \text{ft}) & \text{otherwise} \end{cases} \right] + \left[\begin{cases} R_{LL3}(x) \cdot \left(y - l_{t_3} \right) & \text{if } l_{t_3} \leq y \leq l_{t_{j+2}} \\ (0 \cdot \text{kip} \cdot \text{ft}) & \text{otherwise} \end{cases} \right] \ldots$$
$$+ \left[\begin{cases} R_{LL4}(x) \cdot \left(y - l_{t_4} \right) & \text{if } l_{t_4} \leq y \leq l_{t_{j+2}} \\ (0 \cdot \text{kip} \cdot \text{ft}) & \text{otherwise} \end{cases} \right]$$

Moment Analysis

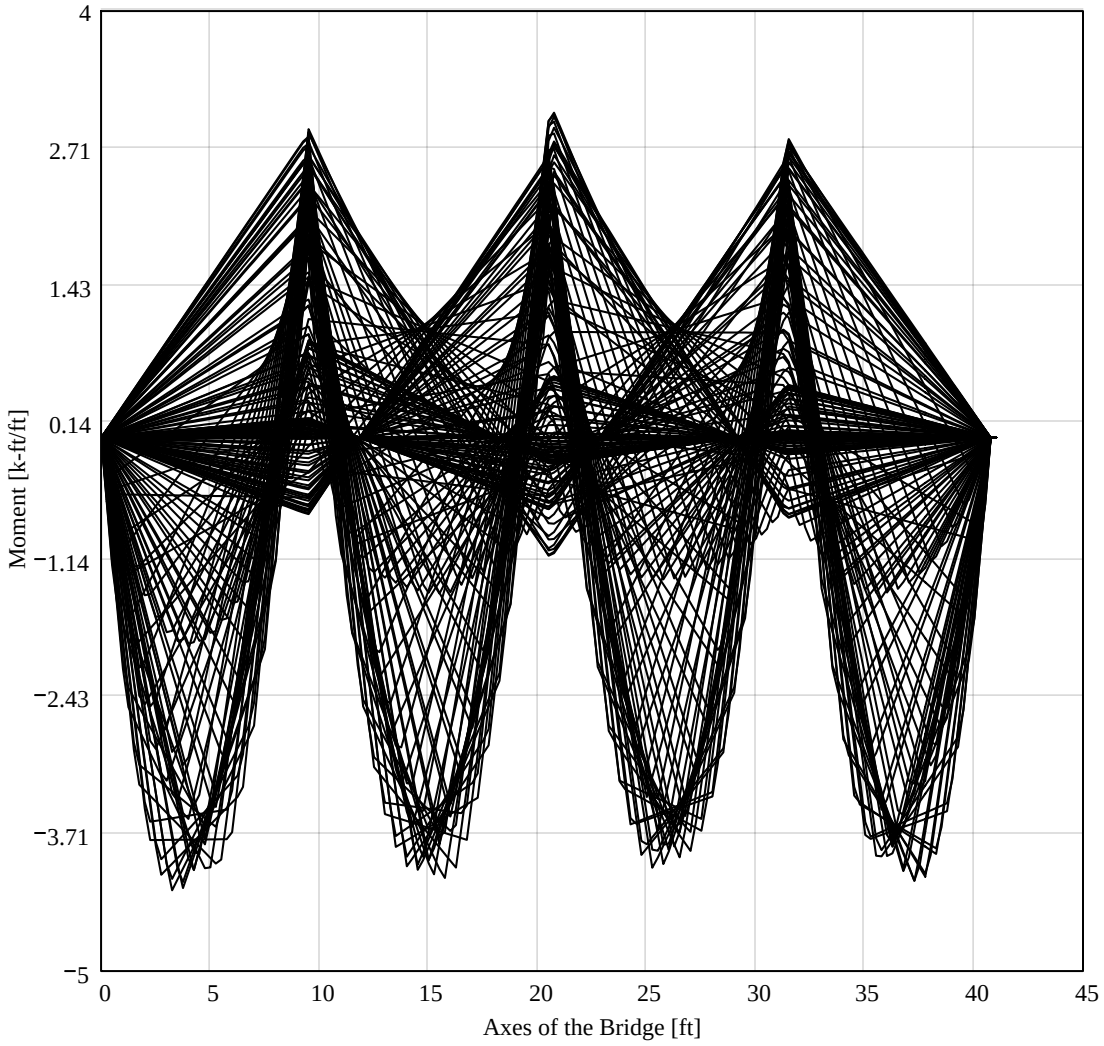

APPENDIX C:

MATERIAL AND CONSTRUCTION SPECIFICATIONS

TABLE OF CONTENTS

A. Construction Practices.....162
A.1 Handling and storage of materials 162
A.2 Placement and assembly of materials 162
A.3 Quality control and inspection 163
B. FRP Composites Bar Systems 164
B.1 General 164
B.1.1 Work to be Provided 164
B.1.2 References 164
B.1.3 Submittals.....165
B.1.3.1 Instructions 165
B.1.3.2 Certificates 165
B.1.3.3 Records.....165
B.1.3.4 Quality Assurance 166
B.1.3.5 Delivery and Storage.....166
B.1.3.6 Safety.....167
B.2 Products.....167
B.2.1 FRP Bars 167
B.2.2 Strength and modulus grades of FRP bars 167
B.2.3 Bar sizes 168
B.2.4 Bar identification.....170
B.2.5 Straight bars.....171
B.2.6 Bent bars.....171
B.2.7 Cementitious Grout 171
B.2.7.1 Cementitious Grout 172
B.3 Execution.....172
B.3.1 Glass FRP Bars Installation.....172
B.3.2 Carbon FRP Bars Installation.....172
B.3.2.1 Grouting procedure 173

August 18, 2003

MATERIALS AND CONSTRUCTION SPECIFICATIONS

By

Center for Infrastructure Engineering Studies
University of Missouri-Rolla (UMR)

PROJECT 206-IBRC

August 18, 2003

A Construction Practices

FRP reinforcing bars are ordered for specific parts of a structure and are delivered to a job site storage area. Construction operations should be performed in a manner designed to minimize damage to the bars. Similarly to epoxy-coated steel bars, FRP bars should be handled, stored, and placed more carefully than uncoated steel reinforcing bars.

A.1 *Handling and storage of materials*

FRP reinforcing bars are susceptible to surface damage. Puncturing their surface can significantly reduce the strength of the FRP bars. In the case of glass FRP bars, the surface damage can cause a loss of durability due to infiltration of alkalis. The following handling guidelines are recommended to minimize damage to both the bars and the bar handlers:

- FRP reinforcing bars should be handled with work gloves to avoid personal injuries from either exposed fibers or sharp edges;
- FRP bars should not be stored on the ground. Pallets should be placed under the bars to keep them clean and to provide easy handling;
- High temperatures, ultraviolet rays, and chemical substances should be avoided because they can damage FRP bars;
- Occasionally, bars become contaminated with form releasing agents or other substances. Substances that decrease bond should be removed by wiping the bars with solvents before placing FRP bars in concrete form;
- It may be necessary to use a spreader bar so that the FRP bars can be hoisted without excessive bending; and
- When necessary, cutting should be performed with a high-speed grinding cutter or a fine-blade saw. FRP bars should never be sheared. Dust masks, gloves, and glasses for eye protection are recommended when cutting. There is insufficient research available to make any recommendation on treatment of saw-cut bar ends.

A.2 *Placement and assembly of materials*

In general, placing FRP bars is similar to placing steel bars, and common practices should apply with some exceptions for the specifications prepared by the engineer as noted:

- FRP reinforcement should be placed and supported using chairs (preferably plastic or non-corrosive). The requirements for support chairs should is included in the project specifications;

- FRP reinforcement should be secured against displacement while the concrete is being placed. Coated tie wire, plastic or nylon ties, and plastic snap ties can be used in tying the bars.

A.3 *Quality control and inspection*

Quality control should be carried out by lot testing of FRP bars. The manufacturer should supply adequate lot or production run traceability. Tests conducted by the manufacturer or a third-party independent testing agency can be used.

All tests should be performed using the recommended test methods cited in the literature. Material characterization tests that include the following properties should be performed at least once before and after any change in manufacturing process, procedure, or materials:

- Tensile strength, tensile modulus of elasticity, and ultimate strain;
- Fatigue strength;
- Bond strength;
- Coefficient of thermal expansion; and
- Durability in alkaline environment.

To assess quality control of an individual lot of FRP bars, it is recommended to determine tensile strength, tensile modulus of elasticity, and ultimate strain. The manufacturer should furnish upon request a certificate of conformance for any given lot of FRP bars with a description of the test protocol.

B FRP Composites Bar Systems

This specification defines the material and procedural requirements for the preparation and installation of pultruded carbon/epoxy (CFRP) and glass/epoxy (GFRP) composite reinforcing bar systems for reinforcing of PC members. The CFRP and GFRP bars will be installed in accordance with the Contract Drawings.

B.1 *General*

B.1.1 Work to be Provided

The Contractor shall complete the following work as shown on the Contract Drawings, details, and as specified herein:

- Provide access for confined spaces
- Install CFRP and GFRP bar systems
- Provide all required tests and inspections of the strengthened system

B.1.2 References

The publications listed below form a part of this specification to the extent referenced. The publications are referred to within the text by the basic designation only.

AMERICAN SOCIETY FOR TESTING AND MATERIALS (ASTM)

ASTM C 882	Standard Test Method for Bond Strength of Epoxy-Resin Systems Used with Concrete by Slant Shear
ASTM D 638	Standard Test Method for Tensile Properties of Plastics
ASTM D 695	Standard Test Method for Compressive Properties of Rigid Plastics
ASTM D3039	Standard Test Method for Tensile Properties of Polymer Matrix Composite Materials
ASTM D 3171	Standard Test Method for Fiber Content of Resin-Matrix Composites by Matrix Digestion
ASTM D 3379	Standard Test Method for Tensile Strength and Young's Modulus for High-Modulus Single-Filament Materials
ASTM D 4258	Standard Practice for Surface Cleaning Concrete for Coating.
ASTM D 4541	Standard Test Method for Pull-Off Strength of Coatings Using Portable Adhesion Testers

AMERICAN CONCRETE INSTITUTE (ACI)

ACI 515.1R	A Guide to the Use of Waterproofing, Damp proofing, Protective, and Decorative Barrier systems for Concrete.
ACI 440.1R-02	Guide for the Design and Construction of Concrete Reinforced with FRP Bars
ACI 440.2R-02	Guide for the Design and Construction of Externally Bonded FRP Systems for Strengthening Concrete Structures

NATIONAL ASSOCIATION OF CORROSION ENGINEERS (NACE)

NACE RP 0288	Inspection of Linings on Steel and Concrete

INTERNATIONAL CONCRETE REPAIR INSTITUTE

Guideline No. 03732 — Selecting and Specifying Concrete Surface Preparation for Sealers, Coatings, and Polymer Overlays

STEEL STRUCTURES PAINTING COUNCIL (SSPC)

SSPC-PA Guide 3 — A Guide to Safety in Paint Application.

B.1.3 Submittals

Submit the following in accordance with Sections B.1.3.1 to B.1.3.3

B.1.3.1 Instructions

a. GFRP and CFRP Bars

Submit supplier's printed instructions to include brand name, catalog numbers, and names of manufacturers. Include with the instructions the quantity of material to be used per square foot and total quantity of material to be used on the job. Include copies of the Material Safety Data Sheets (MSDS) for all materials to be used at the job site

b. Cementitious Grout

Submit supplier's printed instructions and include brand name, catalog numbers, and names of manufacturers. Include in the instructions detailed mixing and injection procedures, quantity of material to be used per square foot, total quantity of material to be used on the job, minimum and maximum application temperatures, and curing procedures. Include copies of the MSDS for all materials to be used at the job site.

B.1.3.2 Certificates

a. Carbon/Epoxy FRP Bars

For the composite bar, certify conformance to the requirements set forth in Paragraph B.2.2

b. Cementitious Grout

For the Cementitious Grout (CG), certify conformance to the requirements set forth in Paragraph **Error! Reference source not found.**.

B.1.3.3 Records

a. Installers Qualifications

Throughout the progress of the work in this Specification, the Contractor will provide at least one (1) person who is thoroughly familiar with the specified requirements, completely trained and experienced with the necessary skills, and

who will be present on the site and direct all work performed under this Specification.

In performing the work of this Specification, the Contractor will use an adequate number of skilled workmen to ensure the installation is in strict accordance with schedule, Specifications, and procedures required by the Missouri Department of Transportation (MoDOT).

b. Disposal of Material
All polymer resins and adhesives shall be disposed of properly as indicated on the MSDS. All epoxy resins and adhesives shall be stored and transported as indicated on the MSDS. All materials (e.g., epoxies, grout, abrasive media, etc.) shall be contained at the site and in accordance with State Regulation.

B.1.3.4 Quality Assurance

Prior to commencement of any work, the Contractor shall be responsible for arranging and conducting a meeting between the Contractor and MoDOT-designated engineers (Engineer) to discuss the project requirements. The Contractor shall review the requirements of the Specification and overall project requirements. All aspects of the project including containment, environmental control, quality assurance, schedule requirements, and safety shall be reviewed and discussed. The Contractor shall request clarification of any ambiguities, and advise the Engineer of any potential conflicts and/or any technical requirements that appear improper or inappropriate.

The Contractor shall ensure the highest quality of workmanship at all times throughout the progression of the work. Only qualified installers having prior training and experience in the specified surface preparation and carbon laminate applications shall be assigned to perform the work described herein.

B.1.3.5 Delivery and Storage

All materials shall be delivered in “new” condition only, packaged in their original, unopened containers bearing the manufacturer’s name, product identification, batch number(s), and shelf life expiration date.

All materials shall be stored in a covered, well-ventilated area and protected from exposure to any detrimental conditions including, airborne contaminants, dirt, dust, sunlight, extreme cold, heat, rainfall, sparks, or flame.

When requested by Engineer, the Contractor shall provide batch samples of any materials that are used throughout the progression of the work. Batch samples will not exceed 2 percent of the total material used on this job.

B.1.3.6 Safety

The processes described in this Specification involve potentially hazardous operations. The contractor shall take the necessary precautions in accordance with manufacturer's instructions, applicable MSDS, and the MoDOT's site safety requirements to ensure the safeness of all personnel that may be affected by the work described in this Specification.

The Contractor shall be responsible for providing any and all safety equipment required for confined spaces, the use of any products, and/or equipment utilized during the progression of the work.

The Contractor shall establish and maintain safe working conditions throughout the progression of the work. The Contractor shall take immediate action to remedy any safety concerns and unsafe, or potentially unsafe, working conditions.

The Contractor shall provide safe access to all work areas for inspection by Engineer and/or designated representatives.

B.2 *Products*

B.2.1 FRP Bars

GFRP and CFRP bars are the reinforcing elements for the negative moment, positive moment and shear regions of RC and PC bridge members. The bars are pultruded carbon or glass fibers reinforced epoxy.

FRP bars should be designated with different grades according to their engineering characteristics (such as tensile strength and modulus of elasticity). Bar designation should correspond to tensile properties, which should be uniquely marked so that the proper FRP bar is used.

B.2.2 Strength and modulus grades of FRP bars

FRP reinforcing bars are available in different grades of tensile strength and modulus of elasticity. The tensile strength grades are based on the tensile strength of the bar, with the lowest grade being 60,000 psi (414 MPa). Finite strength increments of 10,000 psi (69 MPa) are recognized according to the following designation:

Grade F60: corresponds to a $f^*_{fu} \geq 60{,}000$ psi (414 MPa)
Grade F70: corresponds to a $f^*_{fu} \geq 70{,}000$ psi (483 MPa)
Grade F300: corresponds to a $f^*_{fu} \geq 300{,}000$ psi (2069 MPa).

A minimum Grade F70 is required for the GFRP bars while a grade F250 is required for the CFRP bars.

A modulus of elasticity grade is established similar to the strength grade. For the modulus of elasticity grade, the minimum value is prescribed depending on the fiber type. For design purposes, the engineer can select the minimum modulus of elasticity grade that corresponds to the chosen fiber type for the member or project. For example, an FRP bar specified with a modulus grade of E5.7 indicates that the modulus of the bar should be at least 5700 ksi (39.3 GPa). Manufacturers producing FRP bars with a modulus of elasticity in excess of the minimum specified will have superior FRP bars that can result in savings on the amount of FRP reinforcement used for a particular application.

The modulus of elasticity grades for different types of FRP bars are summarized in Table 1. For all these FRP bars, rupture strain should not be less than 0.005 in./in.

Table 1- Minimum modulus of elasticity, by fiber type, for reinforcing bars

	Modulus grade, $\times 10^3$ ksi (GPa)
GFRP bars	E5.7 (39.3)
CFRP bars	E16.9 (110.3)

B.2.3 Bar sizes

FRP bar sizes are designated by a number corresponding to the approximate nominal diameter in eighths of an inch, similar to standard ASTM steel reinforcing bars. There are 12 standard sizes, as illustrated in

Table 2, which also includes the corresponding metric conversion.

The nominal diameter of a deformed FRP bar is equivalent to that of a plain round bar having the same area as the deformed bar. When the FRP bar is not of the conventional solid round shape (that is, rectangular or hollow), the outside diameter of the bar or the maximum outside dimension of the bar will be provided in addition to the equivalent nominal diameter. The nominal diameter of these unconventional bars would be equivalent to that of a solid plain round bar having the same area.

Table 2 - ASTM standard reinforcing bars

Bar size designation		Nominal diameter, in. (mm)	Area, in.^{2} (mm^2)
Standard	Metric conversion		
No. 2	No. 6	0.250 (6.4)	0.05 (31.6)
No. 3	No. 10	0.375 (9.5)	0.11 (71)
No. 4	No. 13	0.500 (12.7)	0.20 (129)
No. 5	No. 16	0.625 (15.9)	0.31 (199)
No. 6	No. 19	0.750 (19.1)	0.44 (284)
No. 7	No. 22	0.875 (22.2)	0.60 (387)
No. 8	No. 25	1.000 (25.4)	0.79 (510)
No. 9	No. 29	1.128 (28.7)	1.00 (645)
No. 10	No. 32	1.270 (32.3)	1.27 (819)
No. 11	No. 36	1.410 (35.8)	1.56 (1006)
No. 14	No. 43	1.693 (43.0)	2.25 (1452)
No. 18	No. 57	2.257 (57.3)	4.00 (2581)

B.2.4 Bar identification

With the various grades, sizes, and types of FRP bars available, it is necessary to provide some means of easy identification. Each bar producer should label the bars, container/ packaging, or both, with the following information:

- A symbol to identify the producer;
- A letter to indicate the type of fiber (that is, g for glass, c for carbon, a for aramid, or h for a hybrid) followed by the number corresponding to the nominal bar size designation according to the ASTM standard;
- A marking to designate the strength grade;
- A marking to designate the modulus of elasticity of the bar in thousands of ksi; and
- In the case of an unconventional bar (a bar with a cross section that is not uniformly circular or solid), the outside diameter or the maximum outside dimension.

A bond grade will be added when a classification is available. Example of identification symbols are shown below:

XXX - G#4 - F100 - E6.0

where

XXX = manufacturer’s symbol or name;

G#4 = glass FRP bar No. 4 (nominal diameter of 1/2 in.);

F100 = strength grade of at least 100 ksi (f*fu ≥ 100 ksi);

E6.0 = modulus grade of at least 6,000,000 psi.

In the case of a hollow or unconventionally shaped bar, an extra identification should be added to the identification symbol as shown below:

XXX - G#4 - F100 - E6.0 - 0.63

where:

0.63 = maximum outside dimension is 5/8 in.

Markings should be used at the construction site to verify that the specified type, grades, and bar sizes are being used.

B.2.5 Straight bars

Straight bars are cut to a specified length from longer stock lengths in a fabricator's shop or at the manufacturing plant.

B.2.6 Bent bars

Bending FRP rebars made of thermoset resin should be carried out before the resin is fully cured. After the bars have cured, bending or alteration is not possible due to the inflexibility or rigid nature of a cured FRP bar. Because thermoset polymers are highly cross-linked, heating the bar is not allowed as it would lead to a decomposition of the resin, thus a loss of strength in the FRP.

The strength of bent bars varies greatly for the same type of fiber, depending on the bending technique and type of resin used. Therefore, the strength of the bent portion generally should be determined based on suitable tests performed in accordance with recommended test methods cited in the literature. Bars in which the resin has not yet fully cured can be bent, but only according to the manufacturer's specifications and with a gradual transition, avoiding sharp angles that damage the fibers.

B.2.7 Cementitious Grout

After tensioning the carbon bars, they are injected with a Cementitious Grout in the duct work, as shown in the Contract Drawings. The system components must be chemically compatible so that individual properties are not compromised and so that solid bonding is developed.

B.2.7.1 Cementitious Grout

DESCRIPTION		(VALUE)[1]	
		US Customary	SI Units
SHELF LIFE		Nine months in original, unopened bags.	
STORAGE CONDITIONS		Store dry at 40-95F (4-35C). For best results, it is suggested to condition material to 65-75F before using.	
TOTAL CHLORIDE IONS (ASTM C-1152)		less than 0.08% by weight of cementitious material	
FLUIDITY TEST (ASTM C-939)		Immediately after mixing	7-20 seconds
		30 minutes after mixing	7-20 seconds
BLEEDING (ASTM C-940)		4 hours	0%
Compressive Strengths	1 day	3300 psi	22.75 MPa
	3 day	6000 psi	41.37 MPa
	7 day	7500 psi	51.71 MPa
	28 day	8500 psi	58.61 MPa

( )[1] at 72°F (22°C) and 50 percent relative humidity

B.3 *Execution*

B.3.1 Glass FRP Bars Installation

Installation of GFRP bars must be in compliance with the construction practices described in Paragraphs from A.1 to A.3.

B.3.2 Carbon FRP Bars Installation

The installation of the CFRP bars must be in compliance with the construction practices described in Paragraphs from A.1 to A.3.

Since bonded post-tensioning is adopted for the CFRP bars, the operations are carried out as follows:

1. Erection of slab supporting formwork;
2. Fitting of end formwork; placing of stressing anchorages;
3. Placing empty ducts according to placing drawing;
4. Supporting of empty ducts with supporting chairs according to support drawing;
5. Placing of top and bottom reinforcement according to the contractor drawings;
6. Concreting of the section of the slab;
7. Removal of end formwork and forms for the stressing block-outs;
8. Stressing of cables according to stressing program;
9. Stripping of slab supporting formwork;
10. Grouting of cables and removing of block-outs.

B.3.2.1 Grouting procedure

Tendon ducts should be tested with air pressure to proof leak tightness. Testing for leak tightness is an essential step in the procedures to assure high quality grouting. After the grout mix has been confirmed in the suitability tests on site, and all grouting activities including equipment and training of personnel have been properly prepared and / or done, actual grouting of the post-tensioning tendons can commence. This is typically in accordance with the following steps:

1. The grout is mixed in accordance with the Data Sheet provided by the manufacturer.

2. When the properties of the grout are confirmed, grouting proper can commence.

3. The grouting nozzle is fitted to the lowest grout connection or to a cable end as specified in the method statement.

4. Grouting should continue without interruption so that grout flows continuously in the same direction from the inlet to the cable end. While the grout moves as a solid column in upward slopes of the duct, it will often flow faster downhill than the pump provides grout. Hence, it will fill the descending branch of the duct from the following low point backwards / upwards again. This will likely cause entrapment of air at the high point which needs to be expelled via the vent at that location. To allow this to happen, the maximum rate of flow of grout in the duct should be limited to 10 to 12 m/minute.

5. When the grout flows out from the first vent, this vent is not closed until the issuing grout has a comparable viscosity and consistency as that in the mixer. This can be judged visually by experienced staff, and can be confirmed by grout density and flow time measurements. If the flow time at the outlet is less than that at the mixer, the difference should not be more than about 3 seconds. This connection can then be closed. The same criterion applies for all further vent points, including the outlet in the anchorage / cap at the cable end. At all vents, the issuing grout should be collected for environmental reasons and to avoid staining of the structure.

6. If the grouting pressure at the grouting connection approaches 10 bars (e.g. with long cables), the grouting nozzle should be transferred to the next already filled connection and grouting should be continued from there.

7. When the entire cable is filled, i.e. when all the vents have been closed, the pump pressure is slightly raised (about 1 to 3 bars above the grouting pressure depending upon the type of seal at the anchor heads). This pressure is maintained for about one minute. If the pressure can be maintained without significant loss

this can be considered confirmation that the duct system is leak tight. The inlet opening is then also closed. The grouting nozzle can now be removed and fitted to the next cable. If the pressure drops significantly, this indicates leakage. Leaks should then be located and sealed, and any void left should be topped up with grout.

8. It is recommended to prepare a grouting report daily, including all relevant data of the mix, grout testing, identification of the grouted tendons, weather conditions, and grout consumption. Reporting of grout consumption will allow to detect gross errors but will not permit the detection of local voids.